UNIVERSIDADE FEDERAL DE SANTA MARIA CENTRO DE TECNOLOGIA
PROGRAMA DE PÓS-GRADUAÇÃO EM ENGENHARIA QUÍMICA

Maria Caroline Ferreira da Silva

OBTENÇÃO E CARACTERIZAÇÃO DE CARVÃO ATIVADO A PARTIR DE RESÍDUOS DE CASCA DE CASTANHA DO PARÁ (*Bertholletia excelsa*) E SUA APLICAÇÃO NA ADSORÇÃO DE FENOL

Santa Maria, RS
2023

Maria Caroline Ferreira da Silva

OBTENÇÃO E CARACTERIZAÇÃO DE CARVÃO ATIVADO A PARTIR DE RESÍDUOS DE CASCA DE CASTANHA DO PARÁ (*Bertholletia excelsa*) E SUA APLICAÇÃO NA ADSORÇÃO DE FENOL

Dissertação apresentada ao Curso de mestrado do Programa de Pós-Graduação em Engenharia Química, área de concentração da Universidade Federal de Santa Maria (UFSM, RS), como requisito parcial para obtenção do título de **Mestre em Engenharia Química**.

Orientador: Prof. Dr. Guilherme Luiz Dotto
Coorientador: Prof. Dr. Éder Cláudio Lima

Santa Maria, RS
2023

This study was financied in part by the Coordenação de Aperfeiçoamento de Pessoal de Nível Superior - Brasil (CAPES) – Finance Code 001

da Silva, Maria Caroline Ferreira
Obtenção e caracterização de carvão ativado a partir de resíduos de casca de Castanha do Pará (Bertholletia excelsa) e sua aplicação na adsorção de Fenol. / Maria Caroline Ferreira da Silva.- 2023.
116 p.; 30 cm

Orientador: Guilherme Luiz Dotto
Coorientador: Éder Cláudio Lima
Dissertação (mestrado) - Universidade Federal de Santa Maria, Centro de Ciências Naturais e Exatas, Programa de Pós-Graduação em Engenharia Química, RS, 2023

1. Adsorventes 2. Caracterização 3. Isotérma 4. Cinética I. Luiz Dotto, Guilherme II. Lima, Éder Cláudio III. Título.

Sistema de geração automática de ficha catalográfica da UFSM. Dados fornecidos pelo autor(a). Sob supervisão da Direção da Divisão de Processos Técnicos da Biblioteca Central. Bibliotecária responsável Paula Schoenfeldt Patta CRB 10/1728.

Declaro, MARIA CAROLINE FERREIRA DA SILVA, para os devidos fins e sob as penas da lei, que a pesquisa constante neste trabalho de conclusão de curso (Dissertação) foi por mim elaborada e que as informações necessárias objeto de consulta em literatura e outras fontes estão devidamente referenciadas. Declaro, ainda, que este trabalho ou parte dele não foi apresentado anteriormente para obtenção de qualquer outro grau acadêmico, estando ciente de que a inveracidade da presente declaração poderá resultar na anulação da titulação pela Universidade, entre outras consequências legais.

Maria Caroline Ferreira da Silva

OBTENÇÃO E CARACTERIZAÇÃO DE CARVÃO ATIVADO A PARTIR DE RESÍDUOS DE CASCA DE CASTANHA DO PARÁ (*Bertholletia excelsa*) E SUA APLICAÇÃO NA ADSORÇÃO DE FENOL

Dissertação apresentada ao Curso de mestrado do Programa de Pós-Graduação em Engenharia Química, área de concentração da Universidade Federal de Santa Maria (UFSM, RS), como requisito parcial para obtenção do título de **Mestre em Engenharia Química**.

Aprovada em 29 de Março de 2023:

_____

Guilherme Luiz Dotto, Dr (UFSM)
(videoconferencia)

_____

Maria Amélia Zazycki, Dra (UFN)
(videoconferencia)

_____

Jivago Schumacher de Oliveira, Dr (UFN)
(videoconferencia)

Santa Maria, RS

2023

AGRADECIMENTOS

Ao Universo e a toda trajetória vivida, que me fez firme no caminho todo!

Aos meus maiores educadores e pais, Leiza Maria Ferreira da Silva e Zoilo Soares da Silva, sempre foi por vocês.

A minha família toda, em especial aos irmãos Ana Gabriela Ferreira da Silva, Matias Ferreira da Silva, ao cunhado André Alfaro. E ao meu sobrinho Joaquin.

A amiga e parceira, da academia para a vida: Vitória Ximenes. Que esteve junto na Graduação e na Pós, sempre apoiando. Certamente é recíproco o agradecimento de chegarmos até aqui juntas. Mas principalmente no momento que mais precisei ter força, tu esteve lá, obrigada!

A admirável química Sabrina Lutke, que com dedicação foi o pilar deste trabalho. Obrigada Sá, seus ensinamentos foram essenciais, para chegarmos até aqui. Principalmente os puxões de orelha.

Ao meu orientador e professor Dr. Guilherme Dotto, pela maestria e organização da pesquisa. E pelo projeto ENGEPAC, com certeza um grupo é exemplo na área de Adsorção. E pela dedicação ao Programa.

Ao meu coorientador, professor Dr. Éder Lima, pelo apoio e dedicação ao estudo.

Aos amigos e familiares, que sempre me apoiaram.

A minha segunda família, empresa Conplan Sistemas. Do convívio diário e por todo incentivo que tens com seus colaboradores se manterem estudando, e se desenvolvendo.

A Universidade Federal de Santa Maria e ao Programa de Pós-Graduação em Engen Química por ter feito meu sonho de criança em fazer parte desta instituição.

RESUMO

OBTENÇÃO E CARACTERIZAÇÃO DE CARVÃO ATIVADO A PARTIR DE RESÍDUOS DE CASCA DE CASTANHA DO PARÁ (*Bertholletia excelsa*) E SUA APLICAÇÃO NA ADSORÇÃO DE FENOL.

AUTORA: Maria Caroline Ferreira da Silva
ORIENTADOR: Guilherme Luiz Dotto
COORIENTADOR: Éder Lima

A contaminação de águas por compostos orgânicos pode causar danos ao meio ambiente e aos seres humanos. A adsorção é um processo promissor para a remoção desses poluentes. Resíduos agrícolas são uma ótima alternativa como precursores na produção de adsorventes, como é o caso da casca de castanha do Pará (*Bertholletia excelsa*). Neste estudo foram obtidos dois carvões ativados (CA11 e CA105), utilizando ativação química com KOH, em proporções de 1:1 e 1:0,5 respectivamente. Os carvões foram caracterizados e aplicados como adsorventes para remoção de fenol. A caracterização foi realizada usando as técnicas como MEV, FTIR, BET, TGA e DRX. Os dados de caracterização mostraram que ambos os materiais apresentaram propriedades semelhantes, com CA11 exibindo uma área superficial específica ligeiramente maior e várias cavidades arredondadas ao longo da superfície (332,2 $m^2 g^{-1}$) do que CA105 (314,3 $m^2 g^{-1}$). O estudo cinético mostrou que CA11 atingiu o equilíbrio do processo mais rápido que o CA105. As máximas capacidades de adsorção foram 55,16 e 68,52 mg g^{-1}para CA105 e CA11, respectivamente. A aplicação dos materiais no tratamento de um efluente industrial simulado apresentou eficiências de remoção de 28,05% e 48,20% para CA105 e CA11, respectivamente. Portanto, através dos resultados de adsorção, o CA11 mostrou-se mais eficiente quando comparado ao CA105. Este colocado em melhores condições, com relação à adsorção de fenol, foi favorecido na dosagem de adsorvente de 0,75 g L^{-1} e pH 6. A investigação cinética revelou que o sistema atingiu o equilíbrio em cerca de 180 minutos e as curvas cinéticas representadas pelo modelo de Elovich. As isotermas de equilíbrio foram representadas pelo modelo de Sips. Além disso, o aumento da temperatura de 25 para 55 °C favoreceu a adsorção do fenol, aumentando o valor da capacidade máxima de adsorção (q_s) de 82,99 para 99,02 mg g^{-1}. De acordo com os parâmetros termodinâmicos estimados, a adsorção foi espontânea, favorável, endotérmica e governada por interações físicas. Portanto, a casca da castanha do Pará provou ser um bom material para obtenção de carvão ativado, eficiente na remoção de fenol.

Palavras-chaves: Isotermas; Cinética, Caracterização;

ABSTRACT

OBTAINMENT AND CHARACTERIZATION OF ACTIVATED CARBON FROM BRAZIL NUTS (*Bertholletia excelsa*) HULL RESIDUES AND ITS APPLICATION IN THE PHENOL ADSORPTION.

AUTHOR: Maria Caroline Ferreira da Silva
ADVISOR: Guilherme Luiz Dotto
CO-ADVISOR: Éder Lima

The water contamination by organic compounds can cause damage to the environment and human beings. Adsorption is a promising process for removing these pollutants. Agricultural residues are a great alternative as precursors in the production of adsorbents, as is the case of the Brazil nut shell (*Bertholletia excelsa*), where in this study two activated carbons (AC11 and AC 105) were obtained, using chemical activation with KOH, in proportions of 1:1 and 1:0.5 respectively. The coals were characterized and applied as adsorbents for phenol removal. Characterization was performed using techniques such as SEM, FTIR, BET, TGA, and XRD. The characterization data showed that both materials showed similar properties, with AC11 exhibiting a slightly larger specific surface area and several rounded cavities along the surface (332.2 m^2 g^{-1}) than AC105 (314.3 m^2 g^{-1}). The kinetic study showed that AC11 reached process equilibrium faster than AC105. Adsorption maxima were 55.16 and 68.52 mg g^{-1} for AC105 and AC11, respectively. The application of the materials in the treatment of a simulated industrial effluent showed removal efficiencies of 28.05% and 48.20% for AC105 and AC11, respectively. Therefore, through the adsorption results, AC11 was more efficient when compared to AC105. This place in better conditions, with regard to phenol adsorption, was favored in the adsorbent dosage of 0.75 g L^{-1} and pH 6. The kinetic investigation revealed that the system reached equilibrium in about 180 minutes and the kinetic curves represented by the Elovich model. Equilibrium isotherms were represented by the Sips model. Furthermore, increasing the temperature from 25 to 55 °C favored phenol adsorption, increasing the value of the maximum adsorption capacity (q_s) from 82.99 to 99.02 mg g^{-1}. According to the estimated thermodynamic parameters, the adsorption was spontaneous, favorable, endothermic, and governed by physical interactions. Therefore, the bark of the Brazil nut proved to be a good material for obtaining activated carbon efficiently in removing phenol.

Keywords: Isotherms; Kinetics, Characterization;

LISTA DE FIGURAS

REFERENCIAL BIBLIOGRÁFICO

ARTIGO 1

ARTIGO 2

LISTA DE TABELAS

ARTIGO 1

ARTIGO 2

LISTA DE ABREVIATURAS E SIGLAS

ARE - erro médio relativo
BET - Braunauer, Emmett e Teller

BJH - Modelo de adsorção de Barrett, Joyner e Halenda

CA - Carvão ativado com ácido fosfórico

CE - Contaminantes emergentes

DRX - difração de raio X
EDTA - Ácido etilenodiamino tetra-acético

FAO - *Food and Agriculture Organization of the United Nations*

FT-IR - Espectrofotometria na região do infravermelho por transformada de Fourier

IUPAC - International Union of Pure and Applied Chemistry

MEV - microscopia eletrônica de varredura
NA - Não adsorveu

OMS - Organização Mundial da Saúde

pHPCZ- pH do ponto de carga zero

R2adj - coeficiente de determinação ajustado

R^2 - coeficiente de determinação
UV-Vis - Ultravioleta-Visível

LISTA DE SÍMBOLOS

Símbolo	Significado	Unidade
Ce	Concentração do adsorbato na fase aquosa no equilíbrio	[mg L^{-1}]
k1	Constante de velocidade de pseudo-primeira ordem	[min^{-1}]
k2	Constante de velocidade de pseudo-segunda ordem	[g mg^{-1} min^{-1}]
kF	Constante de equilíbrio de Freundlich	[(mg g^{-1}) (mg L^{-1}) $^{-1/nf}$]
KD	Constante de equilíbrio	[-]
kL	Constante de equilíbrio de Langmuir	[L mg^{-1}]
R	Constante dos gases universal	[kJ mol^{-1} K^{-1}]
qe	Quantidade de adsorbato adsorvido no equilíbrio	[mg g^{-1}]
qm	Capacidade máxima de adsorção	[mg g^{-1}]
qt	Quantidade adsorvida no tempo t	[mg g^{-1}]
q1, q2	Quantidade adsorvida no equilíbrio	[mg g^{-1}]
t	Tempo	[min]
T	Temperatura	[K]
$^{1}/nf$	Fator de heterogeneidade	[-]
ΔG^0	Energia livre de Gibbs	[kJ mol^{-1}]
ΔH^0	Entalpia de adsorção	[kJ mol^{-1}]
ΔS^0	Entropia de adsorção	[kJ mol^{-1} K^{-1}]

SUMÁRIO

1. INTRODUÇÃO

A contaminação hídrica devido a atividades agrícolas, industriais e sociais tornou-se um problema crucial para o ambiente e seres vivos. Grandes quantidades de poluentes são lançadas em águas naturais sem qualquer tratamento. Existem vários tipos de contaminantes da água, como contaminantes orgânicos, nutrientes, patógenos, poluentes inorgânicos entre outros. (LIMA, et. 2019). Os compostos fenólicos são contaminantes considerados orgânicos, encontrados em águas residuais produzidas por diversas indústrias. As principais indústrias são de mineração de carvão, refinarias de petróleo, indústria farmacêutica, e têxtil. Além de síntese de resinas, papel e celulose, tintas e indústrias de processamento de madeira (PRIYADHARSHINI e BAKTHAVATSALAM, 2019; CETINKAYA e OZDEMIR, 2018, BARIK et al. 2021).

Algumas das técnicas existentes para os tratamentos de fenol em soluções aquosas tal como oxidação (YAZICI GUVENC et al. 2022), separação por membrana (NGOBENI, et al. 2021), métodos bioquimicos (NOORI, 2019), e adsorção (FENG et al. 2021). A última se destaca por sua alta eficiência, simplicidade operacional, menor custo e capacidade de regeneração. A adsorção é um fenômeno de transferência de massa cuja força motriz é a diferença de concentração entre o adsorvato nas fases fluida e sólida (adsorvente) (DOTTO et al., 2015; FRANCO, 2021).

O carvão ativado (CA) é o adsorvente que com boas características físico-químicas tem sido utilizado para purificação de água por um longo prazo. E se, desenvolvido baseado em materiais precursores, mais baratos, como os resíduos agrícolas, contribui não apenas para a eliminação de um contaminante, mas também para o tratamento e destino correto destes que podem causar sérios problemas ambientais e a saúde pública, sem um descarte e tratamento eficaz (AWASTHI et al., 2022).

Baseado no exposto a cima, objetivou-se a desenvolver e caracterizar um carvão ativado, a partir de resíduos de casca de castanha do Pará (*Bertholletia excelsa)*, avaliando seu potencial adsortivo em contato com fenol, em solução aquosa. Os carvões foram caracterizados com relação às técnicas de Microscopia Eletrônica de Varredura (MEV), Difração de Raios-X (DRX), Espectroscopia no Infravermelho por transformada de Fourier (FTIR), Isotermas de Nitrogênio (BET), e Análise termogravimétrica (TGA), Ponto de carga

zero (pH_{PCZ}). Foram avaliados os parâmetros que influenciam o processo de adsorção, as isotermas de equilíbrio e cinéticos, além de termodinâmicos.

2. **OBJETIVOS**

2.1.OBJETIVO GERAL

O objetivo geral deste trabalho foi obter carvões ativados a partir de resíduos de casca de castanha do Pará (*Bertholletia excelsa)*, e verificar seu potencial adsortivo na remoção de Fenol em meio aquoso.

2.2.OBJETIVO**S** ESPECÍFICOS

- Preparar e caracterizar o carvão utilizando às técnicas como: microscopia eletrônica de varredura (MEV), Análise da área superficial (BET/BJH), Análise termogravimétrica (TGA), Espectroscopia no infravermelho por transformada de Fourier (FTIR), Difração de raio-X (DRX), e Ponto de carga zero (pH_{PCZ});
- Analisar a capacidade de adsorção do CA em diferentes concentrações do agente ativador KOH;
- Estudar e compara-los frente a cinética e o equilíbrio de adsorção do Fenol;
- Verificar e comparar a eficiência de remoção de compostos fenólicos em um efluente simulado.;
- Avaliar a regeneração dos carvão ativado;
- Determinar o carvão vai eficaz dentre os adsorventes desenvolvidos;
- Aplicar o carvão mais eficaz em melhores condições definidas de: temperatura, dosagem, pH e tempo;
- Realizar o estudo da termodinâmica;

3. REVISÃO BIBLIOGRÁFICA

3.1.CONTAMINAÇÃO DOS RECURSOS HÍDRICOS

Os recursos hídricos são cada vez mais ameaçados, à medida que a população cresce, as atividades agrícolas e indústrias se expandem e as mudanças climáticas ameaçam alterar o ciclo natural. Neste contexto, o crescimento industrial repercutiu em um aumento significativo da poluição ambiental, inclusive a poluição de corpos hídricos devido ao descarte inadequado de efluentes. Alguns dos contaminantes podem representar riscos à saúde, enquanto outros podem alterar seu cheiro, sabor e aparência. Várias organizações internacionais como a EPA e OMS, fornecem níveis padrão de impurezas na água potável (AHMED, 2019). A remoção de substâncias orgânicas e inorgânicas e outros poluentes é uma das etapas mais importantes antes de transferir esses resíduos para a natureza (SAID et al., 2023).

3.2.COMPOSTOS FENÓLICOS

Os compostos fenólicos podem ser transportados favoravelmente no ambiente natural devido à sua alta solubilidade em água (CARRILLO E BORTHAKUR, 2021). A (EPA) classificou esses compostos orgânicos como poluentes prioritários. São encontrados em águas residuais produzidas por diversas indústrias. Em geral, petroquímicos, mineração de carvão e refinarias de petróleo são as principais indústrias responsáveis pela liberação de poluentes fenólicos no ambiente receptor. Da mesma forma, efluentes da indústria farmacêutica, têxtil, carvão e etc. (PRIYADHARSHINI E BAKTHAVATSALAM, 2019). Poluentes fenólicos também são biologicamente recalcitrantes. Assim, eles persistem em sistemas de águas residuais em uma concentração muito alta (WEI et al., 2016). Muitas vezes, as águas residuais fenólicas se infiltram no solo e contaminam os rios, lagos, reservatórios de água e até mesmo as plantações adjacentes. Assim, a poluição fenólica da água pode alterar a biota, causando em humanos carcinogenicidade (ACOSTA et al., 2018)

3.2.1. Fenol

Organização Mundial da Saúde (OMS) limita a concentração máxima permitida de fenóis em águas residuais é < 1 mg/L) (MOHAMMADI et al., 2020; DEHMANI et al., 2020). Na água potável, de acordo com o regulamento o limite permitido é 0,002 mg L^{-1}. A poluição por fenol é uma grande preocupação devido à sua alta persistência e caráter tóxico (XIONG et al., 2018). A contaminação em seres humanos com fenol, o sistema nervoso central será inibido e também causará danos ao fígado, rins, trato digestivo e outras doenças (HAN, 2022).

O fenol foi isolado pela primeira vez do alcatrão de hulha em 1834 pelo químico alemão Runge. É um composto aromático e combustível. À temperatura e pressão ambiente é um sólido cristalino higroscópico. Quando puro, o fenol sólido é branco, mas é principalmente colorido devido à presença de impurezas. É caracterizada por um odor pungente doce típico, medicinal ou alcatrão. O fenol é muito solúvel em álcool etílico, em éter e em vários solventes polares, bem como em hidrocarbonetos como o benzeno. Em água tem uma solubilidade limitada e comporta-se como um ácido fraco. Em solventes polares é solúvel, mas em água é limitado com 9,3 g_{fenol} $100ml_{H2O}^{-1}$. Na água tem comportamento de ácido fraco, com pKa 9,89. O peso molecular do Fenol é 94,11, temperatura de fusão: 40,9 °C, e temperatura de ebulição 181,75°C (BUSCA, 2008; OTHMER, 1999; JORDAN, 2002). Na figura 1, pode ser observada a estrutura do fenol.

Figura 1- Extrutura molecular do fenol

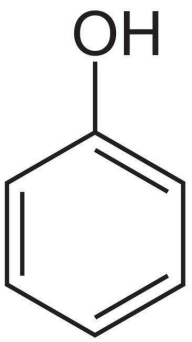

Fonte: (BUSCA, 2008)

O tratamento viável e eficiente para recuperar ou remover fenol ainda é um dos desafios mais importantes. Atualmente, alguns métodos têm sido desenvolvidos para tratar fenol como adsorção, extração, destilação, separação por membrana, oxidação química e degradação catalítica (SAID et al., 2021). Dentre esses métodos, a adsorção é considerada um dos meios mais promissores devido à sua alta eficiência, baixo custo, operação flexível e

menor poluição secundária ao meio ambiente (DEHMANI et al., 2022). Estes incluem carvão ativado, argila, materiais poliméricos, e quitina. Dentre esses materiais, se encontra o carvão ativado comercial apresenta forte afinidade com o fenol. No entanto, os carvões ativados comerciais e seu processo de regeneração são muito caros, tornando o uso desse adsorvente inviável economicamente. Por este motivo é necessário encontrar materiais adsorventes alternativos, que possam substituir e tornar o processo inteiro eficaz (DOTTO, et al. 2015)

3.3.MATERIAIS ADSORVENTES

Os materiais adsorventes mais comuns utilizados na adsorção de fenol e seus compostos são: quitosana (MOTA et al., 2012), zeolita (SYAMSIAH, 2004), e carvão ativado (FROTA, 2023). Os carvões ativados são amplamente e cada vez mais utilizados devido à extensa base de matéria-prima, vários métodos de produção, alta resistência química e térmica , bem como boa adsorção e propriedades catalíticas. A vantagem desses materiais é também a possibilidade de sua modificação abrangente (SERAFIN et al., 2022).

3.3.1. Carvão ativado

O carvão ativado é um material carbonáceo amorfo, que possui uma estrutura interna de poros bem desenvolvida, elevada área superficial e pode possuir a presença de grupos funcionais em sua superfície, que constituem os sítios ativos (VERMA et al., 2021). O carvão ativado é formado de camadas distorcidas de anéis aromáticos de átomos de carbono, que estão empilhadas de forma irregular e unidas entre si formando uma rede tridimensional, como mostra a representação da Figura 2. Os espaços ocos entre essas camadas consistem nos poros do carvão ativado (RODRÍGUEZ-REINOSO; MOLINA-SABIO, 1998).

Levando em consideração que um material para produção de CA deve ter, um elevado teor de carbono e baixo teor de material inorgânico. Os materiais precursores são os resíduos agrícolas. Principalmente sementes, caules, caroços, e cascas de frutas. Que possuem essas características, e são facilmente ativados, baixa degrabilidade e disponíveis em grandes quantidades (LÜTKE, 2019).

Segundo dados da Organização das Nações Unidas para Agricultura e Alimentação (FAO), o Brasil está entre os três maiores produtores mundiais de frutas, com uma produção aproximada de 40 milhões de toneladas por ano. Verifica-se que grande parte dessas frutas é

processada pelas indústrias de polpa e sucos, e cerca de 40% dessas matérias-primas se transformam em resíduos industriais. Desta, temos a castanha, que ultrapassou os 2,4 milhões de toneladas produzidas em 2019. Além disso, a casca representa de 10 a 15% do peso da noz inteira (ZHU, 2022; SHEN, 2023; FAO, 2019;).

O rápido crescimento econômico junto com o crescimento populacional acelerou a geração de resíduos. Agora, a geração de resíduos está se tornando uma das principais preocupações em todo o mundo com sua geração contínua em enorme quantidade. Sendo a gestão dos resíduos agrícolas uma tarefa desafiadora, com uma produção anual de cerca de 1000 milhões de toneladas (GHUO, 2018). Considerando-os como um recurso sustentável para agregação da economia circular. Alguns resíduos agroindustriais são relatados na literatura como materiais precursores para produção de CA para remoção de fenóis, como resíduos de casca de acácia negra (LÜTKE et al., 2019), casca de arroz (FU et al., 2019) e caroço de abacate (RODRIGUES et al., 2011).

3.3.2. Castanha do Pará (*Bertholletia excelsa*)

Nesse contexto, a castanha-do-Brasil (*Bertholletia excelsa*) é uma espécie arbórea de grande porte em toda a região amazônica (BALDONIA et al., 2020). A castanha-do-pará é comercializada em grandes volumes e é um dos produtos florestais não madeireiros mais importantes da América do Sul (FERREIRA et al., 2021). A castanha-do-brasil foi a terceira commodity vegetal mais extraída em 2020, onde foram produzidas mais 33 mil toneladas (IBGE, 2021). Consequentemente, grandes quantidades de cascas de castanha do Brasil são geradas. Assim, a casca da castanha-do-pará é um resíduo agrícola subvalorizado que pode potencialmente ser usado como material precursor para a produção de CA.

No Brasil, temos a Castanha-do-pará (Pará), fruto da nogueira *Bertholletia excelsa*, que tem recebido crescente interesse na última década devido aos seus potenciais efeitos positivos na saúde humana, devido ao seu rico valor nutricional (VÁSQUEZ, 2021; MASSANTINO, 2021). Popularmente conhecida como castanha-do-pará, é encontrada em toda a região amazônica, incluindo Bolívia, Peru, Colômbia, Venezuela e Guiana (BALDONI, et al. 2020). No Brasil, é produzido em Rondônia, Acre, Amazonas, Pará e Roraima (Silva Junior et al., 2017). A castanha é uma fruta importante e amplamente processada na indústria alimentícia, enquanto os resíduos da casca da castanha no processo de descascamento são grandes produzidos para serem manuseados (ZHAO, 2022). Além de fazer o tratamento

adequado pro resíduo, há uma lacuna na literatura, por poucos registros de estudos utilizando a casca de castanha do Pará, no processo de adsorção do fenol. Produzir um CA eficaz a partir desta espécie, é contribuir para o desenvolvimento da área.

3.3.3. Produção do carvão ativado

A produção de um carvão ativado é basicamente dividida em duas etapas principais: a carbonização/pirólise do material precursor e o processo de ativação (BORGES et al., 2003), conforme a figura 2.

Figura 2 - Processo de preparação do carvão ativado

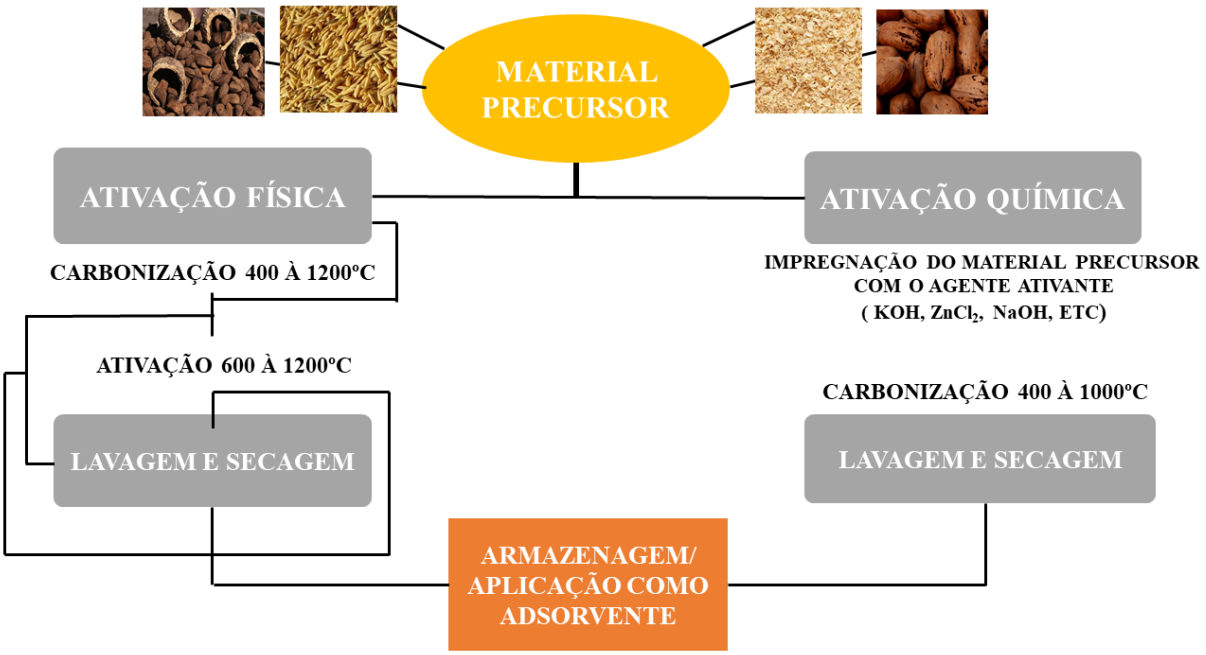

Fonte: (Adaptado de GUPTA; SUHAS, 2009)

A carbonização consiste de uma decomposição térmica do material carbonáceo, em atmosfera inerte a temperatura entre 400-1200 ºC, onde se removem componentes voláteis e gases leves como CO, H_2, CO_2, CH_4 (EL-SHEIKH et al., 2004). Produzindo uma massa de carbono fixa com uma estrutura porosa rudimentar, com poros muito finos e fechados. Segundo McDougall (1991), o objetivo da carbonização é reduzir o teor de voláteis do

material de precursor para converter resultante com mais aoromático (RODRÍGUEZ-REINOSO; MOLINA-SABIO, 1998)

O processo de ativação é uma etapa fundamental no preparo de carvões ativados, sua função principal é alterar as características do carvão para proporcionar melhores resultados através da formação de poros. O objetivo da ativação é basicamente desenvolver mais porosidade e criar algum ordenamento da estrutura que resulta em um sólido altamente poroso (GUO et al, 2009). Com a ativação do material carbonizado há a formação de mesoporos e macroporos (HERNÁNDEZ-MONTOYA, 2012). Resultando em um maior número possível de distribuição de poros, variadas formas e tamanhos, dando origem a um produto com uma alta área superficial específica (BANSAL, 2005).

A ativação pode ser tanto física quanto química. Na ativação física as moléculas se ligam fracamente ao adsorvente, não alterando suas características físicas. O material é tratado termicamente em atmosfera levemente reativas como vapor de água e gás carbônico, ocorrendo simultaneamente a ativação e carbonização, onde são liberados umidade e materiais indesejáveis como alcatrão monóxido e dióxido de carbono, hidrogênio e metano (GONÇALVES et al., 2014; MOHAMAD NOR et al., 2013).).

Na ativação química, ocorre ligações de valências livres das moléculas do adsorvente no adsorbato. Nesse processo utiliza agentes ativantes, que atuam basicamente como agentes desidratantes e oxidantes (MAHAPATRAI; RAMTEKE; PALIWAL, 2012), como ácido fosfórico (H_3PO_4), cloreto de zinco ($ZnCl_2$), hidróxidos de metais alcalinos como o hidróxido de potássio (KOH) ou hidróxido de sódio (NaOH), ou ácido sulfúrico (H_2SO_4) (FOGLER, 1998; YORGUN e YILDIZ, 2015). Além disso, no estágio final no processo de ativação química ocorre a lavagem, onde o carvão ativado é lavado basicamente que irá trazer porosidade no carvão ativado (YAHYA; AL-QODAH E NGAH, 2015).

Neste modo de ativação, os agentes de ativação, reagem iniciando o rompimento das paredes estruturais nas biomassas.

As etapas de pirólise e ativação podem ser realizadas tanto de forma conjunta como separadas. Na forma conjunta o precursor é misturado com agentes de ativação durante a pirólise. Onde que os ativadores químicos são usados em diferentes proporções, atuando de forma a desidratar, influenciando de forma direta a pirólise do precursor, evitando liberação de matéria orgânica volátil através da aromatização do esqueleto do carvão e maior fixação do carbono. Quando da utilização de ativação de forma separada, faz-se a pirólise da amostra, e

logo após é feita a impregnação com o agente escolhido a fim de obter o CA (GUO et al., 2000).

Vantagens do método de ativação após pirolise: Maior rendimento; Menor perda de agentes oxidantes; Simplicidade de ativação, utilização de temperaturas menores de ativação, inclusive para o presente trabalho onde foi utilizada temperatura ambiente. Possibilidade de variação de agente de ativação, pós pirolise.

Já a utilização do método de ativação química, pode apresentar vantagens, como por exemplo de ser conduzido em única etapa pelo emprego de temperaturas mais baixas e tempos de ativação mais curtos, para a obtenção de carvões de elevado rendimento, todavia, pode ser considerado complexo o processo de recuperação e reciclagem de alguns tipos de agentes de ativação, podendo ocorrer geração e possível descarte de líquidos contaminados, com eventual necessidade de tratamento dos efluentes (YANG et al., 2010). De forma geral, o uso de ativação química, pode gerar carvões com poros maiores, mais apropriados a aplicações em fase líquida (SAI E KRISHNAIAH, 2005).

3.4.ADSORÇÃO

A adsorção é um fenômeno físico-químico o qual está relacionado com a transferência de massa no qual as substâncias como os sólidos retem fluidos líquidos ou gasosos. Em outras palavras, o material no qual se deposita na superfície é chamado de adsorbato e a superfície é chamada de adsorvente. E o processo inverso da qual o material se desprende do substrato é chamado de dessorção (MORAES, 2022).

Pode ser classificada em adsorção química (quimissorção) e adsorção física (fisissorção). Sendo, na adsorção química a ligação envolve a troca ou partilha de elétrons entre as moléculas do adsorbato e a superfície do adsorvente, resultando em uma reação química (NASCIMENTO et al., 2020). Segundo RUTHVEN (1984), a quimiossorçao normalmente apresenta características como, formação de uma única camada sobre a superfície sólida, irreversibilidade e liberação de uma quantidade considerável de energia. Por outro lado, na adsorção física, a ligação do adsorbato à superfície do adsorvente envolve uma interação relativamente fraca que pode ser atribuída às forças de Van der Waals, ligações de hidrogênio e dipolo-dipolo (NASCIMENTO et al., 2020; SILVA, 2019; ZAZYCKI, 2019).

Figura 3 - Esquema processo de adsorção.

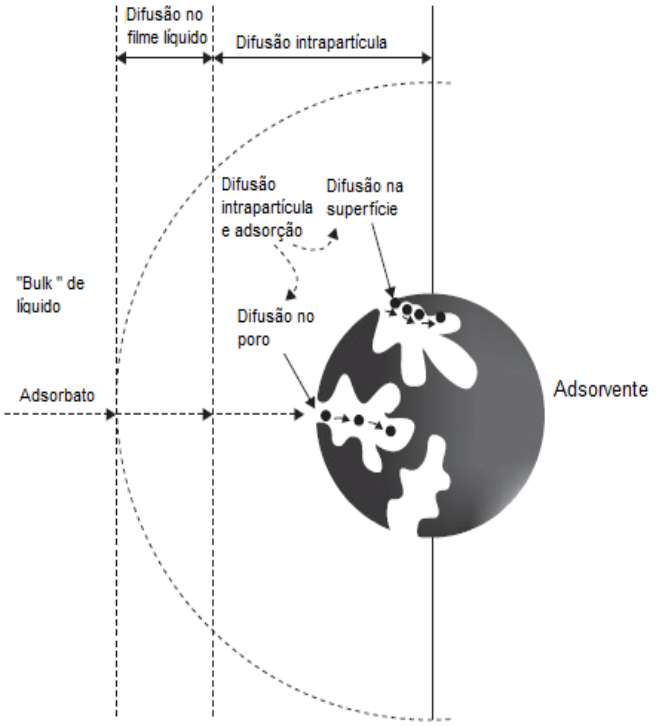

Fonte: (L.B. VALE, 2015)

De acordo com RUTHVEN (1984) na fisissorção, geralmente ocorre a deposição de mais de uma camada de adsorbato sobre a superfície do adsorvente. A adsorção é um método eficiente e de baixo custo para remoção de fenol, apresentando vantagens como baixa emissão de contaminantes secundários, baixo consumo de energia e possibilidade de uso repetido dos adsorventes (SAJID et al., 2018). Vários adsorventes estão disponíveis para a remoção de compostos fenólicos, como carbonos porosos (WANG et al., 2020), lignito (KUŚMIEREK et al., 2020), fotocatalítico (WANG et al., 2021), etc. No entanto, as matérias-primas para a produção desses adsorventes são bastante caras e geralmente levam à contaminação secundária durante os procedimentos de pré-tratamento.

3.4.1. Fatores que influenciam no processo de adsorção

A eficiência da adsorção da fase líquida e, portanto, a operação ideal do processo adsorção depende de vários parâmetros (RÁPÓ e TONK, 2021). Alguns dos fatores físico-químicos que afetam a adsorção, como a natureza do adsorvente (área superficial,

tamanho do poro, densidade, grupos funcionais presentes na superfície e hidrofobidade do adsorvente). Natureza do adsorbato (polaridade, tamanho da molécula, solubilidade) e condições operacionais (temperatura, pH e natureza do solvente) (RAZI et al., 2017; SILVA, 2019; COONEY, 1999).

Área superficial: a intensidade da adsorção é proporcional à área superficial específica, visto que a adsorção é um fenômeno de superfície. Para partículas maiores, a resistência à difusão é menor e grande parte da superfície interna da partícula não é disponibilizada para adsorção (SEKAR et al., 2004).

Parâmetros texturais: relevantes para a adsorção de contaminantes de água com grandes tamanhos moleculares. O tamanho molecular dos adsorbatos afeta a transferência de massa dentro dos mesoporos e microporos e, consequentemente, afeta a acessibilidade dos sítios de ligação disponíveis na estrutura interna do adsorvente. Ou seja, a quantidade adsorvida por unidade de massa de adsorvente é maior quanto mais finamente estiver dividido o adsorvente, e quanto mais poroso for o material (SILVA, 2005).

Tamanho dos poros: as propriedades adsortivas dependem na natureza sólida e do tamanho e distribuição do poro. Esses tamanhos podem ser classificados de acordo com a IUPAC em função do seu diâmetro (THOMMES et al, 2015):

- Macroporos: poros com diâmetros maiores que 50 nm;
- Mesoporos: poros com diâmetros entre 2 e 50 nm;
- Microporos: poros com diâmetros menores que 2 nm.

Temperatura: o efeito da temperatura sobre o sistema afeta a velocidade da adsorção, aumento de energia cinética, na mobilidade das espécies do adsorbato, ainda provocar um aumento na taxa de difusão intrapartícula do adsorbato, danificar a estrutura física do adsorvente (JIMENEZ et al., 2004; RÁPÓ e TONK, 2021. Sendo também, um fator físico-químico significativo, pois afeta o processo de tratamento, mudando a natureza da reação de endotérmica para exotérmica, ou vice-versa (YEOW et al., 2021). Altera na capacidade de adsorção, ou seja, se a capacidade de adsorção aumenta com o aumento da temperatura, então a adsorção é um processo endotérmica. Já a diminuição da capacidade de adsorção com o aumento da temperatura indica que a adsorção é um processo EXOTÉRMICO (YAGUB et al., 2014; ARGUN et al., 2008; BADAWY et al., 2020).

pH: o pH afeta a química da solução de contaminantes, alterando a atividade de grupos funcionais no adsorvente, o grau de ionização do íon adsorvido e a carga superficial do

adsorvente (KHASRI et al., 2021). A variação do pH leva à variação do grau de ionização da molécula adsorvente e das propriedades de superfície do adsorvente (NANDI et al., 2009). Um índice usado para quantificar ou definir a capacidade de uma superfície se tornar positiva ou negativamente carregada em função do pH é chamado ponto de carga zero (pH_{PZC}). A partir do pH da solução é possível determinar o ponto de carga zero e então, a carga superficial de um adsorvente. Para valores de pH inferiores ao ponto de carga zero ($pH < pH_{PZC}$) a carga superficial do adsorvente é positiva e a adsorção de ânions é favorecida; e para valores de pH superiores ao ponto de carga zero ($pH > pH_{PZC}$) a carga superficial é negativa e a adsorção de cátions é favorecida (THUE et al., 2020).

Dosagem: a quantidade de adsorvente utilizado em um processo de adsorção é um parâmetro importante, que influencia o processo através da relação quantitativa da dosagem do adsorvente e a capacidade de remoção do adsorvente para uma dada concentração inicial do poluente (SENTÜRK, 2020; RAPÓ, 2021).

Tempo de contato: fator importante, visto que, indica o comportamento cinético da adsorção de um determinado adsorvente e adsorbato. O tempo de contato ou tempo de residência, é o tempo que envolve a transferência de massa de um ou mais componentes para o adsorvente, ou seja, é o tempo necessário para atingir a concentração de remoção desejada de um poluente no processo de adsorção (NASCIMENTO et al., 2020). Um período rápido necessário para estabelecimento do equilíbrio no processo de adsorção de um poluente pode refletir a eficiência de um adsorvente. Estudos na literatura mostram que a adsorção é rápida nos estágios iniciais do período de contato e, posteriormente, mais lenta próxima ao equilíbrio. Este fato pode estar relacionado com a maior disponibilidade dos sítios de adsorção nos primeiros instantes e que nos momentos posteriores vão sendo ocupados pelas moléculas dos poluentes e com isso variando pouco a capacidade adsorção (KAVEESHWAR et al., 2018).

Concentração inicial: a capacidade de adsorção para remoção de um poluente é altamente dependente da sua concentração inicial, uma vez que, afeta indiretamente a eficiência da remoção do poluente no processo adsorção (YAGUB et al., 2014).

3.5.CINÉTICA DE ADSORÇÃO

A cinética de adsorção descreve a taxa de remoção do adsorbato na fase fluida em relação ao tempo, sendo influenciada pelas características físicas e químicas do adsorvente e adsorbato, e das condições operacionais do processo em estudo. O estudo e os cálculos dos

parâmetros cinéticos é fundamental em um processo de adsorção, visto que com isso, pode-se obter a velocidade de adsorção, o tempo necessário para remover os contaminantes, a quantidade adsorvida do adsorbato e o tempo de residência do adsorbato na interface sólido-líquido (HO e MCKAY, 1999).

Para melhor analise sobre o comportamento cinético de um processo adsortivo, e para o ajuste de curvas experimentais são utilizados modelos matemáticos. O modelo de Elovich, pseudo primeira ordem (PPO), e pseudo segunda ordem (PSO), são alguns exemplos amplamente utilizados em estudos de adsorção, com ênfase em tratamento de soluções aquosas (BONILLA-PETRICIOLET et al., 2019).

3.5.1. Modelo de Elovich

A equação de Elovich descreve a adsorção química. de diferentes espécies químicas em meio líquido, e a quimissorção em adsorventes altamente heterogêneos. (Mclintock, 1976; NASCIMENTO et al., 2014). Baseia-se no princípio em que os sítios/locais de adsorção aumentam exponencialmente, implicando em um processo de adsorção em multicamada, onde cada camada exibe uma energia de ativação diferente para quimissorção (ALBERTI et al., 2012). O modelo de Elovich está apresentado na Equação 1.

$$q_t = (\frac{1}{a})\, ln(1 + abt) \quad (1)$$

onde b é a taxa de adsorção inicial devido a dq/dt com $qt = 0$ (mg g^{-1} min^{-1}) e a é a constante de dessorção do modelo de Elovich (g mg^{-1}).

3.5.2. Modelo pseudo primeira ordem

O modelo de pseudo primeira ordem, de Largergren (1898), baseia-se na capacidade de adsorção, sendo utilizado em processos de adsorção em sistemas sólido/líquido e é representado pela Equação 2. A equação do modelo, assume que a taxa de adsorção é igual ao número de sítios de adsorção livres, e baseado em interações reversíveis (SILVA, 2019).

$$q_t = q_1(1 - e^{-k_1 t}) \quad (2)$$

onde q_t é a quantidade adsorvida no tempo t (mg g^{-1}) e q_1 é o valor teórico da capacidade de adsorção (mg g^{-1}); k_1 é a constante de velocidade de adsorção do modelo pseudo primeira ordem (min^{-1}) e t é o tempo (min).

3.5.3. Modelo pseudo segunda ordem

O modelo de pseudo segunda ordem, proposto por Ho e Mckay (1999), considera que a taxa de adsorção é diretamente relacionada ao quadrado do número de sítios livres. Sendo, a taxa de adsorção, segundo esse modelo, determinada de acordo com a Equação 3.

$$q_t = \frac{t}{(1/k_2 q_2^{\,2}) + (t/q_2)} \tag{3}$$

Onde q_2 é o valor teórico da capacidade de adsorção (mg g^{-1}), k_2 é a constante da taxa de adsorção do modelo pseudo segunda ordem (g mg^{-1} min^{-1}).

O modelo é baseado na capacidade de adsorção do adsorvente, mostrando o comportamento do processo em toda a faixa de tempo de contato. E considera que a adsorção ocorre por natureza química e além de envolver apenas o processo de difusão como no modelo de pseudo primeira ordem, também envolve o mecanismo de difusão interna (ANDIA, 2009; SKODRAS et al., 2008).

3.6.EQUILIBRIO DE ADSORÇÃO

Em sistemas de separação em que são utilizados processos adsortivos, o estudo de equilíbrio fornece informações essenciais para o tratamento. Através dele é possível estimar a capacidade de adsorção de um determinado material, além de descrever o processo revelando qual o tipo de interação existente entre o adsorvente e os contaminantes. Desta forma, se estuda a relação entre a quantidade adsorvida no tempo de equilíbrio (q_e) em diferentes concentrações do adsorvato e sua concentração da fase fluida no equilíbrio (C_e) a uma dada temperatura, obtendo-se a chamada Isoterma de Equilíbrio de Adsorção (NASCIMENTO et al. 2014).

Existem diversos tipos de isotermas, a depender do sistema estudado podem apresentar diferentes formas, isso irá depender da interação adsorvato e adsorvente. Desta

forma para os estudos de sistemas gás-sólido, é utilizada a classificação apresentada pela International Union of Pure And Applied Chemistry (IUPAC), que diferenciam as isotermas em seis diferentes tipos mostrados na Figura 4.

Figura 4 – Tipos de isotermas de acordo com a IUPAC.

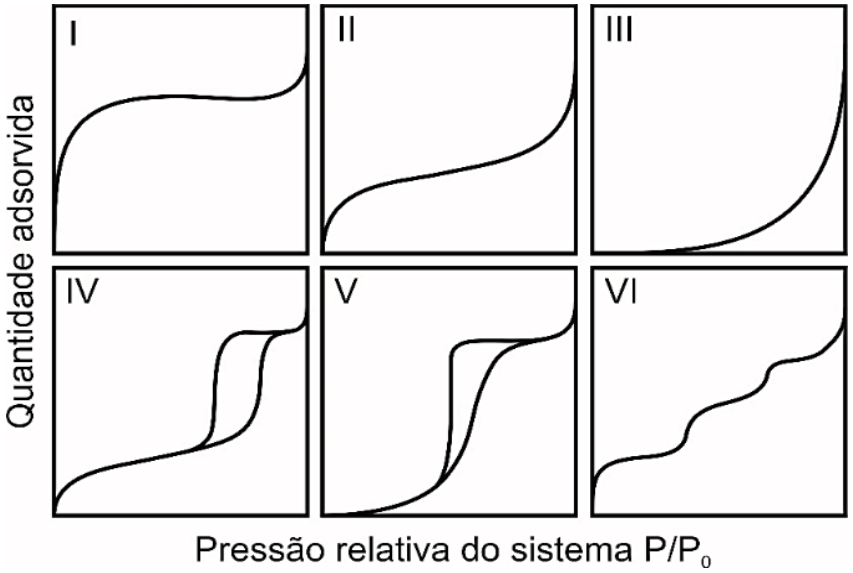

Fonte: Araújo et al. (2018)

O formato de cada isoterma da Figura 4 indica mecanismos de equilíbrio distintos. A curva do tipo I é comumente obtida quando é utilizado materiais sólidos microporosos com área externa pequena (maioria dos carvões ativados e peneiras moleculares). Sendo o processo governado pelo acesso ao volume dos poros. A curva tipo II (também conhecida por curva BET (Braunauer, Emmett e Teller)) é obtida quando são utilizados materiais não porosos ou macro porosos. No início da faixa linear dessa curva indica que já houve a formação da monocamada e as seguintes camadas começaram a ser formadas. A tipo III raramente é encontrada, ela indica que há uma fraca interação entre adsorvente-adsorvato e ocorre em sólidos não porosos. As curvas que apresentam o fenômeno de histerese (IV e V) também são raras de se encontrar. A histerese na IV estar relacionada a condensação capilar dentro de materiais com grandes quantidades de mesoporos. Já a histerese da V está relacionada a fraca interação adsorvato- adsorvente em adsorventes porosos. E por último a isoterma do tipo VI indica a formação de multicamadas em adsorventes homogêneos. Cada degrau está

relacionado a formação de uma camada (MYERS, 1999; RUTHVEN, 1985 Apud CANTELI, 2018).

O estudo das isotermas de equilíbrio é de fundamental importância para avaliar a eficiência de um adsorvente, como sua capacidade máxima de adsorção, por meio dos dados de equilíbrio, conhecidos como isotermas de adsorção. A partir das isotermas de adsorção é possível estabelecer uma relação de equilíbrio entre a concentração do adsorbato na fase fluida e a concentração do adsorbato na superfície do adsorvente em uma dada temperatura (PICCIN et al., 2017; SILVA, 2019). Fornecendo informações sobre o mecanismo de adsorção e sua forma, e podem apresentar diferentes comportamentos típicos, como mostrado na Figura 5.

Figura 5 – Formas típicas de isotermas de adsorção.

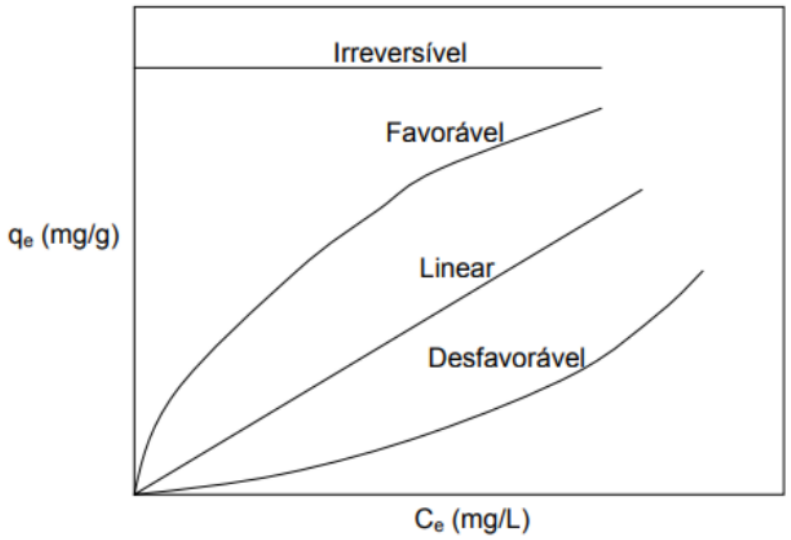

Fonte: (ALVES, 2007).

De acordo com MOREIRA, 2008, abaixo da-se significado as formas de isotermas:

- Isoterma irreversível: a massa de adsorbato retida por unidade de massa do adsorvente independe da concentração de equilíbrio do adsorbato na fase líquida;

-Isoterma favorável: massa do adsorbato retida por unidade de massa do adsorvente é alta para uma baixa concentração de equilíbrio do adsorbato na fase líquida;

-Isoterma linear: a massa de adsorbato retida por unidade de massa do adsorvente é proporcional à concentração de equilíbrio do adsorbato na fase líquida;

-Isoterma desfavorável: a massa de adsorbato retida por unidade de massa do adsorvente é baixa, mesmo para uma alta concentração de equilíbrio do adsorbato na fase líquida.

As isotermas de adsorção são construídas a partir de dados experimentais e podem assumir variadas formas em um gráfico, onde relaciona a capacidade de adsorção (q_e) e a concentração final do adsorbato (C_e), medidas quando o sistema adsortivo atinge o equilíbrio. Dessa forma, a forma da curva de equilíbrio ajuda a explicar certos fenômenos associados à interação entre o adsorbato e o adsorvente. (PICCIN et al., 2017)

Segundo GILES et al (1974) os tipos de isotermas podem ser divididas entre classes (S, L, H, C) e subclasses (1, 2, 3, 4), nesta classificação, as curvas de equilíbrio são identificadas de acordo com à inclinação inicial em quatro classes principais, e os subgrupos são descritos para cada classe, com base nas formas das partes superiores e mudanças de inclinação. A Figura 6 mostra a classificação proposta por GILES et al. (1974).

Figura 6 - Classificação das isotermas de adsorção

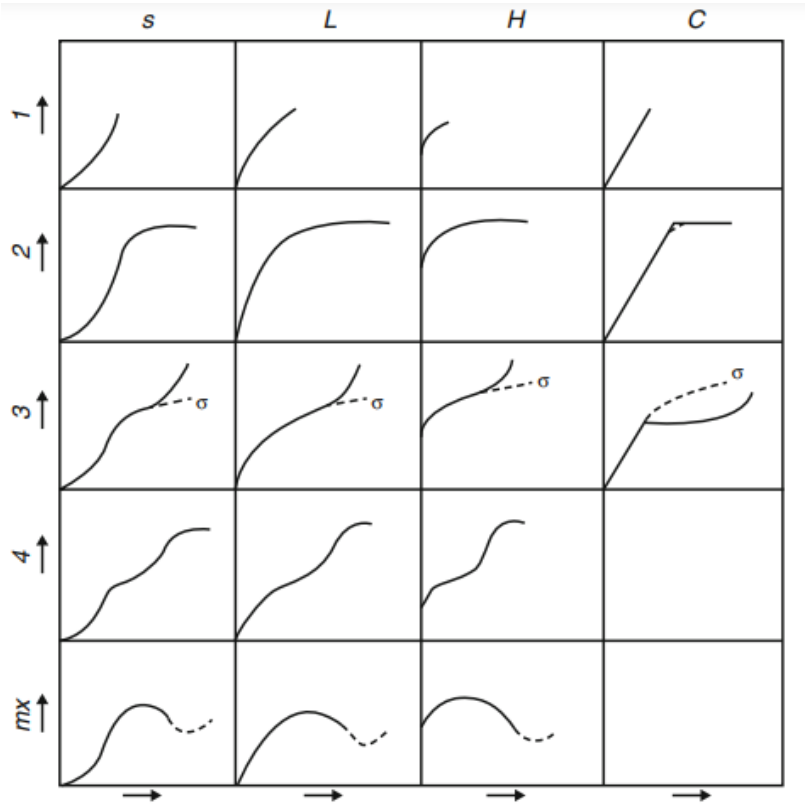

Fonte: (GILES et al. 1974).

Na literatura diversos modelos matemáticos de isotermas de adsorção foram propostos para ajustar e descrever dados de equilíbrio de adsorção, como os modelos de Freundlich, Langmuir e Sips (GILES, et al. 1974

3.6.1. Isoterma de Freundlich

O modelo de Freundlich considera o sólido heterogêneo, aplica uma distribuição exponencial para caracterizar os vários tipos de sítios de adsorção, os quais possuem diferentes energias adsortivas, podendo ser representado pela Equação 4 (FREUNDLICH, 1906).

$$q_e = k_F C_e^{1/nF} \tag{4}$$

Onde, k_F é a constante de Freundlich ((mg g^{-1}) (L $mg^{-1})^{1/n}$), 1/n é o fator de heterogeneidade.

Sendo assim, a isoterma de Freundlich assume que a adsorção ocorre em uma superfície, e a quantidade que é adsorvida aumenta infinitamente com o aumento da concentração (FREUNDLICH, 1906). Além disso, assume, que os sítios com ligação mais forte são ocupados primeiro e que a força de ligação diminui com o aumento do grau de ocupação do sítio, ou seja, prevendo a existência de multicamadas (COLPANI, 2012).

3.6.2. Isoterma de Langmuir

O modelo de isoterma de Langmuir desenvolvido em 1918, foi proposto para explicar a quimissorção com a formação de uma monocamada, e embora apresentem também resultados satisfatórios em dados de adsorção física, demostrado na equação 5. Sendo este um modelo teórico, apresentando os sítios ativos com mesma atividade. E considera que não ocorre interação entre moléculas adsorvidas (NASCIMENTO et al. 2014):

$$q_e = \frac{q_m k_L C_e}{1 + k_L C_e} \tag{5}$$

Em que q_e (mg g^{-1}) representa a quantidade adsorvida na fase sólida, *Ce* (mg L^{-1}) é a concentração na fase líquida no equilíbrio, q_m (mg g^{-1}) a máxima capacidade de cobertura da monocamada, e o K_L (L g^{-1}) parâmetro de afinidade entre o adsorvato e o material.

3.6.3. Isoterma de Sips

O modelo de isoterma de Sips é representado na Equação 6, o modelo representa uma combinação da isoterma de Langmuir e de Freundlich em que, em concentrações baixas, a adsorção reduz-se à isoterma de Freundlich e, em altas concentrações de adsorbato, prevê uma capacidade de adsorção em monocamada, característica da isoterma de Langmuir (SIPS, 1948).

$$q_e = \frac{q_s (k_s C_e)^{m_S}}{1 + (k_s C_e)^{m_S}} \tag{6}$$

onde, k_S é a constante de Sips (L mg^{-1}), q_s é a capacidade máxima de adsorção (mg g^{-1}) e $m_{s\,é}$ a constante exponencial do modelo de Sips.

O modelo de Sips foi desenvolvido para reconhecer e resolver o problema do aumento contínuo da quantidade adsorvida quando a concentração aumenta, o que geralmente é experimentado no modelo de isotermas de Freundlich (SIPS, 1948).

3.7.TERMODINÂMICA

Estimar os parâmetros termodinâmicos de adsorção é fundamental, visto que, fornece informações importantes sobre o processo de adsorção, como a influência da temperatura, características do processo e os mecanismos associados a adsorção (ZAZYCLI, 2019).

Os parâmetros termodinâmicos de adsorção, são a variação da energia livre de Gibbs padrão (ΔG°), variação da entalpia padrão (ΔH°) e variação da entropia padrão (ΔS°). Os valores obtidos no cálculo desses parâmetros indicam a viabilidade do uso de qualquer material como adsorvente, pois revelam se o processo de adsorção é espontâneo, se seu caráter é endotérmico ou exotérmico e avalia o seu grau de desordem (SILVA, 2019; ZAZYCKI, 2019).

A energia livre de Gibbs padrão, pode ser calculada conforme a Equação 7, este parâmetro está relacionado com a espontaneidade do processo de adsorção. Se ΔG° for negativa, o processo é espontâneo e favorável, mas se ΔG° for positiva, o processo é desfavorável e não espontâneo (TRAN et al., 2021)

$$\Delta G^{o} = \Delta H^{o} - T\Delta S^{o} \quad (7)$$

A variação de entalpia indica se o processo de adsorção é exotérmico ou endotérmico. Valores negativos de ΔHº indica que o processo é exotérmico e valores positivos de ΔHº indica que o processo é endotérmico. Além disso, a variação da entalpia está relacionada com a natureza do processo, indicando se a adsorção é física ou química (TRAN et al., 2021). Já variação da entropia (ΔS°) mede o grau de desordem das partículas do sistema no processo (WANG et al., 2019). A variação da entalpia e entropia podem ser estimadas pela equação de Vant´t Hoff (Equações 7, 8 e 9) (LIMA et al., 2019; TRAN et al., 2021; WANG et al., 2019).

$$ln(K_D) = \frac{\Delta S^{o}}{R} - \frac{\Delta H^{o}}{RT} \quad (8)$$

$$K_D = \frac{(1000.K_{s.}.\text{molecular weight of adsorbato}).[\text{adsorbate}]^{\circ}}{\gamma} \quad (9)$$

Onde, K_D é a constante de equilíbrio, R é a constante universal dos gases (8,314 J/mol K), T é a temperatura, K_s é constante do melhor modelo isotérmico ajustado e γ é o coeficiente de atividade.

A partir da Equação 8 é possível construir um gráfico lnK_D em função de 1/T, com os dados experimentais da temperatura e da constante de equilíbrio. Os valores de ΔHº e ΔS° são obtidos a partir da equação da reta do gráfico onde o coeficiente angular representa o valor de ΔHº e o coeficiente linear o valor de ΔS° (SILVA, 2019).

3.8.REGENERAÇÃO

Durante o processo de adsorção, os sítios ativos do sólido adsorvente são ocupados pelo adsorvato, fazendo com que a cada ciclo que o sólido é utilizado mais sítios sejam ocupados, isso ocasiona, a cada vez, uma menor eficiência do processo, até alcançar o estágio do saturamento do sólido, ou seja, o sólido não possui mais capacidade de adsorver e três caminhos devem ser seguidos: a incineração do sólido, a sua disposição em aterros sanitários

ou a sua regeneração, sendo que os dois primeiros são a substituição do sólido saturado por uma nova massa de adsorvente (BORTOLON, 2022).

O objetivo do processo de regeneração é fazer com que a capacidade de adsorção do sólido seja recuperada para sua posterior reutilização, permitindo a realização de um número finito de ciclos de adsorção-regeneração sem causar danos na superfície do adsorvente e perda de massa. Para que seja utilizado o método de regeneração é preciso que ele seja eficiente e barato para que o processo se torne economicamente viável e menos poluente ao meio ambiente quando comparado ao descarte do carvão ativado saturado de poluente (BORTOLON, 2022).

Na regeneração por dessorção o objetivo é apenas a transferência dos compostos adsorvidos, a adsorção é reversível, ou seja, o adsorvato acumulado no sólido pode ser dessorvido, liberando os sítios do carvão. Este método tem como vantagem a facilidade e rapidez do processo, a alta eficiência de regeneração do CA e a possível recuperação de compostos de interesse (BORTOLON, 2022).

Alguns estudos mostraram que os álcoois como etanol e metanol foram capazes de dessorver fenol para um alto grau (MATHEICKAL, 1998; MARTIN, 1984; CHIANG, 1997). Verificou-se que o metanol era vantajoso como uma solução regenerante para carvão ativado carregado por fenol (COONEY, 1983) por ter alta eficiência de regeneração, poderia ser recuperado e é facilmente lavado com água. No entanto, o metanol traz preocupações com a saúde, devido à formação de formaldeído se digerido, o que representa uma das principais desvantagens para sua aplicação no tratamento em soluções aquosas. Como alternativa, o etanol teve um desempenho semelhante ao metanol como regenerante e tem potencial muito menos toxicidade do que o metanol (LASARATI, 2020).

4. RESULTADOS E DISCUSSÕES

Os resultados obtidos neste estudo, juntamente com a discussão estão apresentados na forma de dois artigos científicos, um já publicado e outro submetido a avaliação. O ARTIGO 1 está aceito na revista Chemical Engineering Research and Design (ISSN: 0263-8762) com fator de impacto 4.119, classificada com Qualis A1 na área Engenharias II. Já o ARTIGO 2 foi submetido, a revista Environmental Science And Pollution Research International (ISSN: 0944-1344) com fator de impacto 5.190, classificada com Qualis A2 na área Engenharia II.

ARTIGO 1 - **KOH activated carbons from Brazil nut shell: preparation, characterization, and their application in phenol adsorption**

Maria C. F. da Silva[1], Sabrina F. Lütke[1], Victoria X. Nascimento[1], Éder. C. Lima[2], Guilherme L. Dotto[1*]

[1]Research Group on Adsorptive and Catalytic Process Engineering (ENGEPAC), Federal University of Santa Maria, Av. Roraima, 1000-7, 97105–900 Santa Maria, RS, Brazil

[2]Institute of Chemistry, Federal University of Rio Grande do Sul–UFRGS, Av. Bento Gonçalves 9500, P.O. Box 15003, 91501-970, Porto Alegre, RS, Brazil

*Corresponding author: Research Group on Adsorptive and Catalytic Process Engineering (ENGEPAC), Federal University of Santa Maria, Av. Roraima, 1000-7, 97105–900 Santa Maria, RS, Brazil. Email: guilherme_dotto@yahoo.com.br

Abstract

Activated carbons, named AC105 and AC11 were prepared from Brazil nut shell using the weight ratios of Brazil nut shell: KOH of 1:0.0 and 1:1, respectively. The prepared materials were characterized using different techniques and applied to remove the phenol from aqueous solution through the adsorption process. The characterization data showed that both materials presented similar properties, with AC11 exhibiting a slightly higher specific surface area (332.228 $m^2 g^{-1}$) than AC105 (314.335 $m^2 g^{-1}$). The kinetic study showed that AC11 reached the process equilibrium faster than AC105, and the Elovich model was best suited to the kinetic data for both adsorbents. The equilibrium data followed the Sips model, and the maximum adsorption capacities were 55.16 and 68.52 mg g^{-1} for AC105 and AC11, respectively. The application of the materials in the treatment of a simulated industrial effluent showed the removal efficiencies of 28.05% and 48.20% for AC105 and AC11, respectively. Therefore, through the adsorption results, AC11 proved to be more efficient towards phenol removal and is a promising alternative for the treatment of wastewaters containing this contaminant.

Keywords: Adsorption; Activated carbon; Chemical activation; Kinetic and isotherm models; Phenol; Simulated effluent

1. Introduction

Phenol is widely used in petrochemicals, pharmaceuticals, refineries, coal conversion, wood products, polymers, paint, pesticides, and paper industries. Wastewaters generated by these industries can contain high concentrations of phenol, with the petrochemical and coal conversion industries showing the highest concentrations (200−7000 mg L−1). (Franco et al. 2021). The discharge of wastewaters containing phenol can cause serious environmental and

human health problems. In aquatic organisms, phenol can cause the mortality of several species, inhibit bioluminescence, and affect algae growth, among other effects (Duan et al. 2018). In humans, phenol exposure can cause skin and eye burning, dyspnea, coughing, cyanosis, lung edema, affect the central nervous system, and can intensely damage inner organs including kidneys, liver, spleen, lungs, and heart (Mohammadi et al. 2015). Therefore, there are some limits concerning the presence of phenol in wastewaters. In Brazil, for example, the National Environment Council (CONAMA) established that the phenol concentration in wastewaters must be low as 0.5 mg L^{-1} (CONAMA 2005). Therefore, wastewaters containing phenol must be decontaminated before being discharged into the environment.

Several techniques are used for the treatment of wastewaters containing phenol such as oxidation (Hussain et al. 2013), membrane separation (Raza et al. 2019), reverse osmosis (Al-Obaidi et al. 2017), photocatalytic degradation (Turki et al. 2015), biological removal (Pradeep et al. 2015), and adsorption (Franco et al. 2021). Among these techniques, adsorption stands out due to its high efficiency and simplicity (Ahmaruzzaman 2008). Activated carbon (AC) is one of the adsorbent materials most used by the industry (Kumar et al. 2019). The AC preparation, especially the activation step, has a strong influence on its textural properties and, consequently, on its adsorption efficiency (Wei et al. 2018). The activation step can be carried out by chemical (Yahya et al. 2015), physical (Alvarez et al. 2015), or physicochemical (Prauchner et al. 2016) methods. In chemical activation, potassium hydroxide (KOH), zinc chloride ($ZnCl_2$), and phosphoric acid (H_3PO_4) are the most commonly used activating agents (Kalderis et al., 2008). Literature has shown that the use of KOH as activating agent can contribute to the improvement of the porous structure (Fu et al. 2019).

In addition, the use of agro-industrial wastes as precursor materials for the production of AC is a highly promising alternative, due to its low cost and high availability (Rodrigues et al. 2011). Agroindustrial wastes are generated in large volumes, and their management is crucial to environmental development (Georgin et al. 2018). Some agro-industrial wastes are reported in the literature as precursor materials for AC production for phenol removal such as black wattle bark waste (Lütke et al. 2019), rice husk (Fu et al. 2019), and avocado kernel seed (Rodrigues et al. 2011). In this context, Brazil nut (*Bertholletia excelsa*) is a large tree species, that occurs throughout the Amazon region (Baldonia et al. 2020). Brazil nut is traded in high volumes and is one of the most important non-timber forest products in South America (Ferreira et al. 2021). According to the Brazilian Institute of Geography and Statistics (IBGE), Brazil nut was the third most extracted vegetable commodity in 2020 (33,1 thousand tons were produced) (IBGE, 2021). Consequently, high amounts of Brazil nut shells are generated. Thus, Brazil nut shell is an undervalued agricultural waste, which has great potential to be used as a precursor material for the AC production.

Therefore, this work aimed to prepare ACs from Brazil nut shell, characterize them, and applied them in phenol adsorption from aqueous solution. The ACs were prepared by chemical activation using different KOH weight ratios. Different characterization techniques, such as N_2 adsorption/desorption isotherms, FTIR, XRD, MEV, and TGA were employed to verify the structural differences due to the different KOH weight ratios. The batch adsorption studies considered the kinetic and equilibrium modeling, the possibility of regeneration and reuse of the material, and the efficiency of removing phenolic compounds in a simulated industrial effluent.

2. Material and methods

2.1. Material

Brazil nut shell (*Bertholletia excelsa*) was obtained from the local market. Phenol (94.11 g mol^{-1}, purity of 99.5%) was acquired from Neon (Brazil). A 1000 mg L^{-1} phenol stock solution was prepared and stored in amber bottle, without any pH adjustment. The working solutions at the desired concentrations were prepared by diluting the stock solution with distilled water. All other reagents used in the experiments were of analytical grade

2.2. Preparation of the activated carbons

Two activated carbons, denominated as AC105 and AC11, were prepared with the weight ratios of Brazil nut shell: KOH of 1:0.5 and 1:1, respectively. For preparing CA105, 100.0 g of Brazil nut shell was mixed with 50.0 g of KOH and 50 mL of distilled water. The mixture was stirred with a magnetic stirrer at 90 °C for 2 h, allowing the formation of a homogeneous paste. The obtained paste was oven-dried at 105 °C for 8 h. Then, the dry paste was introduced in a quartz reactor in a conventional furnace (Sanchis, Brazil). The heating procedure was carried out by heating the sample from room temperature until a final temperature of 600 °C at a heating rate of 10 °C min^{-1}. A N_2 flow rate of 150 mL min^{-1} was used. The temperature was kept fixed at 600 °C for 30 min and, after this time, the system was cooled down, still under N_2 atmosphere, until it attains a temperature bellow 200 °C. Upon reaching this temperature, the N_2 flow was interrupted. To remove the inorganics, the pyrolysed material was washed with a 0.1 mol L^{-1} HCl solution (10 mL per gram of pyrolysed

material). The washing was carried out under a reflux system at 80 ºC for 2 h. Subsequently, the material was exhaustively washed with distilled water until the pH of the washing waters attains 7. Finally, the material was oven-dried at 105 °C for 8 h. For preparing CA11, the procedure described above was repeated using 100 g of KOH.

2.3. Characterization of the activated carbons

The textural properties of the produced activated carbons were determined based on nitrogen adsorption/desorption isotherms at 77 K using a volumetric adsorption analyzer (Micromeritcs, ASAP 2020, USA). The Brunauer-Emmett-Teller (BET) method was used to calculate the specific surface area and the Barrett-Joyner-Halenda (BJH) was used to obtain the total pore volume and the average pore size.

Scanning electron microscopy (SEM) (Tescan, MIRA 3, Czech Republic) was used to study surface morphologies of the materials. The SEM images were obtained with a working voltage of 12 kV and magnification of 10000×.

Powder X-ray diffraction (XRD) (Rigaku, Miniflex 300, Japan) analysis was carried out in the following conditions: power source with 30 kV and 10 mA with Cu Kα radiation (λ = 1.54051 Å), Step mode with Scan speed of 0.5 s e Scan step of 0.03°, at angles from 5 to 100°.

Thermogravimetric analysis (TGA) were obtained on a TA instrument (Netzsch, STA 449 F3 Jupiter®, Germany) with a heating rate of 25 °C min^{-1} and N_2 flow rate of 50 mL min^{-1}. Temperature was varied from 20 to 800 °C.

Fourier transform infrared spectroscopy (FTIR) (Shimadzu, Prestige 21210045, Japan) spectra were obtained with a resolution of 4 cm^{-1} in the range from 4000 to 400 cm^{-1}. Diffuse reflectance technique was used, in which the samples were previously dispersed in KBr.

2.4. Phenol adsorption assays

Phenol adsorption kinetic curves were obtained with an initial phenol concentration of 50 mg L^{-1}. 20 mL of the phenol solution were added in Erlenmeyer flasks with 0.02 g of the activated carbon (adsorbent dosage of 1.0 g L^{-1}). The flasks were stirred in a thermostatic agitator (Solab, SL222, Brazil) at 25 °C and stirring rate of 150 rpm for different contact times (0–480 min). The equilibrium curves were obtained with initial phenol concentrations of 25, 50, 75, 100, 125, 150 e 200 mg L^{-1}. The other experimental conditions were the same ones used in the kinetics experiments, except that the flasks were kept under stirring until the system reached equilibrium. For both kinetic and equilibrium experiments, the pH of the phenol solution was 6.9. This pH value is characteristic of the aqueous phenol solution.

After the adsorption experiments, the adsorbent was separated from the liquid phase by centrifugation (LGI Scientific, LGI–DLC–802B, Brazil). The remaining phenol concentration in the liquid phase was measured by UV–vis spectrophometer (Shimadzu, UVmini–1240, Japan) at the maximum wavelength of the phenol molecule (λ_{max} = 270 nm). All assays were conducted in replicate (n = 3) and blank tests were also realized. The adsorption capacity at time t (q_t) and the equilibrium adsorption capacity (q_e) were determined by Eq. (1) and (2), respectively:

$$q_t = \frac{V(C_0 - C_t)}{m} \tag{1}$$

$$q_e = \frac{V(C_0 - C_e)}{m} \tag{2}$$

where C_0 is the initial phenol concentration (mg L^{-1}), C_t is the phenol concentration in liquid phase at time t (mg L^{-1}), C_e is the equilibrium phenol concentration in liquid phase (mg L^{-1}), m is the adsorbent mass (g), and V is the volume of the solution (L).

2.5. Kinetic and equilibrium models and regression analysis

The kinetic data were adjusted to the pseudo-first order (PFO), pseudo-second order (PSO), and Elovich models (Ho and McKay 1998). Eq. (3), (4), and (5) show, respectively, the mathematical expression of these models:

$$q_t = q_1(1 - exp(-k_1 t)) \tag{3}$$

$$q_t = \frac{t}{(1/k_2 q_2^{\,2}) + (t/q_2)} \tag{4}$$

$$q_t = \frac{1}{a} ln(1 + abt) \tag{5}$$

where q_t is the adsorption capacity at time t (mg g^{-1}), q_1 is the adsorption capacity predicted by the pseudo-first model (mg g^{-1}), q_2 is the adsorption capacity predicted by the pseudo-second model (mg g^{-1}), k_1 is the pseudo-first order rate constant (min^{-1}), k_2 is the pseudo-second order rate constant (g mg^{-1} min^{-1}), a is the initial sorption rate of the Elovich model (mg g^{-1} min^{-1}), and b is the constant related to the extent of surface coverage and activation energy for chemisorption of the Elovich model (g mg^{-1}).

Langmuir (Langmuir 1918), Freundlich (Freundlich 1907), and Sips (Sips 1948) models were used for the analysis of the equilibrium data. Eq. (6), (7), and (8) show, respectively, the mathematical expression of these models:

$$q_e = \frac{q_m k_L C_e}{1 + k_L C_e} \tag{6}$$

$$q_e = k_F C_e^{1/nF} \tag{7}$$

$$q_e = \frac{q_s (k_s C_e)^m}{1 + (k_s C_e)^m} \tag{8}$$

where q_e is equilibrium adsorption capacity (mg g^{-1}), Ce is the equilibrium phenol concentration in liquid phase (mg L^{-1}), q_m is the maximum adsorption capacity of the Langmuir model (mg g^{-1}), K_L is the Langmuir equilibrium constant (L mg^{-1}), K_F is the Freundlich equilibrium constant ((mg g^{-1}) (mg $L^{-1})^{-1/nF}$), $1/nF$ is the heterogeneity factor, q_s is the maximum adsorption capacity of the Sips model (mg g^{-1}), k_S is the Sips equilibrium constant (L mg^{-1}), and m the exponent of the Sips model.

The estimation of the parameters of the models was done through nonlinear regression using the Quasi-Newton estimation method. Statistica 7.0 software (Statsoft, USA) was used in the calculations. The fit quality was evaluated by determination coefficient (R^2), adjusted determination coefficient (R^2_{adj}), and average relative error (ARE).

2.6. Regeneration and reuse experiments

To evaluate the possibility of reusing the produced activated carbons, regeneration tests were carried out. First, the activated carbons were loaded with phenol using a 50 mg L^{-1} solution under the same experimental conditions described in section 2.4. After, the adsorbent was separated from the medium by centrifugation and oven-dried at 105 °C for 8 h. In the regeneration step, thermic and chemical regeneration were tested. The thermic regeneration was conducted in a muffle furnace (Quimis, Q.318.24, Brazil) at a temperature of 200 °C for 4 h. For chemical regeneration tests, two different regeneration agents, sodium hydroxide (0.5 mol L^{-1}) and ethanol (purity of 99.8%) were tested. A volume of 20 mL of the regeneration agents were added in Erlenmeyer flasks with the activated carbon previously loaded with phenol and the flasks were stirred for 4 h at 25 °C and stirring rate of 150 rpm. Then, the regenerated adsorbent was separated from the medium by centrifugation (LGI Scientific, LGI–DLC–802B, Brazil) and oven-dried at 105 °C for 8 h. Thereafter, the regenerated

activated carbon were used again for phenol adsorption. This adsorption-regeneration cycle was realized several times.

2.7. Test in a simulated effluent

The efficiency of the produced activated carbons of removing a mixture of phenolic compound from a simulated effluent containing high concentration of salts was tested. The simulated effluent was prepared according Thue et al. (2016) as follows: phenol (60 mg L^{-1}), 2-chlorophenol (10 mg L^{-1}), bisphenol A (10 mg L^{-1}), 2-nitrophenol (10 mg L^{-1}), 4-nitrophenol (10 mg L^{-1}), 2-naphtol (10 mg L^{-1}), hydroquinone (10 mg L^{-1}), resorcinol (10 mg L^{-1}), sodium sulphate (40 mg L^{-1}), sodium carbonate (40 mg L^{-1}), sodium chloride (40 mg L^{-1}) and sodium phosfate (40 mg L^{-1}). The pH of the prepared simulated effluent was 9.0. The experiments were realized with 20 mL of the simulated effluent, temperature of 25 °C and stirring rate of 150 rpm. The adsorbent was added in the dosages of 1.0, 5.0 and 10.0 g L^{-1}. UV–vis absorption spectra of the simulated effluent before and after the adsorption were obtained from 200 to 400 nm (Shimadzu, UV240, Japan). The areas under the absorption bands were used to calculate the removal efficiency.

3. Results and discussion

3.1. Characterization results

3.1.1. Morphological characteristics

Fig. 1 shows the SEM images of AC105 and AC11 with magnifications of 10000×. Both activated carbons showed an irregular and rough surface, with the presence of some grains. The presence of round-shaped cavities was also observed for both materials. It is

possible to observe that AC11 (Fig. 1 (b)) has a rougher surface and a higher quantity of cavities than AC105 (Fig. 1 (a)). Such cavities make it easier for the adsorbate molecules to access the pores, contributing to the adsorption efficiency.

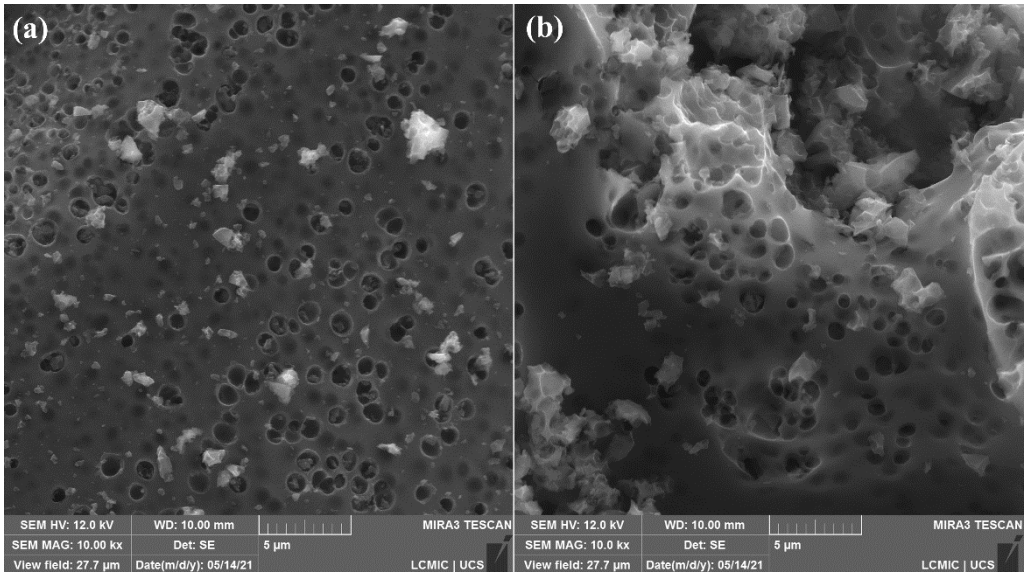

Fig. 1 SEM images of (a) AC105 and (b) AC11.

3.1.2. Textural properties

Fig. 2 shows the N_2 adsorption/desorption isotherms and the pore size distributions for AC105 and AC11. According to the International Union of Pure and Applied Chemistry (IUPAC) classification of adsorption isotherms, both materials exhibited the same isothermal profile, classified as Type IV, accompanied by hysteresis Type H4 (Thommes et al. 2015). Type IV isotherm is a typical characteristic of mesoporous materials. Type H4 hysteresis is frequently associated with narrow slit-shaped pores (Thommes et al. 2015).

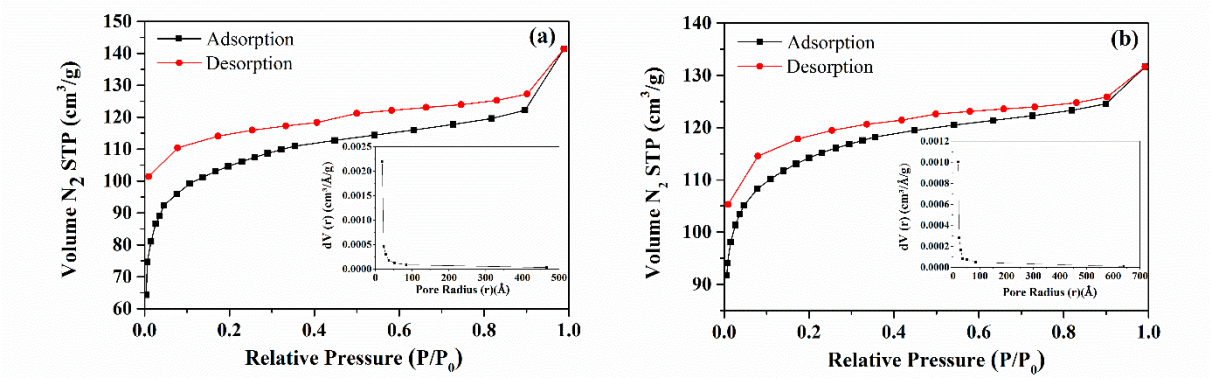

Fig. 2 Nitrogen adsorption/desorption isotherms and the BJH desorption pore size distribution of (a) AC105 and (b) AC11.

Table 1 exhibits the specific surface area (S_{BET}), total pore volume, and average pore size obtained for both materials. According to the literature, in the KOH activation, the activation agent penetrates the pore structure of the carbonaceous precursor material and is converted into other materials, such as K_2O, K_2CO_3, and metallic K. However, the formation of metallic K only occurs if the activation temperature exceeded 700 °C, which did not occur in the present study (pyrolysis temperature was of 600 °C). Therefore, the reactions between the various K compounds with the carbonaceous precursor material can be responsible for generating the pore structure. After the reaction ends, these residual K compounds are removed by washing to obtain abundant pores (Chiang and Juang 2017; Wang et al. 2020). Therefore, it is expected that the increase in the KOH weight ratio to contribute to the increase in the specific surface area, as found by different authors (Muniandy et al. 2014; Singh et al. 2019; Wang et al. 2020). However, in this work AC11 presented a slightly higher BET surface area, even though it was prepared with twice the KOH weight ratio than AC105.

Similarly, the average pore size did not change, regardless of the KOH weight ratio used (Table 1). According to the literature, the increase in the KOH weight ratio leads to a decrease in the pore size due to the collapse of larger pores and the consequent formation of smaller pores (Muniandy et al. 2014; Wang et al. 2020). However, this was not evident in the present work, which may be linked to the weight ratio range chosen.

Table 1. Textural characteristics of the activated carbons.

Activated Carbon	S_{BET} ($m^2\ g^{-1}$)	Total pore volume ($cm^3\ g^{-1}$)	Average pore size (nm)
AC105	314.335	0.044	3.655
AC11	332.228	0.020	3.692

In this work, the average pore size of both materials was around 3.6 nm. According to IUPAC, the pores can be classified as follows: (i) micropores: inner diameter < 2 nm; (ii) mesopores: 2 ≤ inner diameter ≤ 50 nm; and (iii) macropores: inner diameter > 50 nm (Thommes et al. 2015). Therefore, both activated carbons can be classified as mesoporous materials. Besides that, the average pore size presented by both activated carbons is suitable to adsorb phenol, since phenol molecules have an effective molecular diameter of 0.75 nm and can easily penetrate the adsorbent pores (Lütke et al. 2019).

3.1.3. Surface functional groups

Fourier transform infrared spectroscopy (FTIR) was used to identify the main surface functional groups of the activated carbons. The obtained spectra are shown in Fig. 3. The bands observed at 3438 cm^{-1} (AC105) and 3433 cm^{-1} (AC11) can be assigned to the stretching vibrations of O–H bonds from alcohols, phenols, or carboxyls, or even the presence of adsorbed water (Xu et al. 2014). At 1615 cm^{-1} (AC105) and 1634 cm^{-1} (AC11), it is observed the bands related to the C=O bonds of carboxylic groups (Ferreira et al., 2015). The bands at 1564 cm^{-1} (AC105) and 1559 cm^{-1} (AC11) are due to the C=C stretching vibrations of the aromatic rings of the activated carbons' structure (Duan et al. 2017). These aromatic rings result from the dehydration of the carbohydrates during pyrolysis (Machado et al. 2020). Lastly, the bands at 1058 cm^{-1} (AC105) and 1064 cm^{-1} (AC11) are due to the C–O stretching vibrations of hydroxyl in alcohols, phenols, or carboxyls (Xu et al. 2014). According to Du et

al. (2017), the functional groups O–H, C=O, and C–O result from the etching effect that KOH has on the porous carbon network during the activation process.

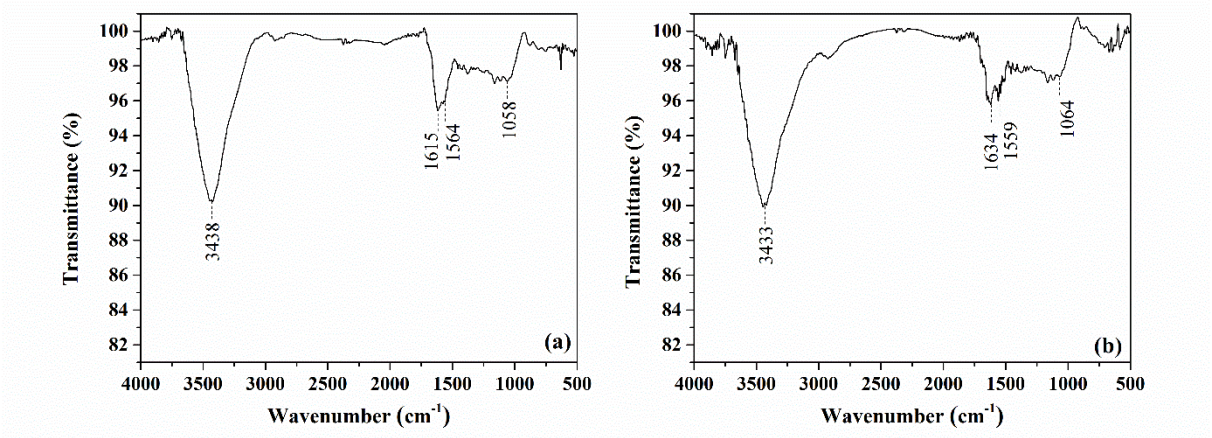

Fig. 3 FTIR vibrational spectra of (a) AC105 and (b) AC11.

3.1.4. Thermogravimetric curves

Fig 4 shows the thermogravimetric curves of the materials. Both curves can be divided into three regions. The first region was 18.13–100.63 °C (AC105) and 19.73–82.23 °C (AC11). The weight loss observed in this section corresponds to the evaporation of moisture from the samples (Thue et al. 2020). The second stage was 100.63–590.63 °C (AC105) and 82.23–599.73 °C (AC11). This stage can be attributed to the loss of water in the interstices of the carbon matrix (Thue et al. 2020). The third stage corresponds to the decomposition of the carbon matrix (Thue et al. 2020). The temperature range for this third region of weight loss was 590.63 (AC105) and 599.73 °C (AC11) to 800.00 °C. The total weight loss was 21.79% and 20.51% for AC105 and AC11, respectively.

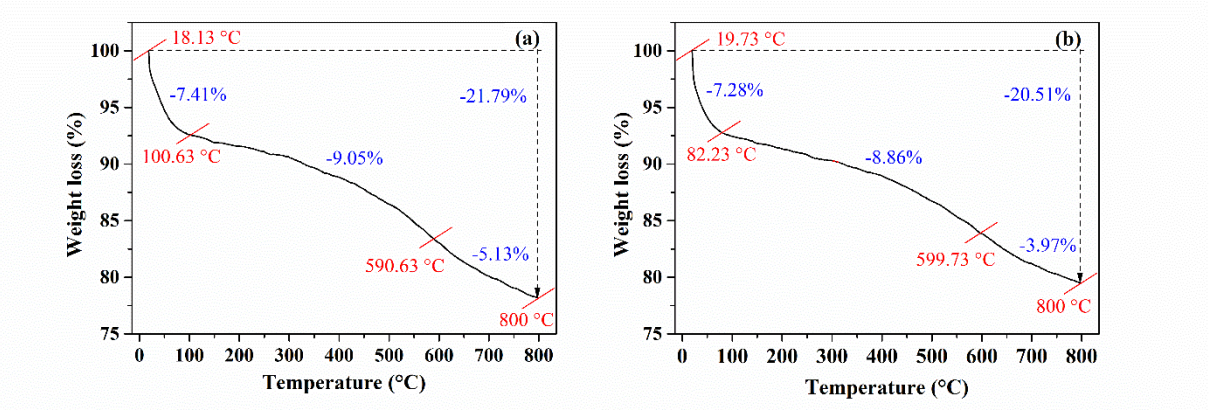

Fig. 4 TGA curves of (a) AC105 and (b) AC11

3.1.5. X–ray diffraction

Fig. 5 shows the XRD diffractograms obtained for AC105 and AC11. Two very broad reflection peaks can be observed at approximately 2θ = 25° and 2θ = 45° for both materials.

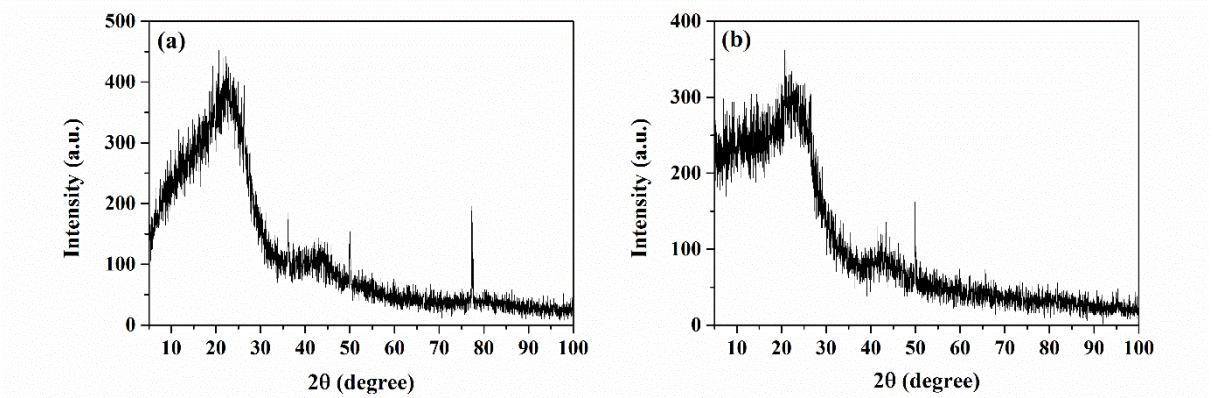

Fig. 5 XRD patterns of AC105 and AC11.

These are typical peaks of disordered aromatic rings structure, indicating the amorphous nature of the materials (Yu-bin et al. 2012). For adsorption purposes, an amorphous nature is generally favorable. An amorphous structure facilitates the entrance of the adsorbate molecules since it has more empty spaces (Zazycki et al. 2018).

3.2. Kinetic study

The kinetic behavior of phenol adsorption on both activated carbons was evaluated employing adsorption capacity curves (q_t) as a function of contact time (t) varying between 0 and 480 min. Fig. 6 shows the kinetic profiles obtained for both materials. As can be observed, in the first minutes the adsorption capacity increased gradually and then tended to the system's equilibrium was achieved. This kinetic behavior occurs due to the progressive occupation of active sites by phenol molecules until reaching saturation (Diel et al. 2021). Besides that, is possible to observe that AC11 exhibited a faster adsorption kinetic (Fig. 6 (b)) than AC105 (Fig. 6 (a)). AC11 reached the equilibrium in around 240 minutes, while AC105 reached the equilibrium in around 360 minutes.

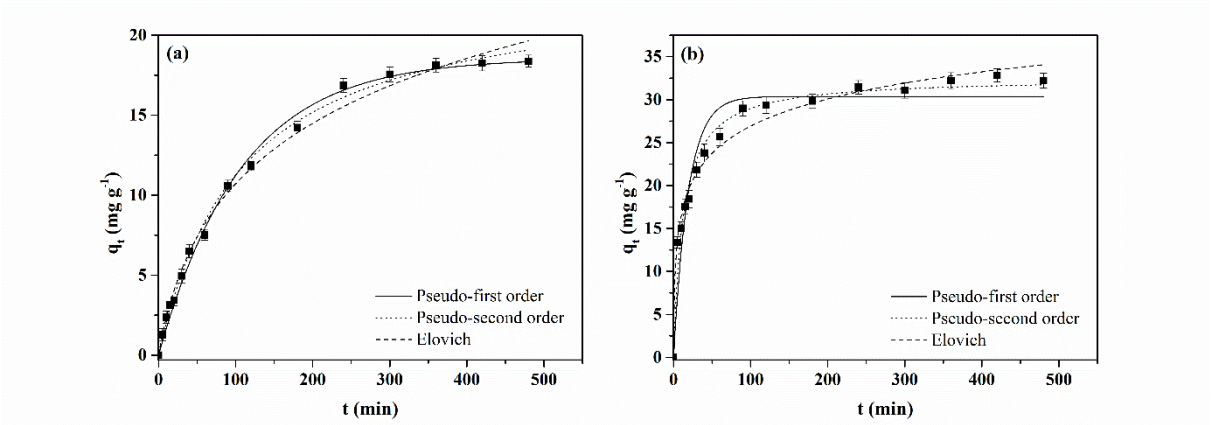

Fig. 6. Kinetic curves of phenol adsorption onto (a) AC105 and (b) AC11 (phenol initial concentration: 50 mg L^{-1}; adsorbent dosage: 1.0 g L^{-1}; temperature: 25 ºC; agitation rate: 150 rpm).

To elucidate the adsorption process, the experimental data of the kinetic curves (Fig. 6) were fitted to the PFO, PSO order, and Elovich models. The parameters of the kinetic models and the criteria for assessing the fit's quality are shown in Table 2. The values of R^2, R^2adj, and *ARE* revealed that the PFO model had the lowest performance among the tested models for predicting the kinetic parameters for both activated carbons. Based on the higher values of

R^2 and R^2_{adj}, and the lower values of ARE, it can be concluded that the Elovich model was the more suitable to describe the phenol adsorption kinetic for AC11. For AC105, the PSO model showed the higher values of R^2 and R^2_{adj}, but the Elovich model showed the lower value of *ARE*. However, for AC105, the predicted value of q_2 (23.32 mg g^{-1}) was considerably different from the experimental value of q_e (18.37 mg g^{-1}). This indicates that the PSO model was not adequate to predict experimental parameters for AC105.

Table 2 Kinetic parameters of phenol adsorption.

Model	Activated carbon	
	AC105	AC11
Pseudo–first order		
q_1 (mg g^{-1})	18.55	30.37
k_1 (min^{-1})	0.0093	0.0524
R^2	0.9950	0.9268
R^2_{adj}	0.9946	0.9216
ARE (%)	8.56	9.19
Pseudo–second order		
q_2 (mg g^{-1})	23.32	32.54
k_2 (g mg^{-1} min^{-1})	0.0004	0.0025
R^2	0.9962	0.9788
R^2_{adj}	0.9959	0.9773
ARE (%)	5.49	4.52
Elovich		
a (g mg^{-1})	0.158	0.219
b (mg g^{-1} min^{-1})	0.280	16.552
R^2	0.9920	0.9834
R^2_{adj}	0.9914	0.9822
ARE (%)	4.49	3.80

Therefore, the Elovich model was established as the most suitable to describe the kinetic data for both adsorbents, assuming that the adsorption occurs by chemisorption and the adsorbing surface is heterogeneous (Hameed and Rahman 2008; Lima et al. 2015; Martins et al. 2015). Mohammadi et al. (2020) also demonstrated that the Elovich model was the most adequate for representing the kinetic data of phenol adsorption onto magnetic activated carbon-cobalt nanoparticles.

3.3. Equilibrium isotherms

The isotherm curves were graphically plotted as the amount of adsorbate present in the adsorbent material (q_e) as a function of the concentration of the adsorbate in the liquid phase (C_e). The curves were obtained at the temperature of 25 °C and initial phenol concentrations of 25–200 mg $L^{-1.}$ Based on the kinetic results, the isotherm curves of both activated carbons were obtained considering a contact time of 360 min, to ensure the equilibrium of the system. Fig. 7 shows the equilibrium curves obtained for both activated carbons. As can be observed, both adsorption isotherms exhibited a concave shape in relation to the concentration, sloped at lower concentrations and tending to plateau at higher concentrations.

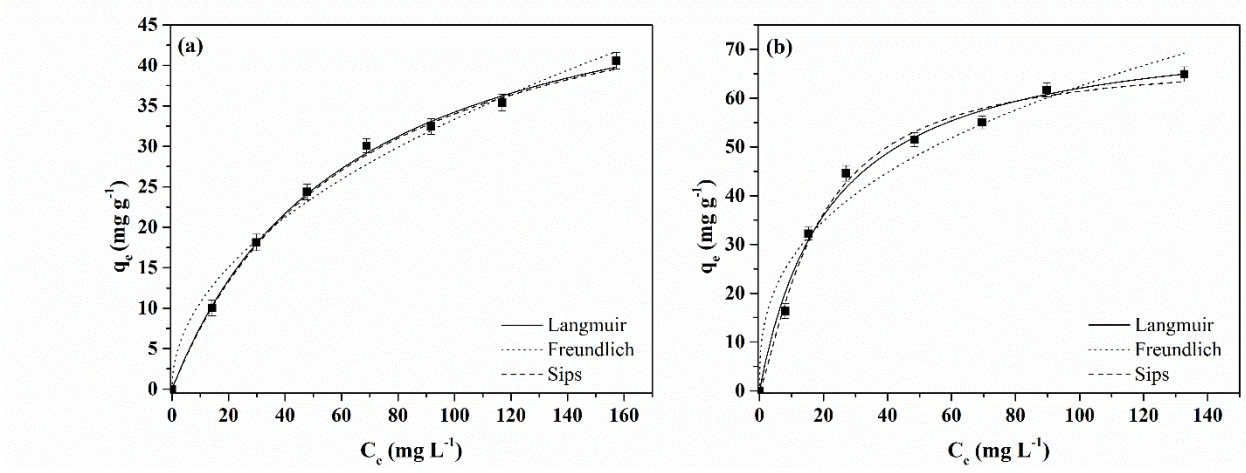

Fig. 7. Equilibrium isotherms of phenol adsorption onto (a) AC105 and (b) AC11 (phenol initial concentration: 25–200 mg L^{-1}; adsorbent dosage: 1.0 g L^{-1}; time: 4 h; temperature: 25 ºC; agitation rate: 150 rpm).

However, the saturation was not achieved in the studied concentration range, which shows that some adsorption sites remained empty. Therefore, according to Giles classification (Giles et al. 1974), the isotherms obtained for both materials can be classified as L1 type. L type isotherms indicate high affinity between the adsorption sites of the adsorbent and the adsorbate molecules, being associated with favorable adsorption. (Giles et al. 1974).

Table 3. Equilibrium parameters of phenol adsorption

Model	Activated carbon	
	AC105	AC11
Langmuir		
q_m (mg g^{-1})	55.61	75.81
k_L (L mg^{-1})	0.016	0.045
R^2	0.9980	0.9912
R^2_{adj}	0.9977	0.9897
ARE (%)	1.75	5.15
Freundlich		
k_F ((mg g^{-1})(L mg^{-1})$^{-1/n}$)	3.43	11.73
1/nF	0.494	0.363
R^2	0.9877	0.9612
R^2_{adj}	0.9856	0.9547
ARE (%)	5.87	10.59
Sips		
q_S (mg g^{-1})	55.16	68.52
k_S (L mg^{-1})	0.016	0.055
m	1.009	1.262
R^2	0.9980	0.9934
R^2_{adj}	0.9977	0.9923
ARE (%)	1.70	4.15

For more information on the equilibrium studies, the isotherm curves were fitted to the Langmuir, Freundlich, and Sips models. Table 3 shows the equilibrium parameters and the criteria for assessing the quality of fit. It was verified that the higher values of R^2 and R^2_{adj}, and the lower values of *ARE* were obtained using the Sips model. Therefore, this model was chosen as the most suitable to represent the equilibrium data for both activated carbons. The Sips model is a combination of the Langmuir and Freundlich models. At low concentrations of adsorbate, the Sips model reduces to the Freundlich model and, at high concentrations, it predicts monolayer formation, which is characteristic of the Langmuir isotherm (Sips 1948). Kamiński et al. (2020) and Ta et al. (2021) also demonstrated that the Sips model was more suitable to represent the equilibrium data of phenol adsorption using activated carbons.

Table 3 also points out that the maximum adsorption capacity of the Sips model (q_s) was higher for AC11 (68.52 mg g^{-1}) than for AC105 (55.16 mg g^{-1}). In general, a higher adsorption capacity is expected for adsorbents with higher surface area, since more active sites are available for adsorption. In fact, as can be observed in Table 1, AC11 presented a slightly superior S_{BET} than AC105. Therefore, this can partially explain the higher adsorption capacity observed for AC11.

In order to compare the maximum adsorption capacity of AC105 and AC11 with other adsorbents developed in the last years to remove phenol, Table 4 presents a brief comparison. Although the data were obtained under different experimental conditions, it is possible to observe a large difference in the maximum adsorption capacities between the materials, ranging from 1.81 to 599.21 mg g^{-1}. Among all adsorbents analyzed, AC11 and AC105 showed intermediate and satisfactory adsorption capacity, indicating that the materials have a high potential to be used as an adsorbent for phenol.

Table 4 Adsorption capacities of different adsorbents for phenol adsorption. [a]Calculated

Adsorbent	Dosage (g L^{-1})	pH	T (°C)	q_m (mg g^{-1})	Reference
AC1105	1.0	6.9	25	55.16	This study
AC111	1.0	6.9	25	68.52	This study
Activated carbon from fruit wastes of *Ceiba speciosa*	0.83	9.0	25	156.7	Franco et al. (2021)
Black wattle bark waste	1.0	6.5	55	98.57	Lütke et al. (2019)
Moroccan clay	5.0[a]	4.0	60	15.11	Dehmani et al. (2020)
Rice husk ash	2.0	9.0	35	13.98	Mandal et al. (2019)
Coffee husk activated carbon	1.0[a]	–	10	205.63	Ta et al. (2021)
Acid-modified Pseudomonas putida-sepiolite/ZIF-8 bio-nanocomposites	1.0[a]	–	–	5.96	Dong et al. (2020)
Reduced graphene oxide	0.4	8.0	30	599.21	Rout and Jena (2022)
Magnetic porous polymer microspheres	0.05	5.47	25	33.83	Özdemir et al. (2019)
Ortho-phosphoric acid-activated biochar from spent tea waste	3.0	8.0	32	154.39	Pathak et al. (2020)
Sulphuric acid-activated biochar from spent tea waste	3.0	8.0	32	185.00	Pathak et al. (2020)
Activated/KOH adsorbent from *Enterolobium contortisiliquum*	20.0	6.0	60	1.81	Lima et al. (2022)
Magnetic activated carbon-cobalt nanoparticles	2.0[a]	7.0	25	107.50	Mohammadi et al. (2020)
Carbonized trace ZIF-8-decorated activated carbon pellets	0.2[a]	–	30	155.24	Yan et al. (2021)
Graphene oxide coated biochar	1.0[a]	7.0	35	23.47	Manna et al. (2019)
Magnetic palm kernel biochar	6.0[a]	8.0	25	10.84	Hairuddin et al. (2019)

3.4. Regeneration study

Regeneration experiments were carried out in order to evaluate the possibility of reusing the activated carbons. The possibility of reusing an adsorbent is an important aspect

from the economic point of view since it allows for prolonged use of the material. In this work, thermic regeneration (200 °C) and chemical regeneration (NaOH 0.5 mol L^{-1} or ethanol 99.8%) were tested. Fig. 8 shows the phenol equilibrium adsorption capacity for four cycles using the different regeneration conditions. It can be observed that the best results were obtained using ethanol for both activated carbons. Rodrigues et al. (2011) also found that ethanol was more efficient than NaOH for regenerating activated carbon after phenol adsorption. Larasati et al. (2020) suggested that ethanol is a better regeneration agent than NaOH since phenol has better solubility and hydrophobicity properties in ethanol.

In addition, it is possible to observe that for AC11 the adsorption capacity decreased by half in the second cycle using ethanol as a regeneration agent (Fig. 8 (b)), while for AC105, the adsorption capacity decreased by only 24% in the second cycle (Fig. 8 (a)). However, the adsorption capacity observed for AC11 in the second cycle is even similar to the adsorption capacity observed for AC105 in the first cycle. This supports that AC11 is a better adsorbent for removing phenol from aqueous solutions than AC105.

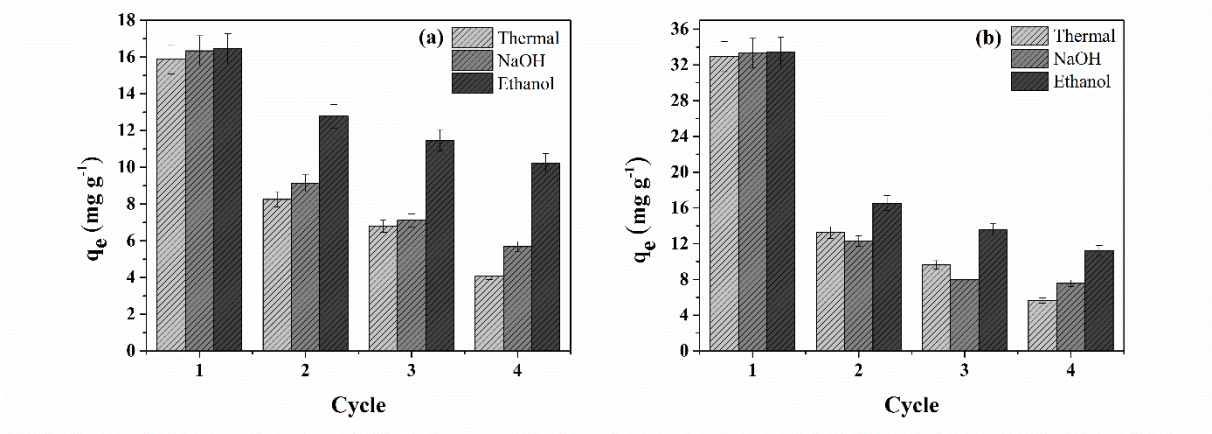

Fig. 8 Reuse cycles of (a) AC105 and (b) AC11 using thermal regeneration and chemical regeneration with NaOH or etanol.

3.5. Adsorption of phenolic compounds in a simulated effluent

A simulated effluent was prepared to evaluate the efficiency of the activated carbons to remove phenolic compounds in a medium with high concentration of salts. The adsorption

tests were carried out with different dosages of the activated carbons and without making any adjustment to the pH, with the simulated solution having the natural pH value of 9.0. Fig 9 shows the absorption spectra in the range of 200 to 400 nm before and after the adsorption. With the dosages of 1, 5, and 10 g L^{-1}, AC105 was able to remove 4.74, 24.01, and 28.05%, of the mixture of phenolic compounds, respectively. CA11 showed better removal efficiency. With the same dosages, AC11 achieved the removal efficiencies of 10.33, 43.96, and 48.20%, respectively. Since the prepared simulated effluent contains several phenolic compounds, in addition to a high concentration of salts, the adsorption sites of the activated carbons were easily saturated. Therefore, the removal efficiencies, even at high dosage, were relatively low.

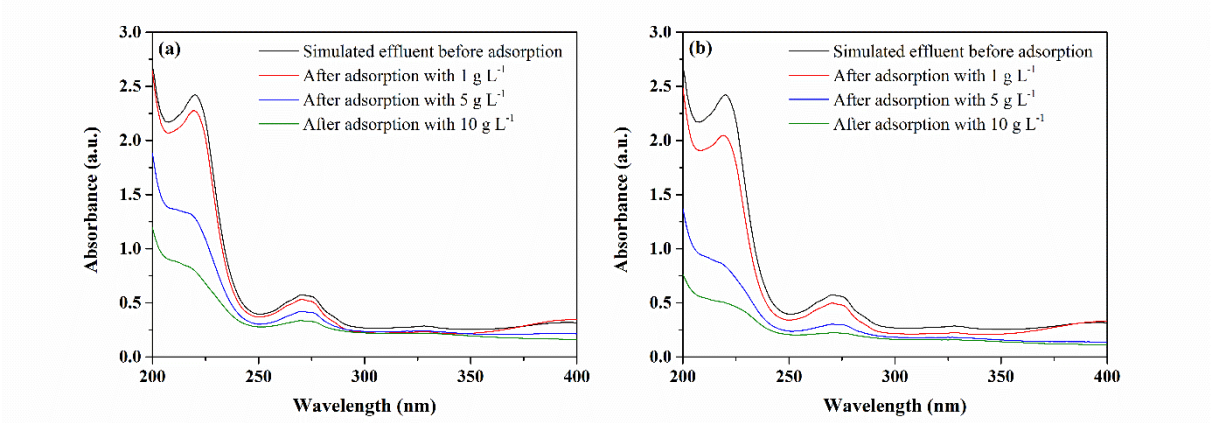

Fig. 9 Absorption spectra of simulated effluent before and after adsorption onto (a) AC105 and (b) AC11 with different dosages.

It is important to add that the spectrum of the untreated effluent (black line) exhibited the existence of a broad band at around 270 nm, corresponding to the maximum absorbance peak of the phenol molecules. The spectrum after the adsorption with AC11 in the dosage of 10 g L^{-1} (green line) showed that this band was efficiently amortized with high reduction in absorbance. This attests to the higher potential of AC11 in removing phenol.

4. Conclusion

In this work, Brazil nut shell was used as precursor material to produce activated carbons with different KOH weight ratios. Both adsorbents were characterized and used as adsorbents to remove phenol from aqueous solution. From the characterization data, it was possible to observe that the materials showed an amorphous structure, with irregular and rough surface, the presence of surface oxygenated functional groups, and average pore size of around 3.6 nm, classified as mesoporous materials. The increase in the KOH weight ratio led to a slight increase in the specific surface area from 314.335 $m^2 g^{-1}$ (AC105) to 332.228 $m^2 g^{-1}$ (AC11). Regarding the phenol adsorption behavior, AC11 exhibited a faster kinetic and higher adsorption capacity. The Elovich model demonstrated a greater prediction capacity for both activated carbons, and, from the equilibrium curves, the Sips model was the most appropriate. The maximum adsorption capacities (q_s) were 55.16 and 68.52 mg g^{-1} for AC105 and AC11, respectively. In the regeneration and reuse studies, AC105 showed better behavior than AC11, with lower decrease in the adsorption capacity throughout the cycles. However, AC11 presented higher adsorption capacity than AC105 when comparing each cycle. The activated carbons were also employed in the treatment of a simulated industrial effluent, showing the removal efficiencies of 28.05% and 48.20% for AC105 and AC11, respectively. These results demonstrated the higher potential of using AC11 instead of AC105 in phenol adsorption from aqueous solution. Further studies on the adsorption conditions are required in order to increase the phenol adsorption capacity using this activated carbon.

References

Ahmaruzzaman M (2008) Adsorption of phenolic compounds on low-cost adsorbents: A review. Adv Colloid Interface Sci 143:48–67. https://doi.org/10.1016/j.cis.2008.07.002

Al-Obaidi MA, Kara-Zaïtri C, Mujtaba IM (2017) Removal of phenol from wastewater using spiral-wound reverse osmosis process: Model development based on experiment and simulation. J Water Process Eng 18:20–28. https://doi.org/10.1016/j.jwpe.2017.05.005

Alvarez J, Lopez G, Amutio M, Bilbao J, Olazar M (2015) Physical Activation of Rice Husk Pyrolysis Char for the Production of High Surface Area Activated Carbons. Ind Eng Chem Res 54:7241−7250. https://doi.org/10.1021/acs.iecr.5b01589

Baldonia AB, Teodoro LPR, Teodorob PE, Toninic H, Tardind FD, Botin AA, Hoogerheide ESS, Botelho SCC, Lulu J, de Farias Neto AL, Azevedo VCR (2020) Genetic diversity of Brazil nut tree (Bertholletia excelsa Bonpl.) in southern Brazilian Amazon. For Ecol Manage 458:117795. https://doi.org/10.1016/j.foreco.2019.117795

Chiang YC, Juang RS (2017) Surface modifications of carbonaceous materials for carbon dioxide adsorption: A review. J Taiwan Inst Chem Eng 71:214–234. https://doi.org/10.1016/j.jtice.2016.12.014

CONAMA (2005) Resolução CONAMA n° 357, de 17 de março de 2005. Conselho Nacional do Meio Ambiente (CONAMA).

Dehmani Y, Sellaoui L, Alghamdi Y, Lainé J, Badawi M, Amhoud A, Bonilla-Petriciolet A, Lamhasni T, Abouarnadasse S (2020) Kinetic, thermodynamic and mechanism study of the adsorption of phenol on Moroccan clay. J Mol Liq 312:113383. https://doi.org/10.1016/j.molliq.2020.113383

Diel JC, Franco DSP, Nunes IS, Pereira HA, Moreira KS, Burgo TAL, Foletto EL, Dotto GL (2021) Carbon nanotubes impregnated with metallic nanoparticles and their application as an adsorbent for the glyphosate removal in an aqueous matrix. J Environ Chem Eng 9:105178. https://doi.org/10.1016/j.jece.2021.105178

Dong R, Chen D, Li N, Xu Q, Li H, He J, Lu J (2020) Removal of phenol from aqueous solution using acid-modified Pseudomonas putida-sepiolite/ZIF-8 bio-nanocomposites.

Chemosphere 239:124708. https://doi.org/10.1016/j.chemosphere.2019.124708

Du W, Sun J, Zan Y, Zhang Z, Ji J, Wang F (2017) Biomass-derived nitrogen-doped hierarchically porous carbon networks as efficient absorbents for phenol removal from wastewater over a wide pH range. RSC Adv 7:46629–46635. https://doi.org/10.1039/C7RA08374B

Duan S, Ma W, Pan Y, Meng F, Yu S, Wu L (2017) Synthesis of magnetic biochar from iron sludge for the enhancement of Cr(VI) removal from solution. J Taiwan Inst Chem Eng 80:835–841. https://doi.org/10.1016/j.jtice.2017.07.002

Duan W, Meng F, Cui H, Lin Y, Wang G, Wu J (2018) Ecotoxicity of phenol and cresols to aquatic organisms: A review. Ecotoxicol Environ Saf 157:441–456. https://doi.org/10.1016/j.ecoenv.2018.03.089

Ferreira MP, Lotte RG, D'Elia FV, Stamatopoulos C, Kim DH, Benjamin AR (2021) Accurate mapping of Brazil nut trees (Bertholletia excelsa) in Amazonian forests using WorldView-3 satellite images and convolutional neural networks. Ecol Inform 63:101302. https://doi.org/10.1016/j.ecoinf.2021.101302

Ferreira SD, Altafini CR, Perondi D, Godinho M (2015) Pyrolysis of Medium Density Fiberboard (MDF) wastes in a screw reactor. Energy Convers Manag 92:223–233. https://doi.org/10.1016/j.enconman.2014.12.032

Franco DSP, Georgin J, Netto MS, Allasia D, Oliveira MLS, Foletto EL, Dotto GL (2021) Highly effective adsorption of synthetic phenol effluent by a novel activated carbon prepared from fruit wastes of the Ceiba speciosa forest species. J Environ Chem Eng 9:105927. https://doi.org/10.1016/j.jece.2021.105927

Freundlich H (1907) Über die Adsorption in Lösungen. Zeitschrift für Phys Chemie 57U 385:470. https://doi.org/10.1515/zpch-1907-5723

Fu Y, Shen Y, Zhang Z, Ge X, Chen M (2019) Activated bio-chars derived from rice husk via

one- and two-step KOH-catalyzed pyrolysis for phenol adsorption. Sci Total Environ 646:1567–1577. https://doi.org/10.1016/j.scitotenv.2018.07.423

Georgin J, Marques BS, Peres EC, Allasia D, Dotto GL (2018) Biosorption of cationic dyes by Pará chestnut husk (Bertholletia excelsa). Water Sci Technol 77:1612–1621. https://doi.org/10.2166/wst.2018.041

Giles CH, Smith D, Huitson A (1974) A general treatment and classification of the solute adsorption isotherm. J Colloid Interface Sci 47:755–765. https://doi.org/10.1016/0021-9797(74)90252-5

Hairuddin MN, Mubarak NM, Khalid M, Abdullah EC, Walvekar R, Karri RR (2019) Magnetic palm kernel biochar potential route for phenol removal from wastewater. Environ Sci Pollut Res 26:35183–35197. https://doi.org/https://doi.org/10.1007/s11356-019-06524-w

Hameed BH, Rahman AA (2008) Removal of phenol from aqueous solutions by adsorption onto activated carbon prepared from biomass material. J Hazard Mater 160:576–581. https://doi.org/10.1016/j.jhazmat.2008.03.028

Ho YS, McKay G (1998) A comparison of chemisorption kinetic models applied to pollutant removal on various sorbents. Process Saf Environ Prot 76:332–340. https://doi.org/10.1205/095758298529696

Hussain SN, Roberts EPL, Asghar HMA, Campen AK, Brown NW (2013) Oxidation of phenol and the adsorption of breakdown products using a graphite adsorbent with electrochemical regeneration. Electrochim Acta 92:20–30. https://doi.org/10.1016/j.electacta.2013.01.020

IBGE (2021) Produção da Extração Vegetal e da Silvicultura 2020. Instituto Brasileiro de Geografia e Estatística (IBGE).

Kalderis D, Koutoulakis D, Paraskeva P, Diamadopoulos E, Otal E, del Valle JO,

Fernández-Pereira C (2008) Adsorption of polluting substances on activated carbons prepared from rice husk and sugarcane bagasse. Chem Eng J 144:42–50. https://doi.org/10.1016/j.cej.2008.01.007

Kamiński W, Kuśmierek K, Świątkowski A, Tomczak E (2020) Simultaneous adsorption of phenol derivatives from water onto spherical activated carbon. Ecol Chem Eng S 27:403–413. https://doi.org/10.2478/eces-2020-0026

Kumar M, Upadhyay SN, Mishra PK (2019) A comparative study of thermochemical characteristics of lignocellulosic biomasses. Bioresour Technol Reports 8:100186. https://doi.org/10.1016/j.biteb.2019.100186

Langmuir I (1918) The adsorption of gases on plane surfaces of glass, mica and platinum. J Am Chem Soc 40:1361–1403. https://doi.org/10.1021/ja02242a004

Larasati A, Fowler GD, Graham NJD (2020) Chemical regeneration of granular activated carbon: preliminary evaluation of alternative regenerant solutions. Environ Sci Water Res Technol 6:2043–2056. https://doi.org/10.1039/d0ew00328j

Lima ÉC, Adebayo MA, Machado FM (2015) Kinetic and Equilibrium Models of Adsorption. In: Bergmann CP, Machado FM (ed) Carbon Nanomaterials as Adsorbents for Environmental and Biological Applications. Springer International Publishing, Switzerland, pp 33–69.

Lima JP, Alvarenga G, Rosa GR, Lopes TJ (2022) Alternative activated/KOH adsorbent for phenol adsorption: experimental , industrial case study and mass transfer interpretation. Environ Sci Pollut Res. https://doi.org/10.1007/s11356-022-21313-8

Lütke SF, Igansi AV, Pegoraro L, Dotto GL, Pinto LAA, Cadaval TRS (2019) Preparation of activated carbon from black wattle bark waste and its application for phenol adsorption. J Environ Chem Eng 7:103396. https://doi.org/10.1016/j.jece.2019.103396

Machado LMM, Lütke SF, Perondi D, Godinho M, Oliveira MLS, Collazzo GC, Dotto GL

(2020) Simultaneous production of mesoporous biochar and palmitic acid by pyrolysis of brewing industry wastes. Waste Manag 113:96–104. https://doi.org/10.1016/j.wasman.2020.05.038

Mandal A, Mukhopadhyay P, Kumar S (2019) The study of adsorption efficiency of rice husk ash for removal of phenol from wastewater with low initial phenol concentration. SN Appl Sci 1:192. https://doi.org/10.1007/s42452-019-0203-3

Manna S, Prakash S, Das P (2019) Synthesis of graphene oxide nano-materials coated bio-char using carbonaceous industrial waste for phenol separation from water. Colloids Surfaces A 581:123818. https://doi.org/10.1016/j.colsurfa.2019.123818

Martins AC, Pezoti O, Cazetta AL, Bedin KC, Yamazaki DAS, Bandoch GFG, Asefa T, Visentainer JV, Almeida VC (2015) Removal of tetracycline by NaOH-activated carbon produced from macadamia nut shells: Kinetic and equilibrium studies. Chem Eng J 260:291–299. https://doi.org/10.1016/j.cej.2014.09.017

Mohammadi S, Kargari A, Sanaeepur H, Abbassian K, Najafi A, Mofarrah E (2015) Phenol removal from industrial wastewaters: a short review. Desalin Water Treat 53:2215–2234. https://doi.org/10.1080/19443994.2014.883327

Mohammadi SZ, Darijani Z, Karimi MA (2020) Fast and efficient removal of phenol by magnetic activated carbon-cobalt nanoparticles. J Alloys Compd 832:154942. https://doi.org/10.1016/j.jallcom.2020.154942

Muniandy L, Adam F, Rahman A, Mohamed AR, Ng EP (2014) The synthesis and characterization of high purity mixed microporous/mesoporous activated carbon from rice husk using chemical activation with NaOH and KOH. Microporous Mesoporous Mater 197:316–323. https://doi.org/10.1016/j.micromeso.2014.06.020

Özdemir İ, Tekin N, Kara A (2019) Magnetic porous polymer microspheres: Synthesis, characterization and adsorption performance for the removal of phenol. J Macromol Sci

Part A 56:564–576. https://doi.org/10.1080/10601325.2019.1586445

Pathak U, Jhunjhunwala A, Roy A, Das P, Kumar T, Mandal T (2020) Efficacy of spent tea waste as chemically impregnated adsorbent involving ortho-phosphoric and sulphuric acid for abatement of aqueous phenol—isotherm, kinetics and artificial neural network modelling. Environ Sci Pollut Res 27:20629–20647. https://doi.org/https://doi.org/10.1007/s11356-019-06014-z

Pradeep NV, Anupama S, Navya K, Shalini HN, Idris M, Hampannavar US (2015) Biological removal of phenol from wastewaters: a mini review. Appl Water Sci 5:105–112. https://doi.org/10.1007/s13201-014-0176-8

Prauchner MJ, Sapag K, Rodríguez-Reinoso F (2016) Tailoring biomass-based activated carbon for CH4 storage by combining chemical activation with H3PO4 or ZnCl2 and physical activation with CO2. Carbon 110:138–147. https://doi.org/10.1016/j.carbon.2016.08.092

Raza W, Lee J, Raza N, Luo Y, Kim K, Yang J (2019) Removal of phenolic compounds from industrial waste water based on membrane-based technologies. J Ind Eng Chem 71:1–18. https://doi.org/10.1016/j.jiec.2018.11.024

Rodrigues LA, da Silva MLCP, Alvarez-Mendes MO, Coutinho AR, Thim GP (2011) Phenol removal from aqueous solution by activated carbon produced from avocado kernel seeds. Chem Eng J 174:49–57. https://doi.org/10.1016/j.cej.2011.08.027

Rout DR, Jena HM (2022) Removal of phenol from aqueous solution using reduced graphene oxide as adsorbent: isotherm, kinetic, and thermodynamic studies. Environ Sci Pollut Res 29:32105–32119. https://doi.org/10.1007/s11356-021-17944-y

Singh J, Bhunia H, Basu S (2019) Adsorption of CO2 on KOH activated carbon adsorbents: Effect of different mass ratios. J Environ Manage 250:109457. https://doi.org/10.1016/j.jenvman.2019.109457

Sips R (1948) On the Structure of a Catalyst Surface. J Chem Phys 16:490–495. https://doi.org/doi.org/10.1063/1.1746922

Ta HS, Van KL, Thi TTL, Nguyen DH (2021) Thermodynamic studies on the adsorption of phenol from aqueous solution by coffee husk activated carbon. Egypt J Chem 64:2355–2367. https://doi.org/10.21608/EJCHEM.2021.30318.2648

Thommes M, Kaneko K, Neimark AV, Olivier JP, Rodriguez-Reinoso F, Rouquerol J, Sing KSW (2015) Physisorption of gases, with special reference to the evaluation of surface area and pore size distribution (IUPAC Technical Report), Pure and Applied Chemistry. https://doi.org/10.1515/pac-2014-1117

Thue PS, Adebayo MA, Lima EC, Sieliechi JM, Machado FM, Dotto GL, Vaghetti JCP, Dias SLP (2016) Preparation, characterization and application of microwave-assisted activated carbons from wood chips for removal of phenol from aqueous solution. J Mol Liq 223:1067–1080. https://doi.org/10.1016/j.molliq.2016.09.032

Thue PS, Umpierres CS, Lima EC, Lima DR, Machado FM, dos Reis GS, da Silva RS, Pavan FA, Tran HN (2020) Single-step pyrolysis for producing magnetic activated carbon from tucumã (Astrocaryum aculeatum) seed and nickel (II) chloride and zinc (II) chloride. Application for removal of nicotinamide and propanolol. J Hazard Mater 398:122903. https://doi.org/10.1016/j.jhazmat.2020.122903

Turki A, Guillard C, Dappozze F, Ksibi Z, Berhault G, Kochkar H (2015) Phenol photocatalytic degradation over anisotropic TiO2 nanomaterials: Kinetic study, adsorption isotherms and formal mechanisms. Appl Catal B Environ 163:404–414. https://doi.org/10.1016/j.apcatb.2014.08.010

Wang J, Lei S, Liang L (2020) Preparation of porous activated carbon from semi-coke by high temperature activation with KOH for the high-efficiency adsorption of aqueous tetracycline. Appl Surf Sci 530:147187. https://doi.org/10.1016/j.apsusc.2020.147187

Wei H, Chen J, Fu N, Chen H, Lin H, Han S (2018) Biomass-derived nitrogen-doped porous carbon with superior capacitive performance and high CO2 capture capacity. Electrochim Acta 266:161–169. https://doi.org/10.1016/j.electacta.2017.12.192

Xu J, Chen L, Qu H, Jiao Y, Xie J, Xing G (2014) Preparation and characterization of activated carbon from reedy grass leaves by chemical activation with H3PO4. Appl Surf Sci 320:674–680. https://doi.org/10.1016/j.apsusc.2014.08.178

Yahya MA, Al-Qodah Z, Ngah CWZ (2015) Agricultural bio-waste materials as potential sustainable precursors used for activated carbon production: A review. Renew Sustain Energy Rev 46:218–235. https://doi.org/10.1016/j.rser.2015.02.051

Yan X, Li Y, Hu X, Feng R, Zhou M, Han D (2021) Enhanced adsorption of phenol from aqueous solution by carbonized trace ZIF-8-decorated activated carbon pellets. Chinese J Chem Eng 33:279–285. https://doi.org/10.1016/j.cjche.2020.06.027

Yu-bin T, Qiang L, Fang-yan C (2012) Preparation and characterization of activated carbon from waste ramulus mori. Chem Eng J 203:19–24. https://doi.org/10.1016/j.cej.2012.07.007

Zazycki MA, Godinho M, Perondi D, Foletto EL, Collazzo GC, Dotto GL (2018) New biochar from pecan nutshells as an alternative adsorbent for removing reactive red 141 from aqueous solutions. J Clean Prod 171:57–65. https://doi.org/10.1016/j.jclepro.2017.10.007

ARTIGO 2 **- Activated carbon prepared from Brazil nut shells toward phenol removal from aqueous solutions**

Maria C. F. da Silva1, Sabrina F. Lütke1, Victoria X. Nascimento1, Éder. C. Lima2, Guilherme L. Dotto1*

1Research Group on Adsorptive and Catalytic Process Engineering (ENGEPAC), Federal University of Santa Maria, Av. Roraima, 1000-7, 97105–900 Santa Maria, RS, Brazil

2Institute of Chemistry, Federal University of Rio Grande do Sul–UFRGS, Av. Bento Gonçalves 9500, P.O. Box 15003, 91501-970, Porto Alegre, RS, Brazil

*Corresponding author: Research Group on Adsorptive and Catalytic Process Engineering (ENGEPAC), Federal University of Santa Maria, Av. Roraima, 1000-7, 97105–900 Santa Maria, RS, Brazil. Email: guilherme_dotto@yahoo.com.br

Abstract

The Brazil nut shell was used as a precursor material for the preparation of activated carbon by chemical activation with potassium hydroxide. The obtained material (BNSAC) was characterized and the adsorptive features towards phenol were investigated. The

characterization results showed that the activated carbon presented several rounded cavities along the surface, with a specific surface area of 332 m^2 g^{-1}. Concerning phenol adsorption, it was favored using an adsorbent dosage of 0.75 g L^{-1} and pH 6. The kinetic investigation revealed that the system approached the equilibrium in around 180 minutes and the kinetic curves were represented by the Elovich model. The equilibrium isotherms were well represented by the Sips model. In addition, the increase in temperature from 25 to 55 °C favored the phenol adsorption, increasing the maximum adsorption capacity value (qs) from 82.99 to 99.02 mg g^{-1}. According to the estimated thermodynamic parameters, the adsorption was spontaneous, favorable, endothermic, and governed by physical interactions. Therefore, the Brazil nut shell proved to be a good precursor material to prepare efficient activated carbon for phenol removal.

Keywords: Adsorbent; Adsorption thermodynamics; Agricultural waste; Kinetic and isotherm modeling; KOH activation; Phenol;

1. Introduction

Accelerated waste generation due to rapid economic growth has become one of the major concerns around the world (Awasthi et al. 2022). Among the waste generated in large amounts are those generated by agricultural activities (Awogbemi et al. 2021). The agricultural sector produces several types of agricultural waste with huge annual production and, usually, they are dumped or burned under open field conditions, resulting in environmental problems (Awasthi et al. 2022; Thines et al. 2017). Therefore, the management of agricultural waste is a challenging task. A proposal for the management of these residues is their use as precursor materials for activated carbon (AC) production (Aguilar-Rosero et al.

2022). For instance, activated carbon was prepared from wastes of the Ceiba speciosa forest species (Franco et al. 2021), tangerine seed (Wang et al. 2020c), pecan nutshells (Zazycki et al. 2018), rice and coffee husk wastes (Paredes-Laverde et al. 2021), date seeds (Ogungbenro et al. 2020), among others. In this context, the Brazil nut shells are a promising agricultural was for AC production. Brazil nut tree (Bertholletia excelsa) grows throughout the Amazon region, including Brazil, Bolivia, Peru, Colombia, Venezuela, and Guyana (Baldoni et al. 2020). The nutritional characteristics and the bioactive compounds present in Brazil nuts have increased interest in their consumption in the last decade, as this can bring beneficial effects for human health (Vasquez et al. 2021). In 2020, 33 thousand tons of Brazil nuts were produced in Brazil (IBGE 2021). As the shell represents a considerable part of the Brazil nut weight, this means a high amount of waste to be handled and its use for AC production is a possibility.

Regarding the AC preparation, the activation step can be carried out by chemical, physical, or a combination of both methods (Bedia et al. 2018). Chemical activation, when compared to physical activation, has several advantages, such as the reduction of tar production during pyrolysis, increasing efficiency and leading to a high carbon yield, and the lower temperatures and shorter times required for pyrolysis (Gao et al. 2020; Kwiatkowski and Broniek 2017). In addition, chemical activation can be performed in a single step. In the one-step chemical activation, the activating agents are previously impregnated in the precursor material, which is then subjected to pyrolysis, i.e., pyrolysis and activation occur simultaneously (Cheng et al. 2021; Gao et al. 2020). All these advantages result in lower energy consumption, which implies lower production costs (Kwiatkowski and Broniek 2017). In this context, KOH is widely reported as a chemical activated agent for AC production from a wide range of precursor materials as it leads to a good development of the porous structure, with the creation of high surface area and pore volume (Cao et al. 2021; Huang et al. 2019;

Jawad et al. 2021; Oginni et al. 2019; Yang et al. 2018). In addition, KOH has the advantage of being less expensive and less corrosive to the reactors when compared to other chemical activating agents, such as acids (Ghosh and Barron 2017).

Activated carbon is a very versatile material and has several applications (Neme et al. 2022). Its use as an adsorbent is perhaps one of the most common. Adsorption processes can benefit from AC characteristics such as high surface area and total pore volume and the presence of surface functional groups (Rashid et al. 2019). In the literature, activated carbon has already been reported, for example, for the removal of heavy metals (Nasseh et al. 2021; Zhang et al. 2021), fluoride (Araga et al. 2017), dyes (Streit et al. 2019), pharmaceutical compounds (Georgin et al. 2021b; Streit et al. 2021) and herbicides (Georgin et al. 2022; de Salomón et al. 2021). In addition, phenol adsorption on AC has been extensively reported (Franco et al. 2021; Iheanacho et al. 2021; Lütke et al. 2019; Lv et al. 2020; Thue et al. 2016). Phenol is classified as a priority contaminant by several international regulatory bodies (Fseha et al. 2023; Hairuddin et al. 2019). Wastewaters containing high phenol concentrations are generated by several industrial sectors, such as textile processing, petrochemicals, pharmaceutical manufacture, oil refining, coke oven plants, coal conversion, leather manufacturing, and resin synthesis, among others (Li et al. 2019; Panigrahy et al. 2022). Coke ovens and coal conversion, for example, generate wastewater containing phenol concentrations as high as 3900 mg L^{-1} and 7000 mg L^{-1}, respectively (Mohd 2022). The discharge of these wastewaters containing phenol can lead to several risks to human beings, animals, aquatic life, and other organisms (Mohamad Said et al. 2021a). Highlighting the effects in humans, phenol can lead to a series of acute as well as chronic effects, causing abnormal breathing, tremor, failure, liver and kidney damage, central nervous system disruption, and even coma and death (Mohamad Said et al. 2021a; Othmani et al. 2022). Therefore, the treatment of wastewater containing phenol before disposal is of high concern.

Faced with the challenge of managing the large amount of Brazil nut shells waste in addition to the deleterious effects of phenol on the environment and human health, the aim of this work was to evaluate the potential of activated carbon from Brazil nut shell waste (BNSAC) towards phenol removal from an aqueous medium. BNSAC was produced following a one-step chemical activation method using KOH as activating agent. The material was characterized by Scanning Electron Microscopy (SEM), Fourier Transform Infrared Spectroscopy (FTIR), N2 adsorption/desorption isotherms, and point of zero charge (pHPZC). The phenol adsorption on BNSAC was evaluated regarding the effect of the adsorbent dosage and pH of the solution, in addition to kinetics, equilibrium, and thermodynamics. Therefore, the present work contemplates both the managing of an abundant agricultural waste, adding value to it and avoiding its inappropriate disposal, and the reduction of water contamination caused by phenol.

2. Material and methods

2.1 Material

Brazil nut shells, used as the precursor material for the production of the activated carbon, were obtained from the local market. Phenol (94.11 g mol–1, purity 99.5%) acquired from Neon (Brazil), was used to make a stock phenol solution (1000 mg L–1), without pH adjustment. Working solutions at the desired concentrations were prepared by diluting this solution with distilled water. All other reagents used in the experiments were of analytical grade.

2.2 Production of the activated carbon

For the BNSAC production, the Brazil nut shell was firstly impregnated with KOH in the weight ratio of 1:1 and then it was pyrolyzed in a quartz reactor in a conventional furnace (Sanchis, Brazil) at 600 ºC. After the pyrolysis, the obtained material was cooled, acid-washed, and dried. More detail about the preparation process can be found in a previous work (da Silva et al. 2022).

2.3 Characterization of the activated carbon

BNSAC was characterized in terms of surface morphology by scanning electron microscopy (SEM), surface functional groups by Fourier transform infrared spectroscopy (FTIR), and textural properties by N2 adsorption/desorption isotherms. For more details about these characterization techniques, see Supplementary Material (S1). Also, the point of zero charge (pHPZC) of the adsorbent was obtained. For this determination, 11 Erlenmeyer flasks containing 0.02 g of BNSAC and 20 mL of pH-adjusted 0.1 mol L–1 NaCl solutions (pH 2–12, adjusted with HCl or NaOH) were kept under constant stirring at 150 rpm (Solab, SL 222, Brazil) at 25 °C for 24 h. After, the adsorbent was separated from the solution by filtration, and the final pH was measured. The pHPZC was determined from the initial pH versus the final pH plot (Netto et al. 2021).

2.4 Phenol adsorption experiments

Dosage and pH experiments were performed using 20 mL of 50 mg L–1 phenol solution, at the temperature of 25 °C, and agitation rate of 150 rpm, using a thermostatic

stirrer (Solab, SL 222, Brazil). To assess the impact of adsorbent dosage on phenol adsorption, assays were performed by varying the dosage from 0.25 to 1.5 g L–1. The dosage experiments were performed using the characteristic pH of the aqueous phenol solution (pH 6.9). The pH assays were performed by varying the pH of the phenol solution (2, 4, 6, 8, and 10, adjusted with HCl or NaOH) using the most suitable adsorbent dosage previously defined.

The phenol adsorption kinetics was studied from 0 to 300 min, using 20 mL of phenol solutions at different initial concentrations (25, 50, 100, 150, and 200 mg L–1), the best adsorbent dosage and pH previously defined, temperature of 25 °C and agitation rate of 150 rpm. The equilibrium curves were obtained under the same conditions as the kinetic curves, except that four different temperatures were studied (25, 35, 45, and 55 °C) and the experiments were carried out until the equilibrium of the system was reached.

After each adsorption assay, the adsorbent was separated from the liquid phase by centrifugation (LGI Scientific, LGI–DLC–802B, Brazil). The phenol concentration remaining in the liquid phase was measured by a UV-vis spectrophotometer (Shimadzu, UVmini-1240, Japão) at the maximum absorption wavelength of phenol (λmax = 270 nm). All experiments were performed in replicate (n = 3) and blank tests were also performed. The adsorption capacity at the time t (qt), the equilibrium adsorption capacity (qe), and the removal percentage (R, %) were determined by Eq. (1), (2), and (3), respectively:

$$q_t = \frac{V(C_0 - C_t)}{m} \quad (1)$$

$$q_e = \frac{V(C_0 - C_e)}{m} \quad (2)$$

$$R\,(\%) = \frac{(C_0 - C_e)}{C_e}\,100 \quad (3)$$

Where: C_0 is the initial phenol concentration (mg L^{-1}), C_t is the phenol concentration in the liquid phase at time t (mg L^{-1}), C_e is the equilibrium phenol concentration in the liquid phase (mg L^{-1}), m is the adsorbent mass (g), and V is the volume of the solution (L).

2.5 Kinetic and equilibrium modeling and adsorption thermodynamic

See Supplementary Material (S2).

3. Results and discussion

3.1 Characterization of the activated carbon

Fig. 1 SEM image of BNSAC with a magnification of 5000×. It is possible to observe that the material has a rough and irregular surface, and exhibited a sponge-like morphology with many cavities spread over the entire surface (Nazir et al. 2022). Such cavities are mostly round in shape and are randomly distributed. These features can be attributed to the KOH effect, which leads to the creation of extra pores during the pyrolysis and activation process (Cao et al. 2021; Nazir et al. 2022).

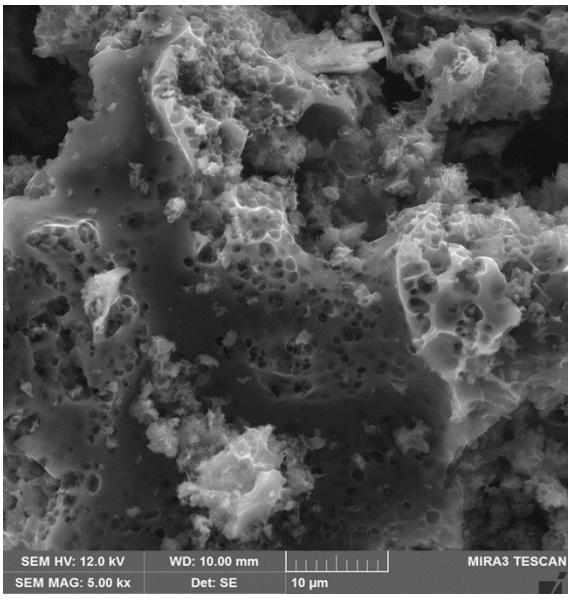

Fig. 1 SEM image of BNSAC (magnification of 5000×).

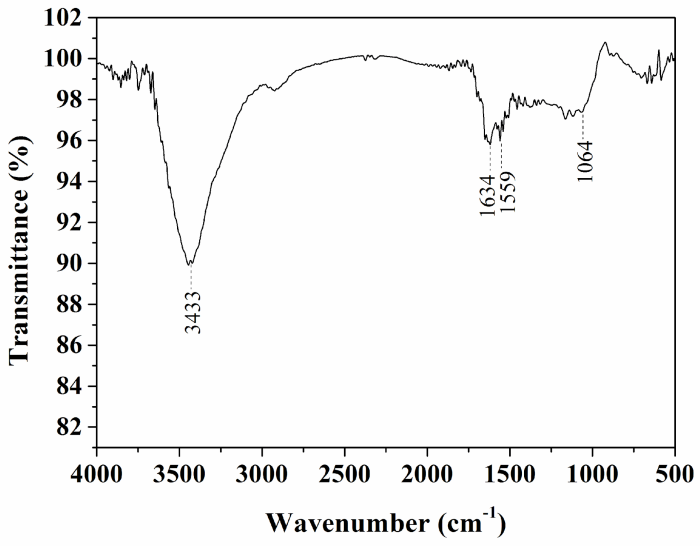

At the high temperature of pyrolysis, KOH undergoes several oxidation reactions. The formed K compounds are incorporated into the carbon skeleton, resulting in its expansion and leading to the development of the porous structure. After the acid washes, these compounds are removed, releasing the formed pores (Cao et al. 2021; Chiang and Juang 2017; J. Wang et al. 2020a). The main surface functional groups of BNSAC were identified through FTIR spectra (Fig. 2). It was possible to identify the main bands usually found in activated carbons, which are 3433 cm–1, 1634 cm–1, 1559 cm–1, and 1064 cm–1. The band at 3433 cm–1 refers to the hydroxyl O–H stretch of alcohols, phenols, or carboxyls. In addition, this band can also be related to adsorbed water (Ogungbenro et al. 2020). The band at 1634 cm–1 is attributed to the C=O stretching vibrations of carboxylic groups (Ferreira et al., 2015). The band observed at 1594 cm–1 is due to the stretching of C=C bonds of the aromatic rings of the activated carbon (Nizam et al. 2021). Lastly, the band 1064 cm−1 is corresponding to the C–O stretching vibrations (Machado et al. 2020a).

Fig. 2 FTIR spectrum of BNSAC.

The N_2 adsorption/desorption isotherms and the BJH pore size distribution of the BNSAC are shown in Fig. 3. According to IUPAC, the isotherm profile exhibited is Type IV, typical of mesoporous materials, and a hysteresis loop Type H4, often associated with narrow slit-shaped pores (Thommes et al. 2015). The specific surface area (SBET) was 332.228 m^2 g^{-1}, total pore volume 0.020 cm^3 g^{-1}, and average pore size 3.69 nm. Therefore, according to the IUPAC classification of pores, BNSAC can be classified as a mesoporous material (Thommes et al. 2015).

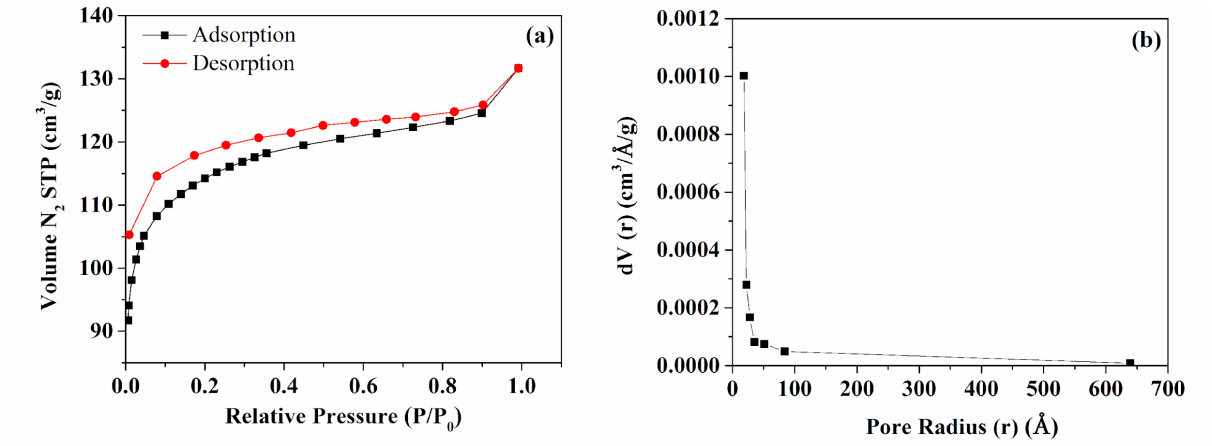

Fig. 3 (a) Nitrogen adsorption/desorption isotherms and (b) BJH pore size distributio of BNSAC.

Determining the pH_{PZC} value of the adsorbent is important in adsorption processes, as it indicates the most adequate pH range for the adsorption of anionic or cationic species. According to Fig. 4, BNSAC exhibited a pH_{PZC} value of 6.0. This means that when the pH of

the solution is lower than 6.0 (pH<pHPZC), some surface functional groups of BNSAC are protonated, making its surface positively charged and favoring the adsorption of anionic species. On the other hand, when the pH of the solution is higher than 6.0 (pH>pHPZC), some surface functional groups release H+, making the BNSAC surface negatively charged and favoring the adsorption (Machado et al. 2020b). In addition, since this value is in the acid region, it is suggested that the acidic surface groups on the adsorbent surface are predominant (Al-Lagtah et al. 2016). Similar pHPZC values for activated carbons were found in the literature (Cunha et al. 2020; Leite et al. 2018; Machado et al. 2020b; Pauletto et al. 2021).

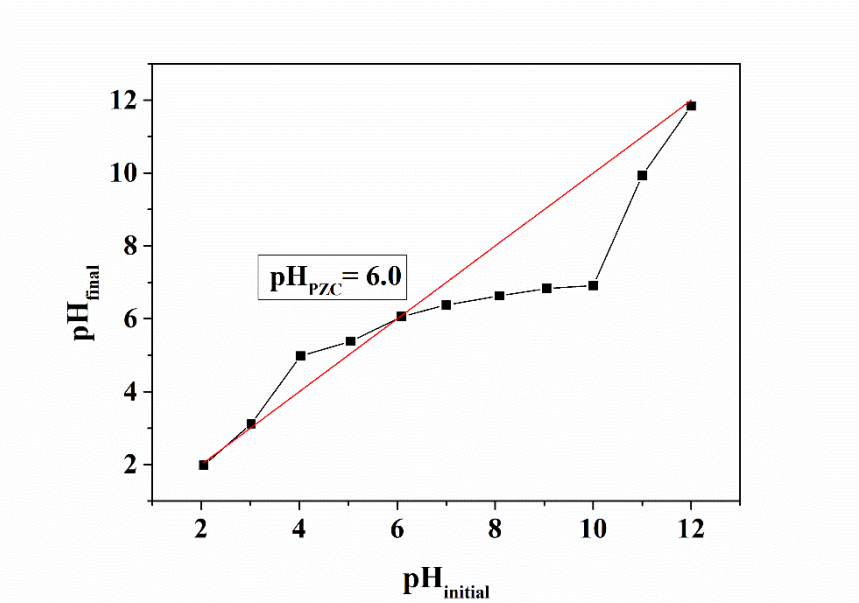

Fig. 4 Determination of the pHPZC of BNSAC

3.2 Adsorption results

3.2.1 Dosage effect

Fig. 5 shows the dosage effect results on phenol adsorption. The adsorption capacity (q) and the removal percentage (R) were evaluated. The removal percentage increased from around 26% to around 70% with the increasing adsorbent dosage from 0.25 g L^{-1} to 1.50 g L^{-1}. This increase is related to the higher number of available adsorption sites with higher dosages. The adsorption capacity revealed an opposite behavior to the removal percentage, decreasing from around 50 mg g−1 to around 25 mg g^{-1} when the adsorbent dosage increased from 0.25 g L^{-1} to 1.50 g L^{-1}.

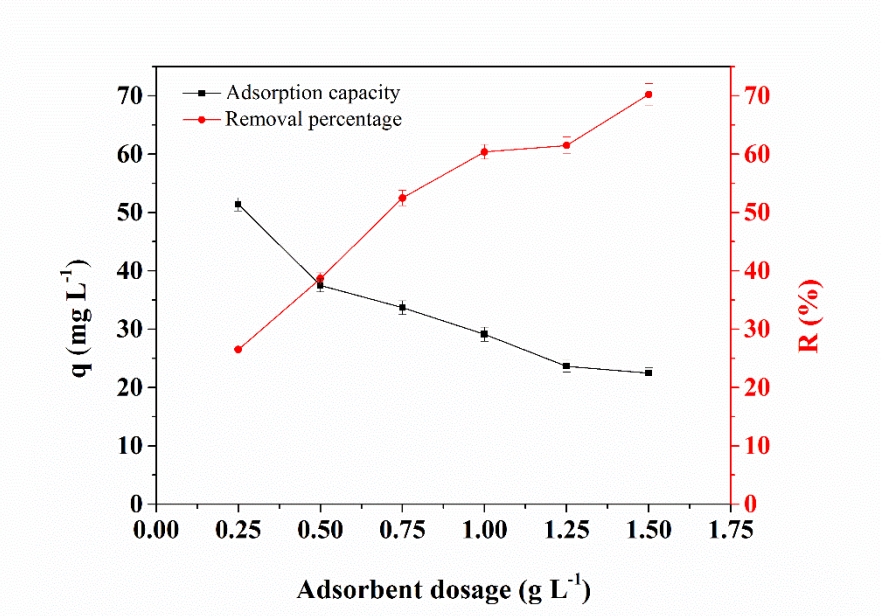

Fig. 5 Effect of BNSAC dosage in the phenol adsorption.

With high adsorbent dosages, some adsorption sites may remain unoccupied, resulting in an overdosage, which can explain this opposite trend observed for the adsorption capacity (Netto et al. 2022). In general, the intersection point between the adsorption capacity and the removal percentage is considered for the choice of the most adequate adsorbent dosage. However, the removal percentage observed at the intersection point (dosage of 0.5 g L−1) was only 40%. Therefore, the dosage of 0.75 g L−1 was chosen for carrying out further

experiments, since it provided a good adsorption capacity value and, concurrently, a more adequate removal percentage

3.2.2 pH effect

Since in the pH range from 2 to 8, the adsorption capacity was similar, pH 6 was chosen for further adsorption studies. The choice of this condition (pH 6) also avoids the addition of large amounts of acid or bases to adjust the pH of the solutions.

Fig. 6 shows the effect of the pH of the solution on the phenol adsorption capacity. As can be observed, pH did not have a very important influence on the adsorption, with the adsorption capacity remaining around 35 mg g−1 in the pH range of 2 to 8. At pH 10, a slightly more pronounced decrease in the adsorption capacity was observed. This can be explained based on the form that phenol molecules are found in different pH values and the surface charge of the adsorbent.

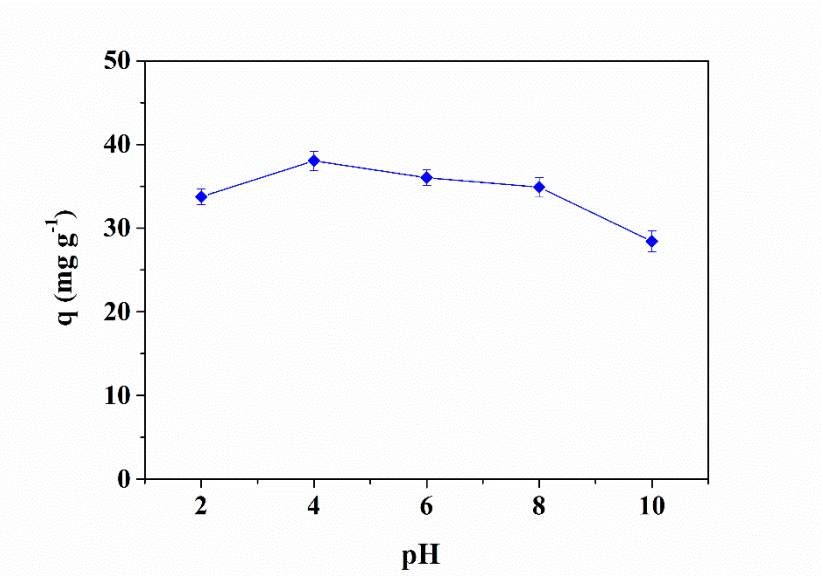

Fig. 6 Effect of the pH of the solution in the phenol adsorption.

The pHPZC of the adsorbent was found to be 6.0 (Fig. 4). Therefore, at pH 6 BNSAC has a neutral surface charge while at more acidic pH values, it has a positive surface charge.

Above pH 6, BNSAC becomes negatively charged due to the deprotonation of some surface functional groups. In addition, above pH 8, the neutral phenol molecules start to transform into phenolate (with a negative charge) due to deprotonation (Franco et al. 2021). However, at pH 8 there is only a very small molar fraction of phenolate in the solution, which does not lead to a large decrease in the adsorption capacity. On the other hand, at pH 10, the molar fraction of phenol molecules that are in the form of phenolate is about 0.5. This leads to a large decrease in the adsorption capacity since the negative surface charge of the adsorbent and the negative charge of the phenolate molecule repel each other.

3.2.3 Adsorption kinetics

The adsorption kinetic study was carried out using different initial phenol concentrations (25, 50, 100, 150, and 200 mg L−1). The obtained kinetic profiles are shown in Fig. 7. As can be observed, the adsorption capacities sharply increased until 60 minutes and, after this time, the increase was gradual. This behavior is associated with the fact that, at the beginning of the adsorption process, the adsorbent has fully available adsorption sites. Over time, these sites are occupied, making the access of the adsorbate molecules to the remaining sites more difficult, and, consequently, the adsorption rate becomes slower (Diel et al. 2021).

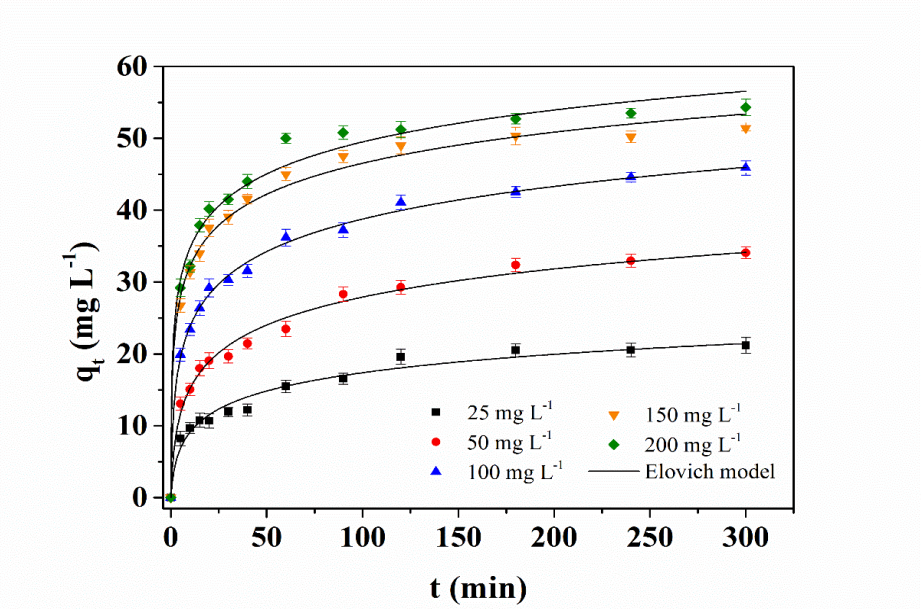

Fig. 7 Kinetic curve of the phenol adsorption onto BNSAC.

In addition, for all initial phenol concentrations, the system approached the equilibrium in around 180 min. As expected, an increase in the adsorption capacity and adsorption rate was observed with increasing initial concentration. This can be explained due to the increase in the mass transfer, leading to an increase in the adsorbate concentration at the surface of the adsorbent (Franco et al. 2021; Georgin et al. 2021a).

To obtain more information on the kinetic study, the kinetic models of pseudo-first-order (PFO), pseudo-second-order (PSO), and Elovich models were used for fitting the experimental data. The estimated kinetic parameters are depicted in Table 1. With higher values of R2 and R2adj and lower values of ARE, the Elovich model proved to be the most adequate to represent the kinetic data of the phenol adsorption on BNSAC. From Table 1 it is also possible to verify that the α parameter increased from 3.9376 mg g–1 min–1 to 142.73 mg g–1 min–1 with increasing initial phenol concentration from 25 mg L–1 to 200 mg L–1.

This trend confirms that the increase in the initial phenol concentration led to faster adsorption. Other authors also found that the Elovich model was the most suitable to represent

the phenol adsorption kinetics on different adsorbents (Li et al. 2013a; Mohammadi et al. 2020; Wang et al. 2020b; Yakub et al. 2020).

Table 1. Kinetic parameters for the phenol adsorption on BNSAC.

Model	Initial phenol concentration (mg L^{-1})				
	25	50	100	150	200
Pseudo-first-order					
q_e (mg g^{-1})	19.23	30.12	40.10	47.10	50.07
k_1 (min^{-1})	0.0410	0.0486	0.0716	0.1007	0.1040
R^2	0.8539	0.8657	0.8844	0.9209	0.9243
R^2_{adj}	0.8247	0.8388	0.8612	0.9051	0.9092
ARE (%)	15.47	14.07	10.81	8.31	7.27
Pseudo-second-order					
q_e (mg g^{-1})	21.26	33.34	43.88	50.64	53.68
k_2 (g mg^{-1} min^{-1})	0.0028	0.0020	0.0024	0.0031	0.0031
R^2	0.9276	0.9436	0.9600	0.9819	0.9812
R^2_{adj}	0.9131	0.9323	0.9520	0.9783	0.9774
ARE (%)	11.13	8.76	6.16	3.79	3.74
Elovich					
α (mg g^{-1} min^{-1})	3.9376	7.6749	24.17	108.58	142.73
β (g mg^{-1})	0.2687	0.1760	0.1525	0.1604	0.1557
R^2	0.9756	0.9897	0.9970	0.9923	0.9867
R^2_{adj}	0.9707	0.9876	0.9966	0.9908	0.9840
ARE (%)	5.67	3.49	1.60	2.39	2.91

3.2.4 Adsorption equilibrium

The equilibrium isotherms of the phenol adsorption on the activated were obtained for different temperatures (25−55 °C) using initial phenol concentrations in the range of 25−200 mg L−1. Fig. 8 shows the obtained curves of the amount of phenol present in the adsorbent at the equilibrium (qe) as a function of the equilibrium phenol concentration in the liquid phase

(Ce). According to the Giles classification, the curves can be classified as L1-type isotherms (Giles et al. 1974). L-type isotherms suggest that the adsorbate molecules and the adsorption sites have a high affinity (Giles et al. 1974).

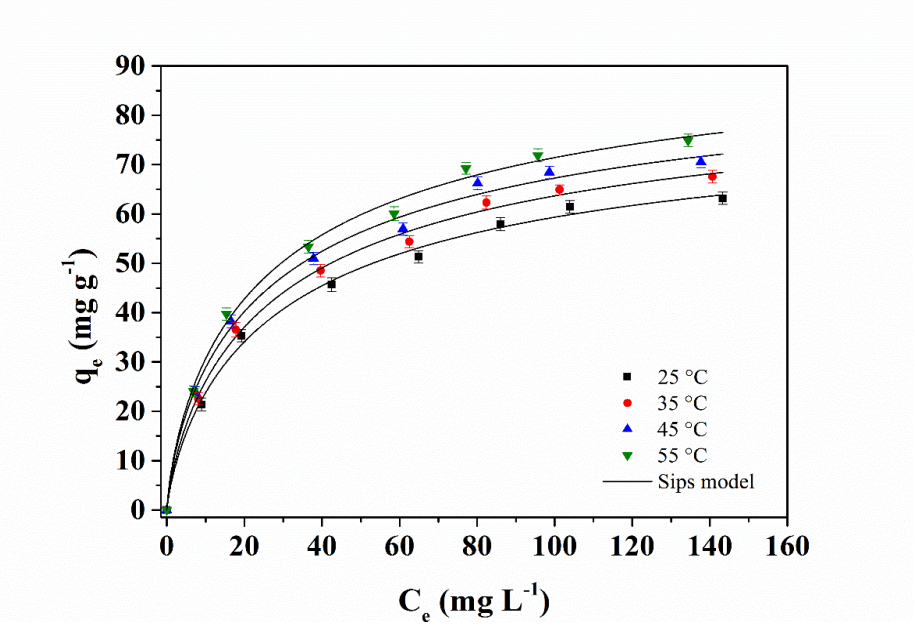

Fig. 8 Equilibrium isotherms of the phenol adsorption onto BNSAC.

In addition, it was possible to observe that the initial portion of the curves was more inclined at higher temperatures, and higher adsorption capacities were found with the increase in temperature. Increasing the temperature from 25 °C to 55 °C led to an increase in the adsorption capacity. This positive effect of the temperature on the adsorption capacity suggests that the phenol adsorption on BNSAC was endothermic.

Langmuir, Freundlich, and Sips isotherms models were adjusted to the equilibrium experimental data. The estimated parameters of each one of these isotherm models are listed in Table 2. The Sips model presented higher values of R2 and R2adj and lower values of ARE when compared to the Langmuir and Freundlich isotherm models. Therefore, the Sips isotherm was chosen as the best model. In the literature, other authors demonstrated that the

Sips model was adequate to describe the phenol adsorption equilibrium data (Istratie et al. 2019; Li et al. 2013b; Mohamad Said et al. 2021b; Ta et al. 2021).

It is also worth mentioning that the qS and kS values increased with increasing temperature, corroborating the information that the increase in temperature favored the adsorption process. At 55 °C, the qS value was 99.02 mg g−1.

Table 2. Equilibrium parameters for the phenol adsorption on BNSAC.

Model	Temperature (°C)			
	25	35	45	55
Langmuir				
q_m (mg g^{-1})	72.36	76.78	79.58	84.06
K_L (L mg^{-1})	0.0451	0.0477	0.0529	0.0539
R^2	0.9950	0.9952	0.9933	0.9937
R^2_{adj}	0.9930	0.9933	0.9906	0.9912
ARE (%)	2.64	2.80	3.29	3.25
Freundlich				
K_F ((mg g^{-1})(L mg^{-1})$^{-1/nF}$)	12.1304	13.2119	14.6214	15.2357
1/nF	0.3437	0.3411	0.3318	0.3365
R^2	0.9870	0.9872	0.9863	0.9863
R^2_{adj}	0.9818	0.9821	0.9808	0.9908
ARE (%)	5.20	4.99	4.93	5.25
Sips				
q_S (mg g^{-1})	82.99	88.82	93.92	99.02
K_S (L mg^{-1})	0.0318	0.0327	0.0341	0.0349
m	0.7954	0.7836	0.7551	0.7608
R^2	0.9967	0.9972	0.9961	0.9965
R^2_{adj}	0.9942	0.9951	0.9932	0.9939
ARE (%)	2.42	2.08	2.22	2.40

3.2.5 Thermodynamics parameters

The thermodynamic parameters of the phenol adsorption onto the activated are shown in Table 3. The equilibrium constant of the Sips model (kS) was used to estimate the thermodynamic equilibrium constant (KD) since this isotherm model showed to be to most suitable to describe the experimental equilibrium data. The R2 value of the Van't Hoff graph was 0.9896. The negative ΔG^{o} values (Table 3) indicated that the phenol adsorption on BNSAC was a spontaneous and favorable process. In addition, more negative ΔG° values were obtained with increasing temperature, indicating that the adsorption was favored at higher temperatures. The positive ΔH^{o} value indicated endothermic adsorption, which corroborates with the temperature dependence observed in the equilibrium isotherms (Fig. 8). Since the magnitude of the ΔH^{o} value was lower than 20 kJ mol−1, it is suggested that the phenol adsorption on BNSAC was a physical process (Bonilla-Petriciolet et al. 2019). This enthalpy change value is frequently associated with van der Waals interactions, hydrogen bond interactions, π-π interactions, and electron donor-acceptor interactions as reported by other studies in the literature (Franco et al. 2021; Rodrigues et al. 2011; Sun et al. 2019; Thue et al. 2016). Electrostatic interactions, which involve the attraction between positive and negative charges, can be ruled out in the phenol adsorption on BNSAC. Since at the pH of the solution (pH 6.0), BNSAC has zero net surface charge (pH=pHPZC) and the phenol molecules exist as neutral species, electrostatic interactions are not able to occur. This also corroborates with the observed low effect of the pH of the solution on the phenol adsorption capacity (Fig. 6). When the main adsorption mechanism is the electrostatic interaction, pH is expected to have an important effect on the adsorption capacity (Thue et al. 2016). However, this was not observed in the present work, which indicates that the phenol adsorption on BNSAC is controlled by mechanisms other than electrostatic interaction. These are the van

der Waals interactions, hydrogen bond interactions, π-π interactions, and electron donor-acceptor interactions.

The ΔS° value was also positive, indicating that the disorder at the solid-liquid interface increased during the adsorption (Al-Trawneh et al. 2021; Zhou et al. 2017). Finally, comparing ΔHº and ΔSº values, it is possible to verify that the phenol adsorption on BNSAC was an entropy-controlled phenomenon, only the ΔSº contributed to obtaining negative ΔGº values (Lütke et al. 2019). Similar results were found for the phenol adsorption on activated carbon from black wattle bark waste (Lütke et al. 2019), activated carbon from fruit wastes of the Ceiba speciosa forest species (Franco et al. 2021), and activated carbons from wood chips (Thue et al. 2016).

Table 3. Thermodynamic parameters of the phenol adsorption on BNSAC.

Temperature (ºC)	K_D	$\Delta G°$ (kJ mol^{-1})	$\Delta H°$ (kJ mol^{-1})	$\Delta S°$ (kJ mol^{-1} K^{-1})
25	2992.698	−19.84	2.612	0.07529
35	3077.397	−20.59		
45	3209.151	−21.34		
55	3284.439	−22.10		

4. Conclusion

In this research, the agricultural waste Brazil nut shells were used for the preparation of activated carbon using chemical activation with KOH. Then, the obtained material was used as an alternative adsorbent for phenol removal from aqueous medium. The characterization results demonstrated a typical activated carbon structure, showing rounded cavities scattered randomly over the entire surface, the presence of oxygenated surface functional groups, good textural properties, and point of zero charge value of 6.0. In addition, BNSAC was characterized as a mesoporous material (average pore size of 3.69 nm). Regarding the phenol adsorption experiments, the most adequate adsorption dosage and pH

were 0.75 g L−1 and 6, respectively. The kinetic curves were well represented by the Elovich model. The Sips model was the most adequate to represent the adsorption equilibrium curves, with a maximum adsorption capacity value (qs) of 99.02 mg g−1 (obtained at the temperature of 55 °C). The estimated enthalpy change value confirmed that the phenol adsorption on BNSAC was an endothermic process and suggested that it was governed by physical interactions. These results showed that the BNSAC has good potential as an adsorbent for phenol removal, contributing both to the management of agricultural waste and the treatment of wastewater contaminated with phenol.

References

Aguilar-Rosero J, Urbina-López ME, Rodríguez-González BE, León-Villegas SX, Luna-Cruz IE, Cárdenas-Chávez DL (2022) Development and Characterization of Bioadsorbents Derived from Different Agricultural Wastes for Water Reclamation: A Review. Appl Sci 12:2740. https://doi.org/10.3390/app12052740

Al-Lagtah NMA, Al-Muhtaseb AH, Ahmad MNM, Salameh Y (2016) Chemical and physical characteristics of optimal synthesised activated carbons from grass-derived sulfonated lignin versus commercial activated carbons. Microporous Mesoporous Mater 225:504–514. https://doi.org/10.1016/j.micromeso.2016.01.043

Al-Trawneh SA, Jiries AG, Alshahateet SF, Sagadevan S (2021) Phenol removal from aqueous solution using synthetic V-shaped organic adsorbent: Kinetics, isotherm, and thermodynamics studies. Chem Phys Lett 781:138959. https://doi.org/10.1016/j.cplett.2021.138959

Araga R, Soni S, Sharma CS (2017) Fluoride adsorption from aqueous solution using activated carbon obtained from KOH-treated jamun (Syzygium cumini) seed. J Environ Chem Eng 5:5608–5616. https://doi.org/10.1016/j.jece.2017.10.023

Awasthi MK, Sindhu R, Sirohi R, Kumar V, Ahluwalia V, Binod P, Juneja A, Kumar D, Yan B, Sarsaiya S, Zhang Z, Pandey A, Taherzadeh MJ (2022) Agricultural waste biorefinery development towards circular bioeconomy. Renew Sustain Energy Rev 158:112122. https://doi.org/10.1016/j.rser.2022.112122

Awogbemi O, Kallon DVV, Aigbodion VS (2021) Trends in the development and utilization of agricultural wastes as heterogeneous catalyst for biodiesel production. J Energy Inst 98:244–258. https://doi.org/10.1016/j.joei.2021.06.017

Baldoni AB, Teodoro LPR, Teodoro PE, Tonini H, Tardin FD, Botin AA, Hoogerheide ESS, Botelho SCC, Lulu J, de Farias Neto AL, Azevedo VCR (2020) Genetic diversity of Brazil nut tree (Bertholletia excelsa Bonpl.) in southern Brazilian Amazon. For Ecol Manage 458:117795. https://doi.org/10.1016/j.foreco.2019.117795

Bedia J, Peñas-Garzón M, Gómez-Avilés A, Rodriguez J, Belver C (2018) A Review on the Synthesis and Characterization of Biomass-Derived Carbons for Adsorption of Emerging Contaminants from Water. J Carbon Res 4:63. https://doi.org/10.3390/c4040063

Bonilla-Petriciolet A, Mendoza-Castillo DI, Dotto GL, Duran-Valle CJ (2019) Adsorption in Water Treatment. Chem Mol Sci Chem Eng 1–19. https://doi.org/10.1016/b978-0-12-409547-2.14390-2

Cao Y, Han K, Teng Z, Li J, Ji T, Li X, Zhang J (2021) Optimized synergistic preparation of nitrogen-doped porous carbon derived from gasified carbon for supercapacitors. J Alloys Compd 860:158385. https://doi.org/10.1016/j.jallcom.2020.158385

Cheng J, Hu SC. Sun GT, Kang K, Zhu MQ, Geng ZC (2021) Comparison of activated carbons prepared by one-step and two-step chemical activation process based on

cotton stalk for supercapacitors application. Energy 215:119144. https://doi.org/10.1016/j.energy.2020.119144

Chiang YC, Juang RS (2017) Surface modifications of carbonaceous materials for carbon dioxide adsorption: A review. J Taiwan Inst Chem Eng 71:214–234. https://doi.org/10.1016/j.jtice.2016.12.014

Cunha MR, Lima EC, Lima DR, da Silva RS, Thue PS, Seliem MK, Sher F, dos Reis GS, Larsson SH (2020) Removal of captopril pharmaceutical from synthetic pharmaceutical-industry wastewaters: Use of activated carbon derived from Butia catarinensis. J Environ Chem Eng 8:104506. https://doi.org/10.1016/j.jece.2020.104506

da Silva MCF, Schnorr C, Lütke SF, Knani S, Nascimento VX, Lima EC, Thue PS, Vieillard J, Silva LFO, Dotto GL (2022) KOH activated carbons from Brazil nut shell: preparation, characterization, and their application in phenol adsorption. Chem Eng Res Des 187:387–396. https://doi.org/https://doi.org/10.1016/j.cherd.2022.09.012

de Salomón YLO, Georgin J, Franco DSP, Netto MS, Foletto EL, Allasia D, Dotto GL (2021) Application of seed residues from Anadenanthera macrocarpa and Cedrela fissilis as alternative adsorbents for remarkable removal of methylene blue dye in aqueous solutions. Environ Sci Pollut Res 28:2342–2354. https://doi.org/10.1007/s11356-020-10635-0

Diel JC, Franco DSP, Nunes IS, Pereira HA, Moreira KS, Burgo TAL, Foletto EL, Dotto GL (2021) Carbon nanotubes impregnated with metallic nanoparticles and their application as an adsorbent for the glyphosate removal in an aqueous matrix. J Environ Chem Eng 9:105178. https://doi.org/10.1016/j.jece.2021.105178

Ferreira SD, Altafini CR, Perondi D, Godinho M (2015) Pyrolysis of Medium Density Fiberboard (MDF) wastes in a screw reactor. Energy Convers Manag 92:223–233. https://doi.org/10.1016/j.enconman.2014.12.032

Franco DSP, Georgin J, Netto MS, Allasia D, Oliveira MLS, Foletto EL, Dotto GL (2021) Highly effective adsorption of synthetic phenol effluent by a novel activated carbon prepared from fruit wastes of the Ceiba speciosa forest species. J Environ Chem Eng 9:105927. https://doi.org/10.1016/j.jece.2021.105927

Fseha YH, Shaheen J, Sizirici B (2023) Phenol contaminated municipal wastewater treatment using date palm frond biochar: Optimization using response surface methodology. Emerg Contam 9:100202. https://doi.org/10.1016/j.emcon.2022.100202

Gao Y, Yue Q, Gao B, Li A (2020) Insight into activated carbon from different kinds of chemical activating agents: A review. Sci Total Environ 746:141094. https://doi.org/10.1016/j.scitotenv.2020.141094

Georgin J, Franco DSP, Netto MS, Allasia D, Foletto EL, Oliveira LFS, Dotto GL (2021a) Transforming shrub waste into a high-efficiency adsorbent : Application of Physalis peruvian chalice treated with strong acid to remove the 2,4-dichlorophenoxyacetic acid herbicide. J Environ Chem Eng 9:104574. https://doi.org/10.1016/j.jece.2020.104574

Georgin J, Pinto D, Franco DSP, Netto MS, Lazarotto JS, Allasia DG, Tassi R, Silva LFO, Dotto GL (2022) Improved Adsorption of the Toxic Herbicide Diuron Using Activated Carbon Obtained from Residual Cassava Biomass (Manihot esculenta). Molecules 27:7574. https://doi.org/10.3390/molecules27217574

Georgin J, Salomón YLO, Franco DSP, Netto MS, Piccilli DGA, Perondi D, Silva LFO, Foletto EL, Dotto GL (2021b) Development of highly porous activated carbon from Jacaranda mimosifolia seed pods for remarkable removal of aqueous-phase ketoprofen. J Environ Chem Eng 9:105676. https://doi.org/10.1016/j.jece.2021.105676

Ghosh S, Barron AR (2017) The effect of KOH concentration on chemical activation of porous carbon sorbents for carbon dioxide uptake and carbon dioxide-methane selectivity:

The relative formation of micro- (<2 nm) versus meso- (>2 nm) porosity. Sustain. Energy Fuels 1:806–813. https://doi.org/10.1039/c6se00102e

Giles CH, Smith D, Huitson A (1974) A general treatment and classification of the solute adsorption isotherm. J Colloid Interface Sci 47:755–765. https://doi.org/10.1016/0021-9797(74)90252-5

Hairuddin MN, Mubarak NM, Khalid M, Abdullah EC, Walvekar R, Karri RR (2019) Magnetic palm kernel biochar potential route for phenol removal from wastewater. Environ Sci Pollut Res 26:35183–35197. https://doi.org/https://doi.org/10.1007/s11356-019-06524-w

Huang G, Liu Y, Wu X, Cai J (2019) Activated carbons prepared by the KOH activation of a hydrochar from garlic peel and their CO2 adsorption performance. New Carbon Mater 34:247–257. https://doi.org/10.1016/S1872-5805(19)60014-4

IBGE (2021) Produção da Extração Vegetal e da Silvicultura 2020. Instituto Brasileiro de Geografia e Estatística (IBGE).

Iheanacho OC, Nwabanne JT, Obi CC, Onu CE (2021) Packed bed column adsorption of phenol onto corn cob activated carbon: linear and nonlinear kinetics modeling. South African J Chem Eng 36:80–93. https://doi.org/10.1016/j.sajce.2021.02.003

Istratie R, Stoia M, Păcurariu C, Locovei C (2019) Single and simultaneous adsorption of methyl orange and phenol onto magnetic iron oxide/carbon nanocomposites. Arab J Chem 12:3704–3722. https://doi.org/10.1016/j.arabjc.2015.12.012

Jawad AH, Saud Abdulhameed A, Wilson LD, Syed-Hassan SSA, ALOthman ZA, Rizwan Khan M (2021) High surface area and mesoporous activated carbon from KOH-activated dragon fruit peels for methylene blue dye adsorption: Optimization and mechanism study. Chinese J Chem Eng 32:281–290. https://doi.org/10.1016/j.cjche.2020.09.070

Kwiatkowski M, Broniek E (2017) An analysis of the porous structure of activated carbons obtained from hazelnut shells by various physical and chemical methods of activation. Colloids Surfaces A Physicochem Eng Asp 529:443–453. https://doi.org/10.1016/j.colsurfa.2017.06.028

Leite AB, Saucier C, Lima EC, dos Reis GS, Umpierres CS, Mello BL, Shirmardi M, Dias SLP, Sampaio CH (2018) Activated carbons from avocado seed: optimisation and application for removal of several emerging organic compounds. Environ Sci Pollut Res 25:7647–7661. https://doi.org/10.1007/s11356-017-1105-9

Li B, Sun K, Guo Y, Tian J, Xue Y, Sun D (2013a) Adsorption kinetics of phenol from water on Fe/AC. Fuel 110:99–106. https://doi.org/10.1016/j.fuel.2012.10.043

Li C, Xu M, Sun X, Han S, Wu X, Liu YN, Huang J, Deng S (2013b) Chemical modification of Amberlite XAD-4 by carbonyl groups for phenol adsorption from wastewater. Chem Eng J 229:20–26. https://doi.org/10.1016/j.cej.2013.05.090

Li H, Meng F, Duan W, Lin Y, Zheng Y (2019) Biodegradation of phenol in saline or hypersaline environments by bacteria: A review. Ecotoxicol Environ Saf 184: 109658. https://doi.org/10.1016/j.ecoenv.2019.109658

Lütke SF, Igansi AV, Pegoraro L, Dotto GL, Pinto LAA, Cadaval TRS (2019) Preparation of activated carbon from black wattle bark waste and its application for phenol adsorption. J Environ Chem Eng 7:103396. https://doi.org/10.1016/j.jece.2019.103396

Lv S, Li C, Mi J, Meng H (2020) A functional activated carbon for efficient adsorption of phenol derived from pyrolysis of rice husk, KOH-activation and EDTA-4Na-modification. Appl Surf Sci 510:145425. https://doi.org/10.1016/j.apsusc.2020.145425

Machado LMM, Lütke SF, Perondi D, Godinho M, Oliveira MLS, Collazzo GC, Dotto GL (2020a) Simultaneous production of mesoporous biochar and palmitic acid by pyrolysis of

brewing industry wastes. Waste Manag 113:96–104. https://doi.org/10.1016/j.wasman.2020.05.038

Machado LMM, Lütke SF, Perondi D, Godinho M, Oliveira MLS, Collazzo GC, Dotto GL (2020b). Treatment of effluents containing 2-chlorophenol by adsorption onto chemically and physically activated biochars. J Environ Chem Eng 8:104473. https://doi.org/10.1016/j.jece.2020.104473

Mohamad Said KA, Ismail AF, Abdul Karim Z, Abdullah MS, Hafeez A (2021ª) A review of technologies for the phenolic compounds recovery and phenol removal from wastewater. Process Saf Environ Prot 151:257–289. https://doi.org/10.1016/j.psep.2021.05.015

Mohamad Said KA, Ismail AF, Zulhairun AK, Abdullah MS, Usman J, Azali MA, Azali, M (2021b) Zinc ferrite migration dependence on magnetic induce membrane for phenol removal: Adsorption reaction and diffusion study. J Environ Chem Eng 9:105036. https://doi.org/10.1016/j.jece.2021.105036

Mohammadi SZ, Darijani Z, Karimi MA (2020) Fast and efficient removal of phenol by magnetic activated carbon-cobalt nanoparticles. J Alloys Compd 832:154942. https://doi.org/10.1016/j.jallcom.2020.154942

Mohd A (2022) Presence of phenol in wastewater effluent and its removal: an overview. Int J Environ Anal Chem 102:1362–1384. https://doi.org/10.1080/03067319.2020.1738412

Nasseh N, Khosravi R, Rumman GA, Ghadirian M, Eslami H, Khoshnamvand M, Al-Musawi TJ, Khosravi A (2021) Adsorption of Cr(VI) ions onto powdered activated carbon synthesized from Peganum harmala seeds by ultrasonic waves activation. Environ Technol Innov 21:101277. https://doi.org/10.1016/j.eti.2020.101277

Nazir G, Rehman A, Hussain S, Ikram M, Park SJ (2022) Supercapacitor performance based on nitrogen and sulfur co-doped hierarchically porous carbons: Superior rate capability and cycle stability. Int J Energy Res 46:15602–15616. https://doi.org/10.1002/er.8256

Neme I, Gonfa G, Masi C (2022) Preparation and characterization of activated carbon from castor seed hull by chemical activation with H3PO4. Results Mater 15:100304. https://doi.org/10.1016/j.rinma.2022.100304

Netto MS, Georgin J, Franco DSP, Mallmann ES, Foletto EL, Godinho M, Pinto D, Dotto GL (2022) Effective adsorptive removal of atrazine herbicide in river waters by a novel hydrochar derived from Prunus serrulata bark. Environ Sci Pollut Res 29:3672–3685. https://doi.org/https://doi.org/10.1007/s11356-021-15366-4

Netto MS, Oliveira JS, Salau NPG, Dotto GL (2021) Analysis of adsorption isotherms of Ag+, Co+2 , and Cu+2 onto zeolites using computational intelligence models. J Environ Chem Eng 9:104960. https://doi.org/10.1016/j.jece.2020.104960

Nizam NUM, Hanafiah MM, Mahmoudi E, Halim AA, Mohammad AW (2021) The removal of anionic and cationic dyes from an aqueous solution using biomass-based activated carbon. Sci Rep 11:8623. https://doi.org/10.1038/s41598-021-88084-z

Oginni O, Singh K, Oporto G, Dawson-Andoh B, McDonald L, Sabolsky E (2019) Influence of one-step and two-step KOH activation on activated carbon characteristics. Bioresour Technol Reports 7:100266. https://doi.org/10.1016/j.biteb.2019.100266

Ogungbenro AE, Quang DV, Al-Ali KA, Vega LF, Abu-Zahra MRM (2020) Synthesis and characterization of activated carbon from biomass date seeds for carbon dioxide adsorption. J Environ Chem Eng 8:104257. https://doi.org/10.1016/j.jece.2020.104257

Othmani A, Magdouli S, Senthil Kumar P, Kapoor A, Chellam PV, Gökkuş O (2022) Agricultural waste materials for adsorptive removal of phenols, chromium (VI) and cadmium

(II) from wastewater: A review. Environ Res 204:111916. https://doi.org/10.1016/j.envres.2021.111916

Panigrahy N, Priyadarshini A, Sahoo MM, Verma AK, Daverey A, Sahoo NK (2022) A comprehensive review on eco-toxicity and biodegradation of phenolics: Recent progress and future outlook. Environ Technol Innov 27:102423. https://doi.org/10.1016/j.eti.2022.102423

Paredes-Laverde M, Salamanca M, Diaz-Corrales JD, Flórez E, Silva-Agredo J, Torres-Palma RA (2021) Understanding the removal of an anionic dye in textile wastewaters by adsorption on ZnCl2activated carbons from rice and coffee husk wastes: A combined experimental and theoretical study. J Environ Chem Eng 9:105685. https://doi.org/10.1016/j.jece.2021.105685

Pauletto PS, Lütke SF, Dotto GL, Salau NPG (2021) Forecasting the multicomponent adsorption of nimesulide and paracetamol through artificial neural network. Chem Eng J 412:127527. https://doi.org/10.1016/j.cej.2020.127527

Rashid J, Tehreem F, Rehman A, Kumar R (2019) Synthesis using natural functionalization of activated carbon from pumpkin peels for decolourization of aqueous methylene blue. Sci Total Environ 671:369–376. https://doi.org/10.1016/j.scitotenv.2019.03.363

Rodrigues LA, da Silva MLCP, Alvarez-Mendes MO, Coutinho AR, Thim GP (2011) Phenol removal from aqueous solution by activated carbon produced from avocado kernel seeds. Chem Eng J 174:49–57. https://doi.org/10.1016/j.cej.2011.08.027

Streit AFM, Collazzo GC, Druzian SP, Verdi RS, Foletto EL, Oliveira LFS, Dotto GL (2021) Adsorption of ibuprofen, ketoprofen, and paracetamol onto activated carbon prepared from effluent treatment plant sludge of the beverage industry. Chemosphere 262:128322. https://doi.org/10.1016/j.chemosphere.2020.128322

Streit AFM, Côrtes LN, Druzian SP, Godinho M, Collazzo GC, Perondi D, Dotto GL (2019) Development of high quality activated carbon from biological sludge and its application for dyes removal from aqueous solutions. Sci Total Environ 660:277–287. https://doi.org/10.1016/j.scitotenv.2019.01.027

Sun J, Liu X, Zhang F, Zhou J, Wu J, Alsaedi A, Hayat T, Li J (2019) Insight into the mechanism of adsorption of phenol and resorcinol on activated carbons with different oxidation degrees. Colloids Surfaces A Physicochem Eng Asp 563:22–30. https://doi.org/10.1016/j.colsurfa.2018.11.042

Ta HS, Van KL, Thi TTL, Nguyen, DH (2021) Thermodynamic studies on the adsorption of phenol from aqueous solution by coffee husk activated carbon. Egypt J Chem 64:2355–2367. https://doi.org/10.21608/EJCHEM.2021.30318.2648

Thines KR, Abdullah EC, Mubarak NM, Ruthiraan M (2017) Synthesis of magnetic biochar from agricultural waste biomass to enhancing route for waste water and polymer application: A review. Renew Sustain Energy Rev 67:257–276. https://doi.org/10.1016/j.rser.2016.09.057

Thommes M, Kaneko K, Neimark AV, Olivier JP, Rodriguez-Reinoso F, Rouquerol J, Sing KSW (2015) Physisorption of gases, with special reference to the evaluation of surface area and pore size distribution (IUPAC Technical Report). https://doi.org/10.1515/pac-2014-1117

Thue PS, Adebayo MA, Lima EC, Sieliechi JM, Machado FM, Dotto GL, Vaghetti JCP, Dias SLP (2016) Preparation, characterization and application of microwave-assisted activated carbons from wood chips for removal of phenol from aqueous solution. J Mol Liq 223:1067–1080. https://doi.org/10.1016/j.molliq.2016.09.032

Vasquez WV, Hernández DM, del Hierro JN, Martin D, Cano MP, Fornari T (2021) Supercritical carbon dioxide extraction of oil and minor lipid compounds of cake byproduct

from Brazil nut (Bertholletia excelsa) beverage production. J Supercrit Fluids 171:105188. https://doi.org/10.1016/j.supflu.2021.105188

Wang J, Lei S, Liang L (2020a) Preparation of porous activated carbon from semi-coke by high temperature activation with KOH for the high-efficiency adsorption of aqueous tetracycline. Appl Surf Sci 530:147187. https://doi.org/10.1016/j.apsusc.2020.147187

Wang X, Chen A, Chen B, Wang L (2020b) Adsorption of phenol and bisphenol A on river sediments: Effects of particle size , humic acid, pH and temperature. Ecotoxicol Environ Saf 204:111093. https://doi.org/10.1016/j.ecoenv.2020.111093

Wang Y, Wang S, Xie T, Cao J (2020c) Activated carbon derived from waste tangerine seed for the high-performance adsorption of carbamate pesticides from water and plant. Bioresour Technol 316:123929. https://doi.org/10.1016/j.biortech.2020.123929

Yakub E, Agarry SE, Omoruwou F, Owabor CN (2020) Comparative study of the batch adsorption kinetics and mass transfer in phenol-sand and phenol-clay adsorption systems. Part Sci Technol 38:801–811. https://doi.org/10.1080/02726351.2019.1616862

Yang K, Zhu L, Yang J, Lin D (2018) Adsorption and correlations of selected aromatic compounds on a KOH-activated carbon with large surface area. Sci Total Environ 618:1677–1684. https://doi.org/10.1016/j.scitotenv.2017.10.018

Zazycki MA, Godinho M, Perondi D, Foletto EL, Collazzo GC, Dotto GL (2018) New biochar from pecan nutshells as an alternative adsorbent for removing reactive red 141 from aqueous solutions. J Clean Prod 171:57–65. https://doi.org/10.1016/j.jclepro.2017.10.007

Zhang Z, Wang T, Zhang H, Liu Y, Xing B (2021) Adsorption of Pb(II) and Cd(II) by magnetic activated carbon and its mechanism. Sci Total Environ 757:143910. https://doi.org/10.1016/j.scitotenv.2020.143910

Zhou Y, Liu X, Tang L, Zhang F, Zeng G, Peng X, Luo L, Deng Y, Pang Y, Zhang J (2017) Insight into highly efficient co-removal of p-nitrophenol and lead by nitrogen-functionalized magnetic ordered mesoporous carbon: Performance and modelling. J Hazard Mater 333:80–87. https://doi.org/10.1016/j.jhazmat.2017.03.031

Supplementary Material

S1. Characterization of the activated carbon

Scanning electron microscopy (SEM) (Tescan, MIRA 3, Czech Republic) was used to study the morphological features of the activated carbon surface. The SEM images were obtained at a working voltage of 12 kV and magnification of 5000×. Fourier transform infrared spectroscopy (FTIR) (Shimadzu, Prestige 21210045, Japan) spectra were obtained before and after the phenol adsorption. The spectra were obtained in the range of 4000 to 500 cm^{-1} with a resolution of 4 cm^{-1}. The analysis was performed using the diffuse reflectance technique with KBr. The textural properties of the activated carbon were determined based on N_2 adsorption-desorption isotherms at 77 K using a volumetric adsorption analyzer (Micromeritcs, ASAP 2020, USA). To determine the specific surface area, total pore volume, and average pore size, BET (Brunauer-Emmett-Teller) and BJH (Barrett-Joyner-Halenda) methods were used.

S2. Kinetic, equilibrium, and thermodynamic modeling

The adsorption kinetic data were evaluated by the pseudo-first-order (PFO), pseudo-second-order (PSO), and Elovich models (Ho and McKay 1998), which are represented in Eq. (1), (2), and (3), respectively:

$$q_t = q_e\left(1 - exp\left(-k_1 t\right)\right) \quad (1)$$

$$q_t = \frac{k_2 q_e^2 t}{1 + q_e k_2 t} \quad (2)$$

$$q_t = \frac{1}{\beta} ln(1 + \alpha\beta t) \quad (3)$$

Where: q_t is the adsorption capacity at time t (mg g^{-1}), qe is the adsorption capacity at the equilibrium (mg g^{-1}), k_1 is the pseudo-first-order rate constant (min^{-1}), and k_2 is the pseudo-second-order rate constant (g mg^{-1} min^{-1}), α is the initial sorption rate of the Elovich model (mg g^{-1} min^{-1}), and β is the constant related to the extent of surface coverage and activation energy for chemisorption of the Elovich model (g mg^{-1}).

Freundlich (Freundlich 1907), Langmuir (Langmuir 1918), and Sips (Sips 1948) models were used to interpret the equilibrium data. Eq. (4), (5), and (5) show, respectively, the mathematical expression of these models:

$$q_e = \frac{q_m K_L C_e}{1 + K_L C_e} \quad (4)$$

$$q_e = K_F C_e^{1/nF} \quad (5)$$

$$q_e = \frac{q_s \left(K_s C_e\right)^m}{1 + \left(K_s C_e\right)^m} \quad (6)$$

Where: q_e is the equilibrium adsorption capacity (mg g^{-1}), Ce is the equilibrium concentration in the liquid phase (mg L^{-1}), q_m is the maximum adsorption capacity of the Langmuir model (mg g^{-1}), K_L is the Langmuir equilibrium constant (L mg^{-1}), K_F is the Freundlich equilibrium constant ((mg g^{-1}) (mg L^{-1}) $^{-1/nF}$), $1/nF$ is the heterogeneity factor, q_s is

the maximum adsorption capacity of the Sips model (mg g^{-1}), K_S is the Sips equilibrium constant (L mg^{-1}), and m is the exponent of the Sips model.

The parameters of the models were estimated by nonlinear regression, using the Statistica 7.0 software (Statsoft, EUA). The validity of the kinetic and isotherm models was assessed by determination coefficient (R^2), adjusted determination coefficient (R^2_{adj}), and average relative error (*ARE*). R^2, $R^2_{adj,}$ and *ARE*, were calculated according to Eq. (7), (8), and (9), respectively:

$$R^2 = \left(\frac{\sum_i^n \left(q_{i,exp} - \bar{q}_{exp}\right)^2 - \sum_i^n \left(q_{i,exp} - q_{i,model}\right)^2}{\sum_i^n \left(q_{i,exp} - \bar{q}_{exp}\right)^2} \right) \tag{7}$$

$$R^2_{adj} = 1 - \left(1 - R^2\right)\left(\frac{n-1}{n-p-1}\right) \tag{8}$$

$$ARE = \frac{100\%}{n} \sum_i^n \left| \frac{q_{i,exp} - q_{i,model}}{q_{i,model}} \right| \tag{9}$$

Where: $q_{i,model}$ is the individual theoretical adsorption capacity value predicted by the model, $q_{i,exp}$ is the individual experimental adsorption capacity value, $\bar{q}_{exp}$ is the average of all experimental adsorption capacity values measured; n is the number of experimental points, and p is the number of parameters in the fitting model.

The thermodynamic parameters Gibb's free energy change (ΔG^o, kJ mol^{-1}), enthalpy change (ΔH^o, kJ mol^{-1}), and entropy change (ΔS^o, J mol^{-1} K^{-1}) were calculated according to Eq. (10), (11), and (12) (Lima et al. 2019, Wang et al. 2019):

$$\Delta G^o = -RT\,ln(K_D) \tag{10}$$

$$ln(K_D) = \frac{\Delta S^o}{R} - \frac{\Delta H^o}{RT} \tag{11}$$

$$K_D = \frac{(1000 \cdot K_{s.} \cdot \mathrm{M_w}) \cdot [\mathrm{adsorbate}]^o}{\gamma} \tag{12}$$

Where: T is the absolute temperature (K), R is the universal gas constant (8.31×10^{-3} kJ mol^{-1} K^{-1}), K_D is the thermodynamic equilibrium constant, K_s is the equilibrium constant of the best isotherm model (in the case here, is the Sips equilibrium constant), [adsorbate]º is the standard concentration of the adsorbate (1 mol L^{-1}), and γ is the coefficient of activity (dimensionless).

The thermodynamic parameters were determined by linear regression, and R^2 was used as an indicator of fit quality.

References

Freundlich H (1907) Über die Adsorption in Lösungen. Zeitschrift für Phys Chemie 57U: 385–470z. https://doi.org/10.1515/zpch-1907-5723

Ho YS, McKay G (1998) A comparison of chemisorption kinetic models applied to pollutant removal on various sorbents. Process Saf Environ Prot 76:332–340. https://doi.org/10.1205/095758298529696

Langmuir I (1918) The adsorption of gases on plane surfaces of glass, mica and platinum. J Am Chem Soc 40:1361–1403. https://doi.org/10.1021/ja02242a004

Lima EC, Hosseini-Bandegharaei A, Moreno-Piraján JC, Anastopoulos I (2019) A critical review of the estimation of the thermodynamic parameters on adsorption equilibria. Wrong use of equilibrium constant in the Van't Hoof equation for calculation of thermodynamic parameters of adsorption. J Mol Liq 273:425–434. https://doi.org/10.1016/j.molliq.2018.10.048

Sips R (1948) On the Structure of a Catalyst Surface. J Chem Phys 16:490–495. https://doi.org/doi.org/10.1063/1.1746922

Wang Y, Li Y, Zhang Y, Wei W (2019) Enhanced brilliant blue FCF adsorption using microwave-hydrothermal synthesized hydroxyapatite nanoparticles. J Dispers Sci Technol 41:1346–1355. https://doi.org/10.1080/01932691.2019.1623695

5. **DISCUSSÕES**

Dois carvões ativados chamados CA105 e CA11 foram preparados a partir da casca de Castanha do Pará (*Bertholletia excelsa*), ativados quimicamente com KOH em diferentes proporções e utilizados na remoção de fenol. Os adsorventes foram caracterizados usando as técnicas de FTIR, BET, TGA, DRX, e MEV. Sendo o trabalho divido em duas etapas: Artigo 1 e Artigo 2.

Na primeira parte do estudo foi demonstrado que ambos os CAs preparados foram adsorventes promissores para remoção do fenol de soluções aquosas, com boa eficiência. Onde, foi evidente que a diferença na proporção de KOH influenciou nas características texturais dos carvões. Assim, o CA11 apresentou os melhores resultados, mostrando-se mais eficiente que o CA105. Nas imagens MEV foi possível observar que o CA11 aparentou ter maior quantidade de cavidades do que CA105, fato que foi confirmado com as análises BET/ BJH, onde CA11 apresentou maior área superficial e volume total de poros. Ou seja, a razão de massa de KOH levou ao aumento da área superficial e do volume total de poros do material obtido. Além disso, estudos preliminares sobre o equilíbrio de adsorção mostraram que a cinética de adsorção do CA11 foi mais rápida do que a CA105 e capacidade de adsorção do CA11 foi mais alta, em torno de 68,52 mg g^{-1} enquanto a do CA105 foi em torno de 55,16 mg g^{-1}. Nesta etapa, que os carvões ativados apresentam potencial para serem reutilizados em mais ciclos de adsorção e que o emprego dos adsorventes no tratamento de um efluente simulado pode ter eficiências de remoção de 28,05% e 48,20%. Sendo assim, por apresentar resultados mais satisfatórios de eficácia, o CA11 foi utilizado na segunda etapa do estudo.

Nesta etapa todos os experimentos foram realizados novamente, e como adicional foi investigado o ponto de carga zero, dosagem do carvão, pH da solução, temperatura, termodinâmica e mecanismo de adsorção frente a descontaminação do fenol. Realizados então testes de dosagem e pH, com resultados igual a: dosagem de 0,75 g L^{-1} e pH 6,0. Definidas as condições mais adequadas do pH e dosagem, as curvas cinéticas de adsorção foram obtidas usando diferentes concentrações iniciais fenol (25–200 mg L^{-1}) em intervalos de tempo definidos (0–180 min). O estudo cinético mostrou que a adsorção foi de forma lenta, independente das concentrações iniciais, o equilíbrio foi alcançado a partir de 180 min. Além disso, com base nos valores mais elevados do coeficiente de determinação (R^2) e menores valores do erro relativo médio (ARE) o modelo de Elovich, foi mais adequado para representar os dados experimentais, confirmando com base na litaratura, além da verificação pelo parâmetro α aumentou de 3,93 mg g^{-1} min^{-1} para 142,73 mg g^{-1} min^{-1} com o aumento da

concentração inicial de fenol. Esta tendência confirma que o aumento na concentração inicial de fenol levou a uma adsorção mais rápida. Pelas isotermas de equilíbrio pode-se observar que o aumento da temperatura de 25 a 55 °C favoreceu a capacidade máxima de adsorção chegando a 99,02 mg g^{-1} em T=55 °C. Os altos valores do coeficiente de determinação (R^2) e os menores valores do erro relativo médio (ARE) mostraram que o modelo de Sips foi o mais adequado para representar os dados de equilíbrio. O modelo indicou que o parâmetro k_S também aumentou com o aumento da temperatura, confirmando que a adsorção foi favorecida em 55°C. Nesta mesma fase, pelos estudos termodinâmicos indicaram a adsorção do fenol foi favorável, espontânea e endotérmica, sendo calculados a partir dos valores da variação da energia livre de Gibbis, entalpia e entropia (ΔG°, ΔHº e ΔS°). E, pelo valor de ΔHº = 20 kJ mol^{-1}, sugere-se que a adsorção de fenol pelo CA, foi um processo físico.

Os resultados demonstraram que os resíduos de casca de castanha do Pará (*Bertholletia excelsa*), são um material promissor a ser utilizado para obtenção de carvão ativado. Os carvões obtidos, principalmente os utilizando maior massa de KOH, foram eficientes para a remoção de fenol, contribuindo para a eliminação de duas problemáticas ambientais como descarte de resíduos e tratamento de efluentes.

6. CONCLUSÃO GERAL

Este trabalho utilizou cascas de castanha-do-pará como material precursor para a produção de carvões ativados com diferentes proporções em massa de KOH. Ambos os adsorventes foram caracterizados e usados para remover fenol de solução aquosa. A partir da caracterização, os materiais apresentaram uma estrutura amorfa, com superfície irregular e rugosa, presença de grupos funcionais oxigenados na superfície e tamanho médio dos poros em torno de 3,6 nm, classificados como materiais mesoporosos. Além disso, a razão de massa de KOH aumentou ligeiramente a área de superfície específica de 314,3 $m^2 g^{-1}$ (CA105) para 332,2 $m^2 g^{-1}$ (CA11). E da mesma forma quando comparados, CA11 exibiu uma cinética mais rápida e maior capacidade de adsorção. As capacidades máximas de adsorção (q_s) foram 55,16 e 68,52 mg g^{-1} para CA105 e CA11. Os carvões ativados também foram usados para tratar um efluente industrial simulado, apresentando eficiências de remoção abaixo de 50% para ambos. Esses resultados demonstraram o maior potencial do uso de CA11 em vez de CA105 na adsorção de fenol a partir de uma solução aquosa.

O carvão com maior eficácia adsortiva foi o CA11, e este apresentou o valor de ponto de carga zero de 6,0. Além disso, pelos experimentos de adsorção de fenol, a dosagem de adsorvent de 0,75 g L^{-1} e o pH igual a 6 foram satisfatórios. As curvas cinéticas foram bem representadas pelo modelo de Elovich. O modelo Sips foi o mais adequado para representar as curvas de equilíbrio de adsorção, com valor máximo da capacidade de adsorção (q_s) de 99,02 mg g^{-1}, obtido na temperatura de 55 °C. O valor estimado da variação de entalpia confirmou que a adsorção de fenol foi um processo endotérmico e sugeriu que foi governado por interações físicas. Esses resultados mostraram que o CA obtido apartir de casca de Castanha do Pará, é potencial adsorvente para remoção de fenol, contribuindo tanto para o gerenciamento de resíduos agrícolas quanto para o tratamento de soluções aquosas contaminados com fenol.

7. SUGESTÕES PARA TRABALHOS FUTURO

- Ativar quimicamente o carvão obtido a partir da casca de castanha do Pará, fazendo-se uso de outros agentes como por exemplo, Cloreto de Zinco ($ZnCl_2$) e Hidróxido de Potássio (H_3PO_4);
- Investigar o processo de adsorção para outros compostos fenólicos (Ex.: 2-clorofenol);
- Realizar o processo de regeneração com outros agentes regenerantes da literatura.

8. REFERENCIAS

ACOSTA TORRES, Juan Camilo; BRISNEDA RODRÍGUEZ, Johnnie Briley. **Propuesta para la reducción de colorante azul índigo en aguas residuales de industria textil mediante la oxido reducción para la empresa comercial Dacetex Ltda**. 2018. Trabalho de Conclusão de Curso. Fundación Universidad de América.

AHMED, M. J. et al. High-performance porous biochar from the pyrolysis of natural and renewable seaweed (Gelidiella acerosa) and its application for the adsorption of methylene blue. **Bioresource technology**, v. 278, p. 159-164, 2019.

ANVISA. Agência Nacional de Vigilância Sanitária, 2005. Resolução – RDC n° 218. Diário Oficial da República Federativa do Brasil.

ARGUN, Mehmet Emin *et al*. Activation of pine cone using Fenton oxidation for Cd (II) and Pb (II) removal. **Bioresource technology**, v. 99, n. 18, p. 8691-8698, 2008.

ARUNPRASATH, T. *et al*. Biodegradation of triphenylmethane dye malachite green by a newly isolated fungus strain. **Biocatalysis and Agricultural Biotechnology**, v. 17, p. 672-679, 2019.

AWASTHI, Mukesh Kumar et al. Agricultural waste biorefinery development towards circular bioeconomy. **Renewable and Sustainable Energy Reviews**, v. 158, p. 112122, 2022.

BADAWY, Abdelrahman A.; IBRAHIM, Shaimaa M.; ESSAWY, Hisham A. Enhancing the textile dye removal from aqueous solution using cobalt ferrite nanoparticles prepared in presence of fulvic acid. **Journal of Inorganic and Organometallic Polymers and Materials**, v. 30, n. 5, p. 1798-1813, 2020.

BALDONI, Aisy Botega et al. Genetic diversity of Brazil nut tree (Bertholletia excelsa Bonpl.) in southern Brazilian Amazon. **Forest Ecology and Management**, v. 458, p. 117795, 2020.

BANSAL, R. C.; DONNET, J. B.; STOECKLI, F. Active Carbon, Marcel Decker. **Inc., New York**, v. 482, 1988.

BARIK, Bapun et al. Ionic liquid assisted mesoporous silica-graphene oxide nanocomposite synthesis and its application for removal of heavy metal ions from water. **Materials Chemistry and Physics**, v. 239, p. 122028, 2020.

BORGES, F. M. et al. Desenvolvimento e criação de uma unidade produtiva de carvão ativado. **ENCONTRO NACIONAL DE ENGENHARIA DE PRODUÇÃO**, v. 21, 2003.

BORTOLON, Eduardo. Regeneração de carvão ativado saturado com cafeína via ozonização. 2022.

BUSCA, Guido et al. Technologies for the removal of phenol from fluid streams: a short review of recent developments. **Journal of hazardous materials**, v. 160, n. 2-3, p. 265-288, 2008.

CARRILLO, James T.; BORTHAKUR, Dulal. Do uncommon plant phenolic compounds have uncommon properties? A mini review on novel flavonoids. **Journal of Bioresources and Bioproducts**, v. 6, n. 4, p. 279-291, 2021.

CETINKAYA, Afsin Y.; OZDEMIR, Oğuz K. Phenol removal from synthetic solution using low pressure membranes coated with graphene oxide and carbon. **Chemical Papers**, v. 72, p. 327-335, 2018.

CHIANG, P. C.; CHANG, E. E.; WU, J. S. Comparison of chemical and thermal regeneration of aromatic compounds on exhausted activated carbon. **Water science and technology**, v. 35, n. 7, p. 279-285, 1997.

COONEY, David O.; NAGERL, Andrew; HINES, Anthony L. Solvent regeneration of activated carbon. **Water Research**, v. 17, n. 4, p. 403-410, 1983.

CUNHA, Mariene R. et al. Conversion of Eragrostis plana Nees leaves to activated carbon by microwave-assisted pyrolysis for the removal of organic emerging contaminants from aqueous solutions. **Environmental Science and Pollution Research**, v. 25, p. 23315-23327, 2018.

DEHMANI, Younes et al. Kinetic, thermodynamic and mechanism study of the adsorption of phenol on Moroccan clay. **Journal of Molecular Liquids**, v. 312, p. 113383, 2020.

DÍAZ-GARDUÑO, B. et al. Environmental risk assessment of effluents as a whole emerging contaminant: Efficiency of alternative tertiary treatments for wastewater depuration. **Water Research**, v. 119, p. 136-149, 2017.

DOS SANTOS, Davis Castro et al. New carbon composite adsorbents for the removal of textile dyes from aqueous solutions: Kinetic, equilibrium, and thermodynamic studies. **Korean Journal of Chemical Engineering**

DOTTO, G. L. et al. Adsorption of methylene blue by ultrasonic surface modified chitin. **Journal of colloid and interface science**, v. 446, p. 133-140, 2015.

DOTTO, Guilherme L.; MCKAY, Gordon. Cenário atual e desafios em adsorção para tratamento de água. **Jornal de engenharia química ambiental** , v. 8, n. 4, pág. 103988, 2020.

DOTTO, Juliana et al. Performance of different coagulants in the coagulation/flocculation process of textile wastewater. **Journal of cleaner production**, v. 208, p. 656-665, 2019.

FANG, Xingyu et al. Enhanced degradation of bisphenol A by mixed ZIF derived CoZn oxide encapsulated N-doped carbon via peroxymonosulfate activation: The importance of N doping amount. **Journal of Hazardous Materials**, v. 419, p. 126363, 2021

FENG, Dongdong et al. Functionalized construction of biochar with hierarchical pore structures and surface O-/N-containing groups for phenol adsorption. **Chemical Engineering Journal**, v. 410, p. 127707, 2021.

FERREIRA, Matheus Pinheiro et al. Accurate mapping of Brazil nut trees (Bertholletia excelsa) in Amazonian forests using WorldView-3 satellite images and convolutional neural networks. **Ecological Informatics**, v. 63, p. 101302, 2021.

FOGLER, William E. et al. Recruitment of hepatic NK cells by IL-12 is dependent on IFN-γ and VCAM-1 and is rapidly down-regulated by a mechanism involving T cells and expression of Fas. **The Journal of Immunology**, v. 161, n. 11, p. 6014-6021, 1998.

FRANCO, Dison SP et al. Highly effective adsorption of synthetic phenol effluent by a novel activated carbon prepared from fruit wastes of the Ceiba speciosa forest species. **Journal of Environmental Chemical Engineering**, v. 9, n. 5, p. 105927, 2021.

FREUNDLICH, H. Z. **Journal of Physical Chemistry,** v. 57, p. 385, 1907.

FROTA, André Madson Araújo. Production, characterization and assessment of sludge-derived biochar for water treatment as a sustainable solution towards a circular economy. 2023.

GAO, Ming et al. Phenol removal via activated carbon from co-pyrolysis of waste coal tar pitch and vinasse. **Korean Journal of Chemical Engineering**, v. 38, p. 64-71, 2021.

GIL, Aida et al. Mixture optimization of anaerobic co-digestion of tomato and cucumber waste. **Environmental technology**, v. 36, n. 20, p. 2628-2636, 2015.

GILES, C. H.; SMITH, D.; HUITSON, A. A general treatment and classification of the solute: part I. theoretical. **J. Colloid Interface Sci**, v. 47, p. 755-765, 1974.

GONZÁLEZ-GARCÍA, P. Activated carbon from lignocellulosics precursors: A review of the synthesis methods, characterization techniques and applications. **Renewable and Sustainable Energy Reviews**, v. 82, p. 1393–1414, 2018.

GUO, Liping et al. Amplified Electrochemical Response of Phenol by Oxygenation of Tyrosinase Coupling with Electrochemical‐chemical‐chemical Redox Cycle. **Electroanalysis**, v. 31, n. 9, p. 1728-1735, 2019.

GUPTA, Tripti *et al*. Adsorption of Indigo Carmine Dye by Acacia nilotica sawdust activated carbon in fixed bed column. **Scientific Reports**, v. 12, n. 1, p. 1-14, 2022.

GUPTA, V. K. e SUHAS. Application of low-cost adsorbents for dye removal–a review. **Journal of environmental management**, v. 90, n. 8, p. 2313-2342, 2009.

GUPTA, V. K.; SUHAS. Application of low-cost adsorbents for dye removal – A review. **Journal of Environmental Management**, v. 90, p. 2313–2342, 2009.

HAN, J. et al. The N-doped activated carbon derived from sugarcane bagasse for CO2 adsorption. **Industrial Crops & Products**, v. 128, p. 290–297, 2019.

HAN, Zhantao *et al*. Magnetite impregnation effects on the sorbent properties of activated carbons and biochars. **Water research**, v. 70, p. 394-403, 2015

HERNÁNDEZ-MONTOYA, Virginia; GARCÍA-SERVIN, Josafat; BUENO-LÓPEZ, José Iván. Thermal treatments and activation procedures used in the preparation of activated carbons. **Lignocellulosic precursors used in the synthesis of activated carbon-characterization techniques and applications in the wastewater treatment**, v. 2, p. 19-36, 2012.

HO, Yuhshan S.; MCKAY, Gordon. A comparison of chemisorption kinetic models applied to pollutant removal on various sorbents. Process safety and environmental protection, v. 76, n. 4, p. 332-340, 1998..

JAGWE, Joseph et al. Synthesis and application of Granular activated carbon from biomass waste materials for water treatment: A review. **Journal of Bioresources and Bioproducts**, v. 6, n. 4, p. 292-322, 2021.

JORDAN, W. et al. J. Ullrich em Ullmann's Encyclopedia of Industrial Chemistry. **Editora VCH** , v. 5, p. 299, 1987.

JUNIOR, EC Silva et al. Natural variation of selenium in Brazil nuts and soils from the Amazon region. **Chemosphere**, v. 188, p. 650-658, 2017.

KHASRI, Azduwin *et al*. Adsorption of Remazol Brilliant Violet 5R dye from aqueous solution onto melunak and rubberwood sawdust based activated carbon: interaction mechanism, isotherm, kinetic and thermodynamic properties. **DWT**, v. 216, p. 401-411, 2021.

KUŚMIEREK, Krzysztof; SPRYNSKYY, Myroslav; ŚWIĄTKOWSKI, Andrzej. Lignito bruto como um adsorvente eficaz de baixo custo para remover fenóis e clorofenóis de soluções aquosas. **Separação Ciência e Tecnologia** , v. 55, n. 10, pág. 1741-1751, 2020.

LAGERGREN, Stan. Zur theorie der sogenannten adsorption geloster stoffe. Kungliga Svenska Vetenskapsakademiens Handlingar, [s. l.], v. 24, n. 4, p. 1–39, 1898.

LANGMUIR, Irving. The adsorption of gases on plane surface of glass, mica and platinum. **Journal of American Chemical Society**, v. 40, p. 1361-1403, 1918

LARASATI, Amanda; FOWLER, Geoffrey D.; GRAHAM, Nigel JD. Chemical regeneration of granular activated carbon: preliminary evaluation of alternative regenerant solutions. **Environmental Science: Water Research & Technology**, v. 6, n. 8, p. 2043-2056, 2020.

LEE, J. D. et al. 9. Química Orgânica. **SUGESTÃO DE CURRÍCULO PARA CURSO DE BACHAREL EM QUÍMICA E QUÍMICA TECNOLÓGICA**, p. 19, 2016.

LIMA, Diana R. et al. Efficient acetaminophen removal from water and hospital effluents treatment by activated carbons derived from Brazil nutshells. **Colloids and Surfaces A: Physicochemical and Engineering Aspects**, v. 583, p. 123966, 2019.

LIMA, Eder C. *et al*. A critical review of the estimation of the thermodynamic parameters on adsorption equilibria. Wrong use of equilibrium constant in the Van't Hoof equation for calculation of thermodynamic parameters of adsorption. **Journal of molecular liquids**, v. 273, p. 425-434, 2019.

LÜTKE, Sabrina F. et al. Preparation of activated carbon from black wattle bark waste and its application for phenol adsorption. **Journal of Environmental Chemical Engineering**, v. 7, n. 5, p. 103396, 2019.

MARTIN, R. J.; NG, W. J. Chemical regeneration of exhausted activated carbon—I. **Water research**, v. 18, n. 1, p. 59-73, 1984.
MASSANTINI, Riccardo; MOSCETTI, Roberto; FRANGIPANE, Maria Teresa. Evaluating progress of chestnut quality: A review of recent developments. **Trends in Food Science & Technology**, v. 113, p. 245-254, 2021.

MATHEICKAL, J. T.; YU, Q.; LINDEN, J. In‐situ regeneration of phenol‐saturated activated carbon using ethanol. **Developments in Chemical Engineering and Mineral Processing**, v. 6, n. 5, p. 263-272, 1998.

MEKHILEF, Saad; SAIDUR, Rahman; KAMALISARVESTANI, Masoud. Effect of dust, humidity and air velocity on efficiency of photovoltaic cells. **Renewable and sustainable energy reviews**, v. 16, n. 5, p. 2920-2925, 2012.

MOHAMAD NOR, N. et al. Synthesis of activated carbon from lignocellulosic biomass and its applications in air pollution control - A review. **Journal of Environmental Chemical Engineering**, v. 1, p. 658–666, 2013.

MOHAMMADI, Sayed Zia; DARIJANI, Zahra; KARIMI, Mohammad Ali. Fast and efficient removal of phenol by magnetic activated carbon-cobalt nanoparticles. **Journal of Alloys and compounds**, v. 832, p. 154942, 2020.

MORAES, Caio Santos de et al. Zeólitas funcionalizadas para a adsorção de miclobutanil em matrizes aquosas. 2022.
MORAES, Caio Santos de et al. Zeólitas funcionalizadas para a adsorção de miclobutanil em matrizes aquosas. 2022.

MOTA, Jackeline Andrade et al. Interação da quitosana com surfactante e fenol em meio aquoso: cinética, equilíbrio e calorimetria. 2012.

MYERS, D. Surfaces, Interfaces, and Colloids: Principles and Applications. 2. ed. **Electronic: John Wiley & Sons**, 1999.

NASCIMENTO, Ronaldo Ferreira do *et al.* Adsorção: aspectos teóricos e aplicações ambientais. 2020.

NASCIMENTO, Victoria X. et al. Adsorptive Features of Magnetic Activated Carbons Prepared by a One-Step Process towards Brilliant Blue Dye. **Molecules**, v. 28, n. 4, p. 1821, 2023.

NGOBENI, Rivoningo; SADARE, Olawumi; DARAMOLA, Michael O. Synthesis and evaluation of HSOD/PSF and SSOD/PSF membranes for removal of phenol from industrial wastewater. **Polymers**, v. 13, n. 8, p. 1253, 2021.

NOORI, Maasume; SADEGHI, Soroor. Novel immobilization of Pseudomonas aeruginosa on graphene oxide and its applications to biodegradation of phenol existing in industrial wastewaters. **Journal of Water Chemistry and Technology**, v. 41, n. 6, p. 363-370, 2019.
.

PICCIN, Jeferson Steffanello *et al*. Adsorption isotherms in liquid phase: experimental, modeling, and interpretations. In: **Adsorption processes for water treatment and purification**. Springer, Cham, 2017. p. 19-51

PRIYADHARSHINI, S. Dayana; BAKTHAVATSALAM, A. K. Optimization of phenol degradation by the microalga Chlorella pyrenoidosa using Plackett–Burman design and response surface methodology. **Bioresource Technology**, v. 207, p. 150-156, 2016.

RÁPÓ, Eszter; TONK, Szende. Factors affecting synthetic dye adsorption; desorption studies: A review of results from the last five years (2017–2021). **Molecules**, v. 26, n. 17, p. 5419, 2021.

RODRIGUES, Liana Alvares. Maria Lucia Caetano Pinto da Silva, Manoel Orlando Alvarez-Mendes, Aparecido dos Reis Coutinho, Gilmar Patrocínio Thim., et al.,"Phenol removal from aqueous solution by activated carbon produced from avocado kernel seeds.". **Chemical Engineering Journal**, v. 174, p. 49-57, 2011.

RODRIGUEZ-NARVAEZ, Oscar M. et al. Treatment technologies for emerging contaminants in water: A review. **Chemical Engineering Journal**, v. 323, p. 361-380, 2017.

RODRIGUEZ-REINOSO, F.; MOLINA-SABIO, M. Textural and chemical characterization of microporous carbons. **Advances in colloid and interface science**, v. 76, p. 271-294, 1998.

RUTHVEN, Douglas M. **Principles of Adsorption and Adsorption Processes**. John Wiley & Sons. New York, 1984.

SAID, Amir. Introduction to Arithmetic Coding--Theory and Practice. **arXiv preprint arXiv:2302.00819**, 2023.

SAID, Hanaa Mohamed et al. Adsorptions of phenol molecules by graphene-based nanostructures, modified with nitrogen and bromine, from petroleum wastewater using molecular dynamics simulation. **Engineering Analysis with Boundary Elements**, v. 150, p. 636-641, 2023.

SAID, Khairul Anwar Mohamad et al. A review of technologies for the phenolic compounds recovery and phenol removal from wastewater. **Process Safety and Environmental Protection**, v. 151, p. 257-289, 2021.

SAJID, Muhammad et al. Remoção de metais pesados e poluentes orgânicos da água usando adsorventes à base de polímeros dendríticos: uma revisão crítica. **Tecnologia de Separação e Purificação** , v. 191, p. 400-423, 2018.

SATYA SAI, P. M.; KRISHNAIAH, K. Development of the pore-size distribution in activated carbon produced from coconut shell char in a fluidized-bed reactor. **Industrial & engineering chemistry research**, v. 44, n. 1, p. 51-60, 2005.

SERAFIN, Jarosław et al. Activated carbons from the Amazonian biomass andiroba shells applied as a CO2 adsorbent and a cheap semiconductor material. **Journal of CO2 Utilization**, v. 62, p. 102071, 2022.
SHEN, Tianhao et al. Comprehensive study on the pyrolysis process of chestnut processing waste (chestnut shells): Kinetic triplet, thermodynamic, in-situ monitoring of evolved gasses and analysis biochar. **Fuel**, v. 331, p. 125944, 2023.

SILVA, Alfredo José Ferreira da. **Adsorção dos íons de cobre usando pó da palha da carnaúba e bentonita: estudo cinético, termodinâmico e de equilíbrio**. 2019. Tese (Doutorado em Engenharia Química) - Universidade Federal do Rio grande do Norte, Natal, RN, 2019.

SILVA, Matheus Almeida. **Modelagem e simulação de desintoxicação de licores simulados de pré-tratamento via adsorção em carvão ativado**. 2022. Trabalho de Conclusão de Curso. Universidade Federal do Rio Grande do Norte.

SYAMSIAH, Siti; HADI, Iwan Santoso. Adsorption cycles and effect of microbial population on phenol removal using natural zeolit. **Separation and purification technology**, v. 34, n. 1-3, p. 125-133, 2004.

TAHERAN, Mehrdad et al. Emerging contaminants: here today, there tomorrow!. **Environmental nanotechnology, monitoring & management**, v. 10, p. 122-126, 2018.

THUE, Pascal S. *et al*. Single-step pyrolysis for producing magnetic activated carbon from tucumã (Astrocaryum aculeatum) seed and nickel (II) chloride and zinc (II) chloride. Application for removal of nicotinamide and propanolol. **Journal of Hazardous Materials**, v. 398, p. 122903, 2020.

TRAN, Hai Nguyen *et al*. Thermodynamic parameters of liquid–phase adsorption process calculated from different equilibrium constants related to adsorption isotherms: A comparison study. **Journal of Environmental Chemical Engineering**, v. 9, n. 6, p. 106674, 2021.

USGS. Contaminantes de preocupação emergente no meio ambiente. Saúde Ambiental - Programa de Hidrologia de Substâncias Tóxicas. Pesquisa Geológica dos EUA. 2017

VASQUEZ, Wilson V. et al. Supercritical carbon dioxide extraction of oil and minor lipid compounds of cake byproduct from Brazil nut (Bertholletia excelsa) beverage production. **The Journal of Supercritical Fluids**, v. 171, p. 105188, 2021.

VERMA, Monu et al. Fabrication of GO–MnO2 nanocomposite using hydrothermal process for cationic and anionic dyes adsorption: Kinetics, isotherm, and reusability. **Journal of Environmental Chemical Engineering**, v. 9, n. 5, p. 106045, 2021.

WANG, Xiangjie et al. Degradação fotocatalítica de dióxido de titânio-turmalina revestido de superfície para autolimpeza de formaldeído emitido de móveis. **Journal of Hazardous Materials** , v. 420, p. 126565, 2021.

WANG, Yan et al. Enhanced brilliant blue FCF adsorption using microwave-hydrothermal synthesized hydroxyapatite nanoparticles. Journal of Dispersion Science and Technology, v. 41, n. 9, p. 1346-1355, 2020.

WEI, Huanming et al. Biomass-derived nitrogen-doped porous carbon with superior capacitive performance and high CO2 capture capacity. **Electrochimica Acta**, v. 266, p. 161-169, 2018.

XIONG, Qiancheng et al. A cellulose acetate/Amygdalus pedunculata shell-derived activated carbon composite monolith for phenol adsorption. **RSC advances**, v. 8, n. 14, p. 7599-7605, 2018.

XU, Ying et al. Novo surfactante Gemini contendo várias aminas montmorilonita modificada como adsorvente para remoção de fenóis. **Ciência Aplicada da Argila** , v. 162, p. 204-213, 2018.

YANG, Yongli; CANNON, Fred S. Biomass activated carbon derived from pine sawdust with steam bursting pretreatment; perfluorooctanoic acid and methylene blue adsorption. **Bioresource technology**, v. 344, p. 126161, 2022.

YAZICI GUVENC, Senem; CAN-GÜVEN, Emine; VARANK, Gamze. Recalcitrant pollutants removal from paper mill wastewater by ferrous ion-and heat-activated persulfate oxidation processes using response surface methodology: a comparison study. **Separation Science and Technology**, v. 57, n. 7, p. 1151-1166, 2022.

ZAZYCKI, Maria Amélia. **Preparação de biochar a partir de matérias–primas alternativas e sua aplicação na adsorção de corantes**. 2019. Tese (Doutorado em Engenharia Química) - Universidade Federal de Santa Maria, Santa Maria, RS, 2019

ZHAO, Lu et al. Recycling chestnut shell for superior peroxymonosulfate activation in contaminants degradation via the synergistic radical/non-radical mechanisms. **Journal of Hazardous Materials**, v. 430, p. 128471, 2022.

ZHOU, Yanbo *et al*. Recent advances for dyes removal using novel adsorbents: a review. **Environmental pollution**, v. 252, p. 352-365, 2019.

ZHU, Ting et al. Ionic liquid and ultrasound-assisted extraction of chestnut shell pigment with good hair dyeing capability. **Journal of Cleaner Production**, v. 335, p. 130195, 2022.

ZOLLINGER, Heinrich. Color chemistry: syntheses, properties, and applications of organic dyes and pigments. **John Wiley & Sons**, 2003.